

AWARD NUMBER: W81XWH-16-1-0190

TITLE: Untapped Therapeutic Targets in the Tumor Microenvironment

PRINCIPAL INVESTIGATOR: Sandra Orsulic, PhD

CONTRACTING ORGANIZATION: Cedars-Sinai Medical Center Los Angeles,
CA 90048

REPORT DATE: Nov 2019

TYPE OF REPORT: Final

PREPARED FOR: U.S. Army Medical Research and Materiel Command
Fort Detrick, Maryland 21702-5012

DISTRIBUTION STATEMENT: Approved for Public Release; Distribution Unlimited

The views, opinions and/or findings contained in this report are those of the author(s) and should not be construed as an official Department of the Army position, policy or decision unless so designated by other documentation.

REPORT DOCUMENTATION PAGE

Form Approved
OMB No. 0704-0188

Public reporting burden for this collection of information is estimated to average 1 hour per response, including the time for reviewing instructions, searching existing data sources, gathering and maintaining the data needed, and completing and reviewing this collection of information. Send comments regarding this burden estimate or any other aspect of this collection of information, including suggestions for reducing this burden to Department of Defense, Washington Headquarters Services, Directorate for Information Operations and Reports (0704-0188), 1215 Jefferson Davis Highway, Suite 1204, Arlington, VA 22202-4302. Respondents should be aware that notwithstanding any other provision of law, no person shall be subject to any penalty for failing to comply with a collection of information if it does not display a currently valid OMB control number. **PLEASE DO NOT RETURN YOUR FORM TO THE ABOVE ADDRESS.**

1. REPORT DATE Nov 2019			Final	3. DATES COVERED 08/01/2016 - 07/31/2019	
4. TITLE AND SUBTITLE Untapped Therapeutic Targets in the Tumor Microenvironment				5a. CONTRACT NUMBER W81XWH-16-1-0190	
				5b. GRANT NUMBER	
				5c. PROGRAM ELEMENT NUMBER	
6. AUTHOR(S) Sandra Orsulic E-Mail: orsulics@csbs.org				5d. PROJECT NUMBER	
				5e. TASK NUMBER	
				5f. WORK UNIT NUMBER	
7. PERFORMING ORGANIZATION NAME(S) AND ADDRESS(ES) Cedars-Sinai Medical Center 8700 Beverly Boulevard Los Angeles, CA 90048				8. PERFORMING ORGANIZATION REPORT NUMBER	
9. SPONSORING / MONITORING AGENCY NAME(S) AND ADDRESS(ES) U.S. Army Medical Research and Materiel Command Fort Detrick, Maryland 21702-5012				10. SPONSOR/MONITOR'S ACRONYM(S)	
				11. SPONSOR/MONITOR'S REPORT NUMBER(S)	
12. DISTRIBUTION / AVAILABILITY STATEMENT Approved for Public Release; Distribution Unlimited					
13. SUPPLEMENTARY NOTES					
14. ABSTRACT Most therapeutic approaches have focused on the tumor cell and its genetic alterations. However, it is becoming clear that the microenvironment plays an important role in tumor evolution. We hypothesized that conventional chemotherapy for ovarian cancer will be more effective if the microenvironment that harbors the resistant cancer cells is simultaneously targeted. Since activated cancer-associated fibroblasts (CAFs) have a prominent role in most aspects of tumor progression, including responses to anticancer agents by forming a physical barrier that prevents chemotherapy access and promotes resistance, we predicted that targeting CAFs would inhibit tumor progression and/or increase chemotherapeutic efficacy. 1. Our attempts to test anti-fibrotic agents showed largely negative results. One confounding factor in these pre-clinical tests was the modest presence of fibrosis in the existing ovarian cancer models. Therefore, we generated two new mouse models that exhibit extensive fibrosis and rapid onset of ovarian carcinomatosis. These models will be a valuable resource for studying the role of fibroblasts in ovarian cancer initiation and progression. 2. We made advances in targeting and characterizing the functional properties of COL11A1, which we previously identified as a molecular target that distinguishes CAFs from other fibroblasts. 3. We largely disproved our hypothesis that induction of terminal differentiation in CAFs may minimize cancer growth.					
15. SUBJECT TERMS Ovarian cancer, tumor microenvironment, tumor progression, cancer-associated fibroblasts					
16. SECURITY CLASSIFICATION OF:			17. LIMITATION OF ABSTRACT	18. NUMBER OF PAGES	19a. NAME OF RESPONSIBLE PERSON
a. REPORT	b. ABSTRACT	c. THIS PAGE			19b. TELEPHONE NUMBER (include area code)
Unclassified	Unclassified	Unclassified	Unclassified	19	USAMRMC

Table of Contents

	<u>Page</u>
1. Introduction.....	1
2. Keywords.....	1
3. Accomplishments.....	1
Major goals of the project.....	1
Major accomplishments.....	4
Major activities.....	4
Specific objectives.....	4
Significant findings or key outcomes.....	4
Other achievements.....	14
4. Impact.....	15
5. Changes/problems.....	15
6. Products.....	16
7. Participants.....	17
8. Special reporting requirements.....	18
9. Appendix.....	19

1. INTRODUCTION:

High grade serous ovarian carcinoma is among the most lethal cancers affecting women in the U.S. While most therapeutic approaches have focused on malignant epithelial tumor cells and their genetic alterations, it is becoming increasingly clear that the tumor microenvironment plays an equally important role in tumor evolution. The presence of cancer cells induces a reaction in the surrounding stromal cells similar to fibrosis after an injury. These reactions can also reduce therapeutic efficacy of chemotherapy by creating a physical barrier for drug transport while providing a protective environment for cancer cells to repopulate after completion of treatment. Thus, it is thought that anti-cancer therapies should target not only malignant cancer cells but also the microenvironment that fosters tumor growth and survival. Our goal is to demonstrate that targeting processes responsible for the formation of cancer-associated fibroblasts (also known as CAFs) in the tumor microenvironment will effectively attenuate tumor growth, improve intratumoral drug delivery and restore anti-tumor immune responses. We are using three different approaches to targeting CAFs. The first approach is to test anti-fibrotic agents for their efficacy in preventing CAF activation and increasing sensitivity to chemotherapy in a mouse model of ovarian cancer that was developed in our laboratory. The second approach is to increase the precision of targeting activated CAFs, by targeting a protein that we previously identified to be present in activated CAFs but absent from fibroblasts associated with non-cancerous conditions such as fibrosis, inflammation, and wound healing. The third approach is to test several agents for their efficacy in inducing CAF-to-cartilage differentiation with the idea that a terminally-differentiated microenvironment cannot protect malignant cells from chemotherapy or foster their dormancy for future recurrence.

2. KEYWORDS:

Ovarian cancer, tumor microenvironment, cancer-associated fibroblasts, fibrosis, targeted therapy, clinical outcome

3. ACCOMPLISHMENTS:

▪ What were the major goals of the project?

Specific Aim 1 (specified in proposal)	Timeline	Percent Completed
Major Task 1 Test the therapeutic efficacy of CTGF, CTSK, FN1, and LOXL2 inhibitors	Months	Cedars-Sinai Medical Center
Subtask 1 Amend approved IACUC protocol 5318 (Mouse Models of Tumor Microenvironment, PI: Orsulic) for local approval and send related material for DoD's approval.	Upon award notice	100%
Subtask 2 Purchase FVB mice, drugs, and reagents; plan experiments.	1-2	100%
Subtask 3 Implant FVB mice with mouse ovarian cancer cells.	2-25	100%

<p>Subtask 4 Treat mice with CTGF, CTSK, FN1, and LOXL2 inhibitors Assess therapeutic efficacy:</p> <ol style="list-style-type: none"> 1. Tumor growth: tumor weight/volume, luciferase whole-animal imaging. 2. Tumor invasion and metastasis: dissection and immunohistochemistry. 3. Stromal differentiation: Masson's trichrome stain, qPCR and immunostaining for myofibroblast markers (α-SMA, fibronectin, COL11A1). 4. Chemotherapy diffusion: quantification of fluorescently-labeled dextran beads. 5. Tumor-infiltrating immune cells: flow cytometric analyses with antibody cocktail (CD3, CD4, CD8a, CD44, CD62L, CD25, Nkp46, F4/80, CD11b, Gr1, Ly6G, CD11c, and FoxP3). 6. Cancer stem cell content: flow cytometric analyses with CD133, CD44, CD24, and CD117. 7. Angiogenesis: CD31 and CD34. 8. Apoptosis, DNA damage: ApopTag, CC3 positivity, PARP cleavage, or histone H2AX phosphorylation. 9. Toxicity: histological analysis of liver, lung, and kidney injury 10. TGFβ signaling: immunodetection of phosphorylated Smad2/3. 	3-30	80%
<p>Subtask 5 Analyze data using statistical methods; replicate experiments if necessary, prepare and submit manuscripts.</p>	3-36	80%
<p>Milestone Achieved Verified therapeutic efficacy of CTGF, CTSK, FN1, and LOXL2 inhibitors.</p>	32	80%
Specific Aim 2 (specified in proposal)	Timeline	Site 1
<p>Major Task 1 Determine the effect of COL11A1 knockdown in human cancer-associated fibroblasts</p>	Months	Cedars-Sinai Medical Center
<p>Subtask 1 Amend approved IACUC protocol 5318 (Mouse Models of Tumor Microenvironment, PI: Orsulic) for local approval and send related material for DoD's approval.</p>	Upon award notice	100%
<p>Subtask 2 Knock out COL11A1 in human cancer-associated fibroblasts using CRISPR.</p>	1-3	100%
<p>Subtask 3 Co-culture COL11A1 knockout cancer-associated fibroblasts with</p>	3-12	80%

ovarian cancer cells under kidney capsule of nude mice; measure cell proliferation, cell death and other parameters.		
Subtask 4 Analyze data using statistical methods; replicate experiments if necessary.	12-18	80%
Milestone Achieved Verified whether COL11A1 in cancer-associated fibroblasts is essential for the tumor promoting effects in a paracrine manner.	18	80%
Major Task 2 Determine the potential of COL11A1 as a therapeutic target	Months	Cedars-Sinai Medical Center
Subtask 1 Amend approved IACUC protocol 5318 (Mouse Models of Tumor Microenvironment, PI: Orsulic) for local approval and send related material for DoD's approval.	Upon award notice	100%
Subtask 2 Purchase FVB mice, drugs and reagents; plan experiments.	1-2	50%
Subtask 3 Implant FVB mice with mouse ovarian cancer cells.	2-25	50%
Subtask 4 Treat mice with COL11A1 neutralizing antibody. Assess therapeutic efficacy as in Aim 1, Task 4.	3-30	50%
Subtask 5 Analyze data using statistical methods; replicate experiments if necessary; prepare and submit manuscripts.	3-36	50%
Milestone Achieved Verified whether COL11A1 is promising as a therapeutic target with high specificity for activated cancer-associated fibroblasts.	36	50%
Specific Aim 3 (specified in proposal)	Timeline	Site 1
Major Task 1 Assess the effect of differentiating cancer-associated fibroblasts into cartilage on tumor progression and chemosensitivity	Months	Cedars-Sinai Medical Center
Subtask 1 Amend approved IACUC protocol 5318 (Mouse Models of Tumor Microenvironment, PI: Orsulic) for local approval and send related material for DoD's approval.	Upon award notice	100%
Subtask 2 Purchase FVB mice, drugs and reagents; plan experiments.	1-2	100%
Subtask 3 Implant FVB mice with mouse ovarian cancer cells.	2-25	100%

Subtask 4 Treat mice with recombinant collagen II, rAAV-FLAG-Sox9, and dexamethasone. Assess therapeutic efficacy as in Aim 1, Task 4.	3-30	100%
Subtask 5 Analyze data using statistical methods; replicate experiments if necessary; prepare and submit manuscripts.	4-36	70%
Milestone Achieved Verified whether agents that induce terminal differentiation of activated cancer-associated fibroblasts are effective in attenuating tumor growth and increasing chemosensitivity.	36	70%

▪ **What was accomplished under these goals?**

1) major activities

Aim 1. Using multiple approaches to targeting CAFs in an immunocompetent mouse model of ovarian cancer that was developed in our laboratory, we failed to show any significant benefits of targeting CAFs. Meanwhile, other groups showed the efficacy of some of the CAF-targeting agents in mouse models of induced fibrosis. We realized that we needed to develop a more fibrotic model of ovarian cancer to demonstrate the efficacy of anti-fibrotic agents. We generated two new mouse models, both of which exhibit extensive fibrosis and rapid onset of ovarian carcinomatosis. Aim 2. We made further advances in characterizing the functional properties of COL11A1, which we previously identified as a molecular target that distinguishes CAFs from other fibroblasts. Aim 3. Contrary to our hypothesis that induction of terminal differentiation in CAFs may minimize cancer growth, we observed increased subcutaneous and intraperitoneal cancer growth in the presence of factors that induce bone/fat differentiation in CAFs, possibly because the same factors serve as growth factors for cancer cells.

2) specific objectives

Our objectives were to: 1) generate suitable mouse ovarian cancer models for testing the efficacy of anti-fibrotic agents in improving ovarian cancer chemosensitivity to cisplatin; 2) increase the specificity of targeting activated CAFs by targeting the CAF-specific protein COL11A1; and 3) identify a method to induce bone/cartilage differentiation of CAFs.

3) significant results or key outcomes, including major findings, developments, or conclusions

AIM 1. Improve therapeutic efficacy by targeting processes involved in CAF activation

CAFs are the most prominent component of the tumor stroma in advanced ovarian cancer. However, it is still not completely understood how the presence of CAFs specifically contribute to tumor progression and therapeutic resistance in ovarian cancer (1). Studies in other solid tumors have shown that CAFs can promote tumor growth, angiogenesis, invasion, and metastasis while at the same time suppressing antitumor immunity and conferring drug resistance and/or limiting access of chemotherapeutics, anti-angiogenic therapies, and immunotherapies. Experimental mouse models that exhibit extensive cancer fibrosis, such as the K-ras^{G12D}

mutation-driven autochthonous pancreatic cancer model and the xenograft 4T1 breast cancer model, have been crucial in proving that CAF-targeting therapeutic approaches can improve tumoral immune response, intratumoral drug delivery, and therapeutic efficacy (2-12). These studies confirmed the key role of CAFs in cancer progression and demonstrated their effectiveness as a therapeutic target. However, our attempts to diminish ovarian cancer growth with anti-fibrotic agents have not been successful (reported in annual progress reports), possibly due to the lack of extensive fibrosis and/or inflammatory reaction in our current ovarian cancer models. Thus, much of our effort during the past year focused on developing syngeneic mouse models of ovarian cancer that accurately model fibroblast activation observed in our previous analyses of human primary and metastatic ovarian cancers (Jia et al. *Scientific Reports* 2016; Jia et al., *Cancer Letters* 2016; Haro and Orsulic, *Frontiers in Cell and Developmental Biology* 2018).

In the first model, we used tight skin (TSK) mice in which fibroblasts are continuously activated due to the overexpression of fibrillin 1 (FBN1) (13, 14). The TSK mouse model has been used extensively to study fibrosis and ECM remodeling (15-18) but has not been used to study cancer progression. In our pilot experiment, compared to wild type (WT) littermates, TSK mice exhibited faster and more invasive ovarian cancer progression after subcutaneous (**Fig. 1A-B**) and intraperitoneal (**Fig. 1C**) injection of ovarian cancer cells, indicating that fibroblast activation may contribute to ovarian cancer progression in this model.

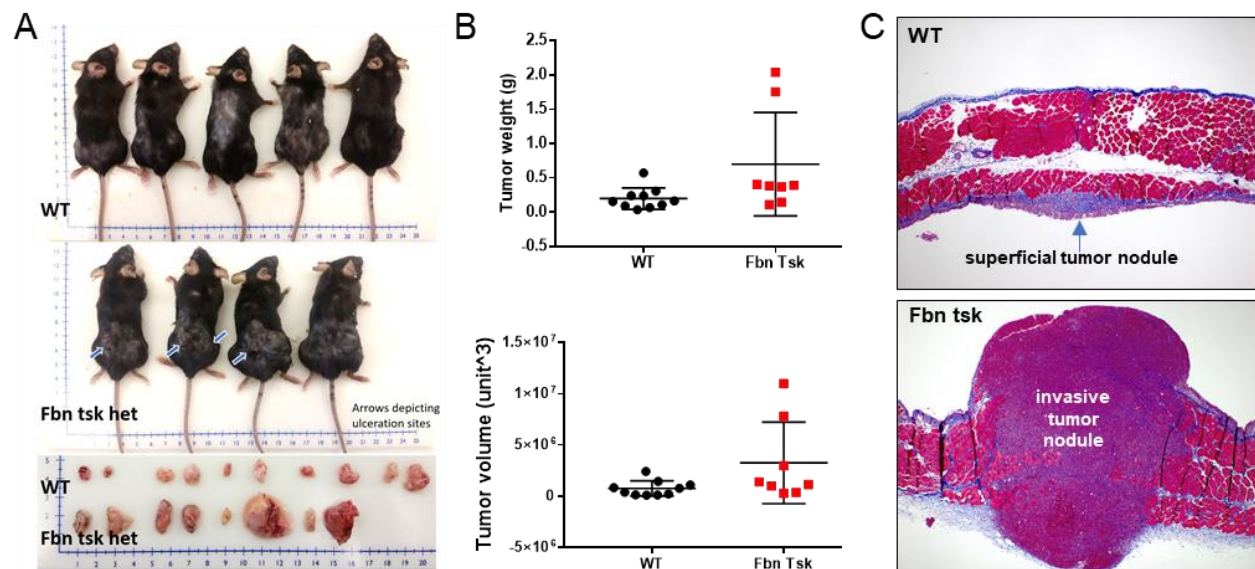


Fig. 1. A mouse model of ovarian cancer in the setting of endogenous CAF activation in the TSK mouse. A) Wild-type (WT) and TSK mice heterozygous for a gain-of-function FBN1 mutation (Fbn tsk het) were subcutaneously injected with syngeneic mouse ovarian cancer cells containing genetic alterations in p53, myc and H-ras (2×10^6 cells in each flank). The subcutaneous tumors were harvested after 18 days when tumors in the TSK mice started to ulcerate. **B)** Tumor weight and volume. **C)** Representative Masson's trichrome-stained sections of ovarian cancer nodules in the diaphragm of WT and TSK mice ($n=5$ /group) 14 days after intraperitoneal injection of 10^6 p53, myc and H-ras cells.

In the second model, we induced an inflammatory reaction and peritoneal fibrosis by intraperitoneal injection of immunocompetent FVB mice with 1 ml PBS (PBS mice) or 1 ml 0.05% NaOCl diluted in PBS (NaOCl mice) (**Fig. 2**). Mice were intraperitoneally injected with 10^6 syngeneic BR-luc mouse ovarian cancer cells 1 day, 3 days, and 5 days after treatment with PBS or NaOCl. Five PBS and 5 NaOCl mice were used for each timepoint. Longitudinal intravital luciferase imaging at 1, 2, 3, and 4 weeks after cancer cell injection showed a marked difference in luciferase signal intensity between PBS and NaOCl mice. In PBS mice, cancer cells were present at the injection site and the omentum, which is the preferred metastatic site for mouse and human ovarian cancer (**Fig. 2A** and data not shown). In contrast, NaOCl mice showed a widespread dissemination of cancer cells throughout the peritoneal cavity (**Fig. 2A** and data not shown), suggesting that the microenvironment in the NaOCl mice allows for better engraftment of cancer cells than in the PBS mice. Four to six weeks after cancer cell injection, mice were euthanized for pathologic analysis. PBS mice usually exhibited tumor nodules confined to the omentum (asterisk in **Fig. 2B**) and diaphragm (arrows in **Fig. 2C**) while all peritoneal surfaces in NaOCl mice were studded with cancer growths (**Fig. 2B** and **C**). It appears that the NaOCl-induced mesothelial injury created favorable conditions for cancer cell attachment and growth on all peritoneal surfaces, including organs rarely colonized by human and mouse ovarian cancer cells, such as the liver and the spleen (**Fig. 2B** and **C**).

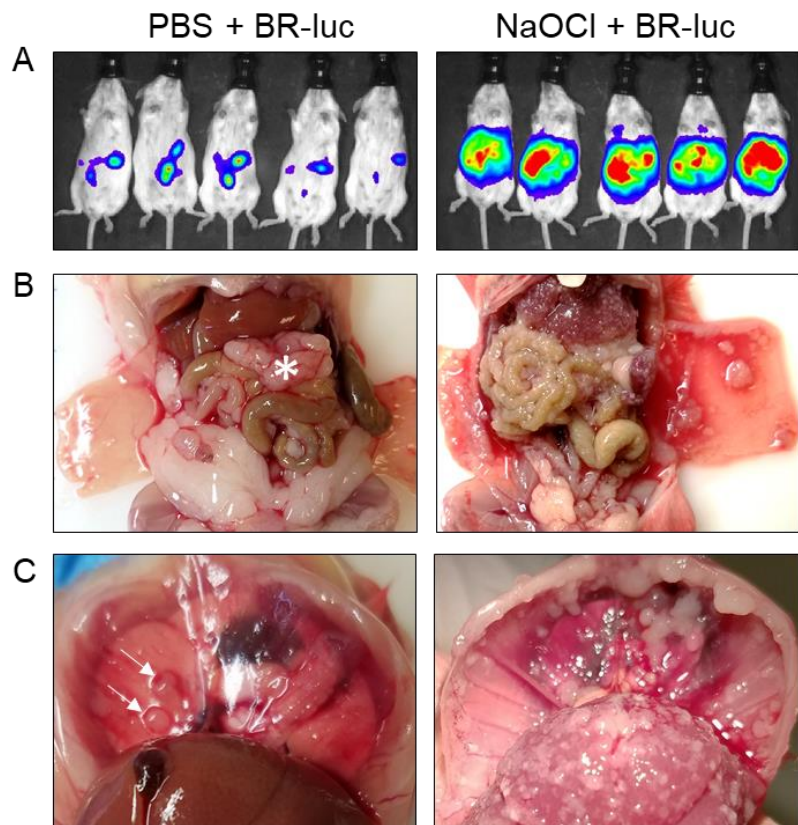


Fig. 2. A mouse model of enhanced ovarian cancer metastasis after induction of peritoneal inflammatory reaction and fibrosis with NaOCl. (A) Representative *in vivo* luciferase imaging of PBS mice and NaOCl mice 2 weeks after intraperitoneal injection of 10^6 BR-luc cells one day after treatment with PBS or NaOCl. In PBS mice, surviving cancer cells are present at the injection site (mechanical injury) and the omentum (preferred metastatic site for mouse and human ovarian cancer). In contrast, NaOCl mice show widespread dissemination of cancer cells throughout the peritoneal cavity. (B-C) Representative images of intraperitoneal tumor spread 6 weeks (PBS mice) or 4 weeks (NaOCl mice) after injection of ovarian cancer cells. In PBS mice, most of the cancer is localized to the omentum (asterisk) and occasional nodules on the diaphragm (arrows). In contrast, NaOCl mice exhibit tumor spread to the omentum, liver, spleen, intestines, peritoneal wall and diaphragm. n=5 mice/group in the pilot experiment and 10 mice/group in the repeated experiment.

To identify cell types involved in mesothelial wound repair on days 1 (expected influx of neutrophils), 3 (expected influx of macrophages) and 7 (expected recruitment of fibroblasts) after injury, we isolated the peritoneal walls from 5 PBS and 5 NaOCl mice for each of the 3 timepoints and conducted RNA sequencing. To date, we have thoroughly analyzed RNA sequencing results for day 3 after injury. Principle Component Analysis (PCA) demonstrated a clear separation of the PBS and NaOCl samples (**Fig. 3A**). Differential gene expression analysis identified 285 upregulated and 78 downregulated genes in the NaOCl mice ($\pm 1.5 \log_2$ fold change; $p < 0.001$) (data not shown). The most downregulated genes in the peritoneal walls of NaOCl mice were uroplakin 3B (*Upk3b*) and leucine rich repeat neuronal 4 (*Lrrn4*) (data not shown), both markers of mesothelial cells (19), which is consistent with injury-induced ablation and/or mesothelial-myofibroblast transition. Gene Ontology analysis of differentially expressed genes showed Immune Responses as the top canonical pathways. Ingenuity Pathway Analysis showed Fc γ Receptor-mediated Phagocytosis in Macrophages and Monocytes as the top canonical pathway. Overlay of the CIBERSORT leukocyte gene signature matrix LM22 (20, 21) identified 24 immune-related genes significantly upregulated in NaOCl mice (**Fig. 3B**). An overlay of these 24 immune-related genes with the ImmGen transcriptome (22, 23) revealed that the peritoneal wall cell infiltrates in NaOCl mice represent subsets of macrophages, monocytes, and neutrophils (**Fig. 3C**). Neutrophils are typically the first immune cells to be recruited to the

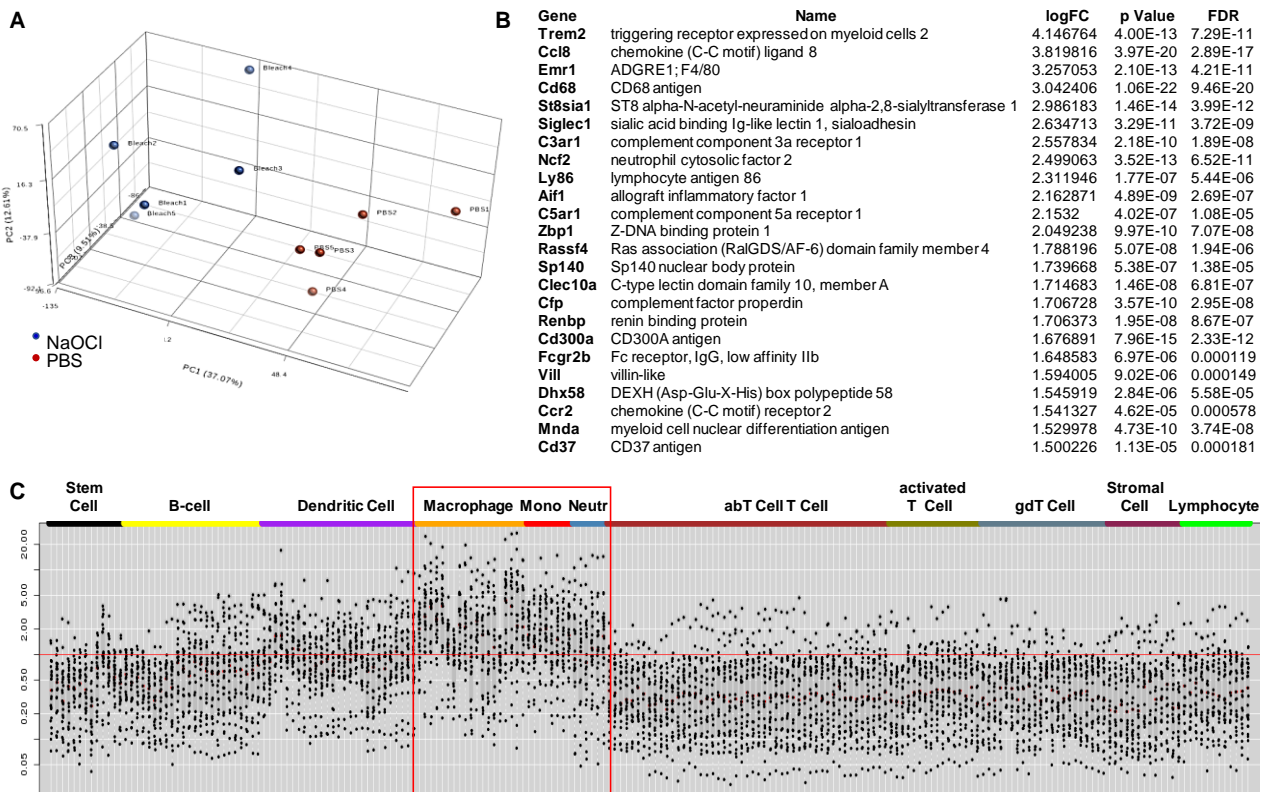


Fig. 3. Differential transcriptomes in peritoneal wall samples from PBS and NaOCl mice on day 3 after treatment. (A) Principle Component Analysis demonstrates a clear separation of the PBS and NaOCl samples. (B) Identification of 24 immune cell markers overrepresented in NaOCl mice that overlap with the CIBERSORT leukocyte gene signature matrix LM22. (C) Expression levels of the 24 genes in different immune and stromal cell subtypes in the ImmGen dataset reveal that these genes are primarily enriched in the transcriptomes of macrophages, monocytes, and neutrophils.

site of injury (24). Importantly, neutrophils were recently identified as the key facilitators of pre-metastatic niche formation in ovarian cancer (25). We confirmed the presence of neutrophils (and/or gMDSCs, which are phenotypically indistinguishable from neutrophils (26, 27)) by flow cytometry of peritoneal lavages and dissociated peritoneal walls at 4h and 24h after treatment with PBS or NaOCl. Increased frequencies of live neutrophils/gMDSCs in peritoneal lavages and walls were observed at both time points (**Fig. 4A-B**). Immunohistochemical staining of peritoneal wall sections with the neutrophil marker NGAL (neutrophil gelatinase-associated lipocalin) confirmed that neutrophils infiltrated blood vessels and submesothelial connective tissue as early as 4h after NaOCl treatment (**Fig. 4C**) and remained in these tissues 24h and 72h after treatment (data not shown).

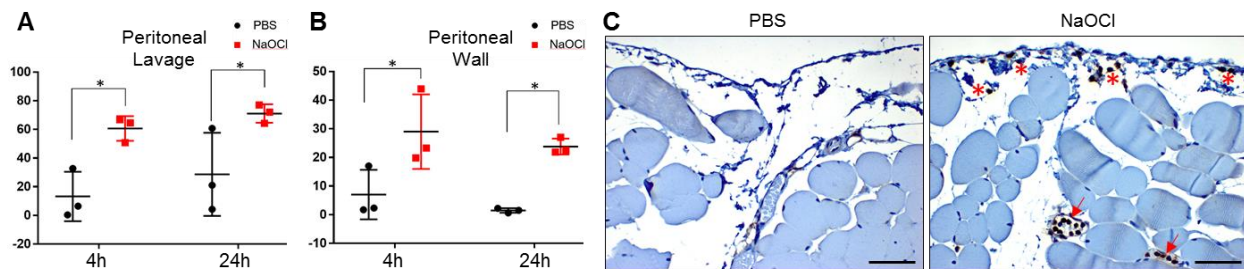


Fig. 4. Early influx of neutrophils in the peritoneum of NaOCl mice. (A-B) Peritoneal lavage (**A**) and dissociated body wall (**B**) neutrophils or granulocytic MDSC (frequency of live cells) 4 hours and 24 hours after intraperitoneal injection of 1 ml PBS or 1 ml 0.05% NaOCl diluted in PBS (n=3 mice per group). *Immune cell marker panel: CD3, CD4, CD8, CD11b, CD11c, CD19, CD45, F4/80, Ly6G, live/dead cells.* * $p < 0.05$. (**C**) Representative images of peritoneal walls (n=5 mice per group) fixed 4 hours after intraperitoneal injection of PBS or NaOCl. Neutrophil gelatinase-associated lipocalin (NGAL) staining shows the influx of neutrophils in the blood vessels (arrows) and submesothelial connective tissue (asterisks) in the peritoneal walls of NaOCl mice. Bar size: 50 μ m.

Upregulation of general macrophage markers F4/80 and CD68 (**Fig. 3B**) suggested that the peritoneal walls of NaOCl mice were infiltrated with macrophages on day 3 after treatment with PBS or NaOCl. Since macrophages comprise multiple subtypes that can be pro- and anti-inflammatory and pro- or anti-tumorigenic (28-31), we screened genes upregulated in NaOCl mice for markers that have been previously associated with specific subsets of macrophages. Among the top upregulated genes were CCL8 and SIGLEC1 (CD169) (**Fig. 3B**). SIGLEC1⁺ macrophages were recently identified in a mouse model of dextran sodium sulfate (DSS)-induced colitis as a specific subpopulation of resident colonic macrophages that secrete the CCL8 chemokine to recruit inflammatory monocytes to the DSS-induced wound (32). Importantly, SIGLEC1⁺ macrophages were the only subpopulation of macrophages capable of secreting CCL8 and specific depletion of SIGLEC1⁺ macrophages or neutralization of CCL8 ameliorated the DSS-induced colitis (32). Relevant to human cancer, SIGLEC1⁺ macrophages and CCL8 were recently associated with aggressive subtypes of breast cancers and CCL8 was shown to recruit monocytes and increase breast cancer cell motility (33). Thus, in our NaOCl model of peritoneal wound repair, we may have identified a specific subset of macrophages

(SIGLEC1⁺ CCL8-secreting) that regulate mesothelial wound repair and the induction of carcinomatosis.

Among the top 20 genes upregulated in the NaOCl peritoneal walls on day 3 after treatment were 4 genes (CCL8, S100A8, SAA3, and LGALS3) that have been previously implicated in fibrosis and pre-metastatic niche formation. CCL8 was shown to trigger the recruitment of pro-inflammatory monocytes (32), fibroblasts (34), and cancer cells (35). S100A8 and SAA3 were identified as components of a lung pre-metastatic niche that potentiate inflammation-like state and facilitate migration of primary tumor cells to the lung (36). LGALS3 was shown to activate fibroblasts to a profibrotic phenotype in rodent models of ischemia-induced renal fibrosis (37), bleomycin-induced lung fibrosis (38), and carbon tetrachloride (CCL₄)-induced liver fibrosis (39). Thus, our model of mesothelial injury is useful for the identification of known (and unknown) genes associated with pre-metastatic niche formation.

We used the 24 immune cell-related genes that were upregulated in the peritoneal walls of NaOCl mice on day 3 after treatment (**Fig. 3B**) to identify other normal or diseased conditions in which this gene set is upregulated (mouse and human SEEK platforms). We have shown that the 24 immune cell-related gene set is upregulated in various types of acute injuries (superficial cut, UV exposure, DSS treatment, bleomycin treatment) in various human and mouse tissues (skin, intestinal mucosa, lung) (**Fig. 5**), suggesting that our mouse model of NaOCl-induced mesothelial injury exhibits a prototypical early wound healing immune response. Because of the largely universal response of epithelial and mesothelial tissues to different types of injury (40), we conclude that our mouse model of chemical injury to the mesothelium is representative of mesothelial injury induced by surgery and cytotoxic chemotherapy in patients undergoing cytoreductive surgery and/or HIPEC.

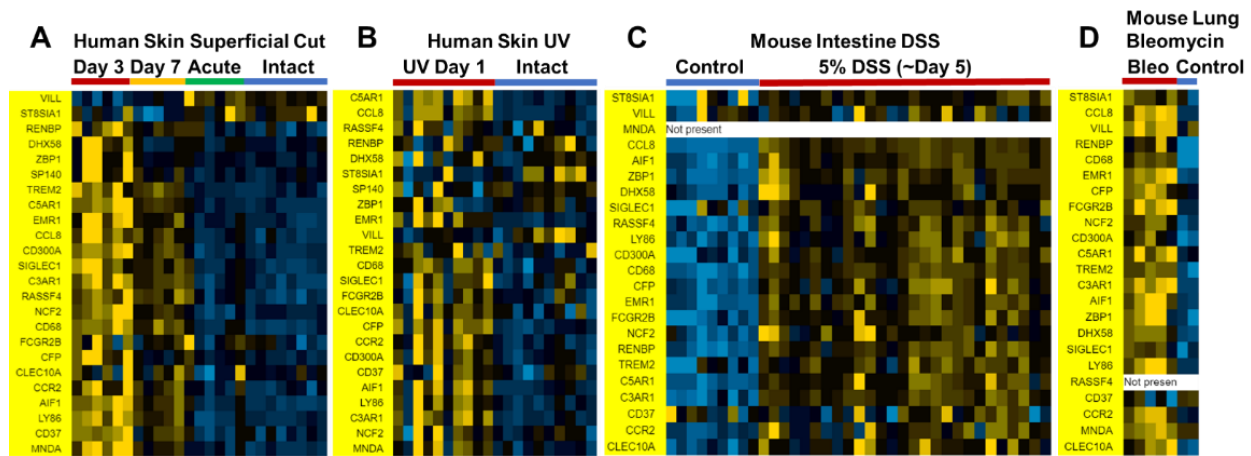


Fig. 5. The set of 24 immune cell-related genes found to be upregulated in peritoneal walls on day 3 after NaOCl treatment is also upregulated in various types of acute injury in diverse human and mouse tissues (A) GSE28914: human skin superficial cut injury. (B) GSE41078: human skin narrowband UVB-induced injury. (C) GSE31906: mouse 5% DSS-induced intestinal mucosa injury. (D) GSE2640: mouse bleomycin-induced lung injury.

In summary, our attempts to test anti-fibrotic agents showed largely negative results (described in annual reports). One confounding factor in these pre-clinical tests was the modest presence of fibrosis in the existing ovarian cancer models. Therefore, we generated two models with endogenous or induced fibrosis. These models will be a valuable resource for studying the role of fibroblasts in ovarian cancer initiation and progression.

AIM 2. Increase specificity of targeting activated CAFs

Our analyses identified COL11A1 as the most specific target for activated CAFs. We hypothesized that targeting COL11A1 function will disable activated CAFs with a minimal effect on normal fibroblasts. The results of *in vitro* and *in vivo* experiments as well as correlative analyses of human samples to test our hypothesis have been provided in our publications (Jia et al., *Cancer Letters* 2016; Haro and Orsulic, *Frontiers in Cell and Developmental Biology* 2018; Ye et al., submitted). We will briefly summarize the main conclusions from the unpublished experiments described in the Annual Progress Reports and focus on experiments conducted in the last year.

Our *in vitro* experiments with cancer-associated fibroblasts (CAFs) and normal fibroblasts (NAFs) showed that only CAFs express COL11A1. However, expression of COL11A1 could be induced and maintained in both CAFs and NAFs by direct co-culture with various ovarian cancer cell lines. *In vivo* subcutaneous co-injection of ovarian cancer cells with either CAFs or NAFs showed that both CAFs and NAFs were able to support the growth of ovarian cancer cells to the same extent, possibly because both types of fibroblasts were activated by the co-injected cancer cells. The effects of neutralizing endogenous COL11A1 with a COL11A1-specific antibody were tested *in vitro* and *in vivo*. The ability of the COL11A1 antibody to suppress CAF function was tested in a collagen contraction assay, where we showed that CAFs contract collagen more effectively than NAFs and that this contraction ability is abrogated in the presence of the COL11A1 antibody (as well as siCOL11A1). However, treatment of tumor-bearing mice with the COL11A1 antibody did not have an effect on tumor growth.

The therapeutic use of antibodies is primarily restricted to extracellular or membrane-bound proteins due to inefficient intracellular delivery of antibodies by endocytosis. To overcome this obstacle, we used biocompatible hyaluronic acid (HA) or polysialic acid (PSA) nanocapsules (NC), capable of releasing small cytostatic drugs into cancer cells (3,4), as vehicles for intracellular delivery of COL11A1 antibodies into CAFs. To test the NCs potential therapeutic utility, we first evaluated their cytotoxicity and intracellular internalization in 781T CAFs. HA-NCs and PSA-NCs showed similar low cytotoxicity levels after 24 hours of treatment (**Fig. 6A**). Next, to assess the intracellular delivery of the COL11A1 antibody, 781T CAFs were treated at different time points with 1.0 mg/mL PSA- or HA-NCs loaded with FITC-labeled antibodies. With a single dose of 1mg/mL of FITC-COL11A1 antibody-NCs, HA-NCs were clearly internalized into the cytoplasm while PSA-NCs were mostly attached to the membrane (**Fig. 6B**). Thus, HA-NCs are effective in delivering COL11A1 antibody into CAFs and are good candidates for *in vivo* testing.

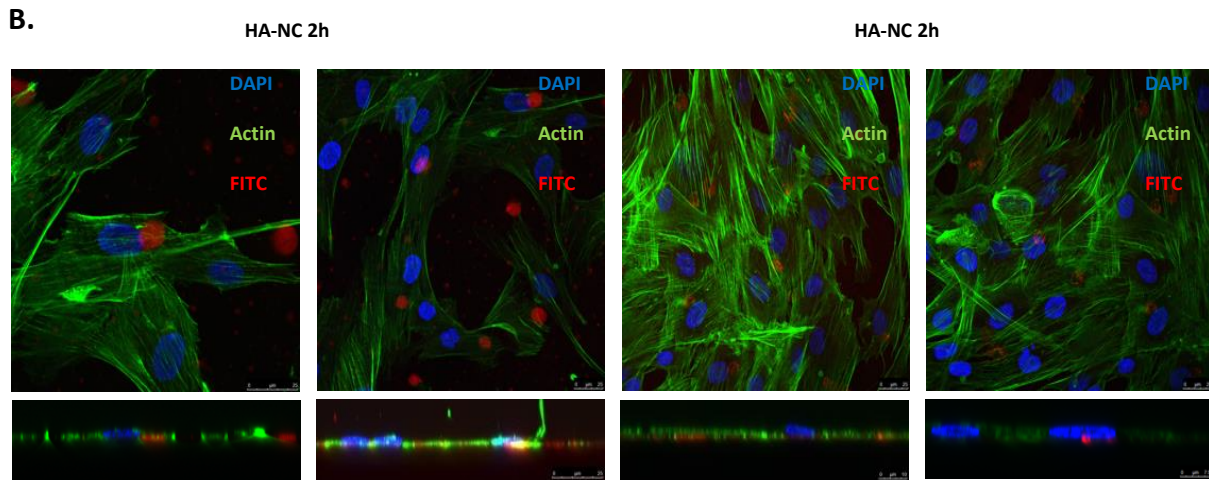
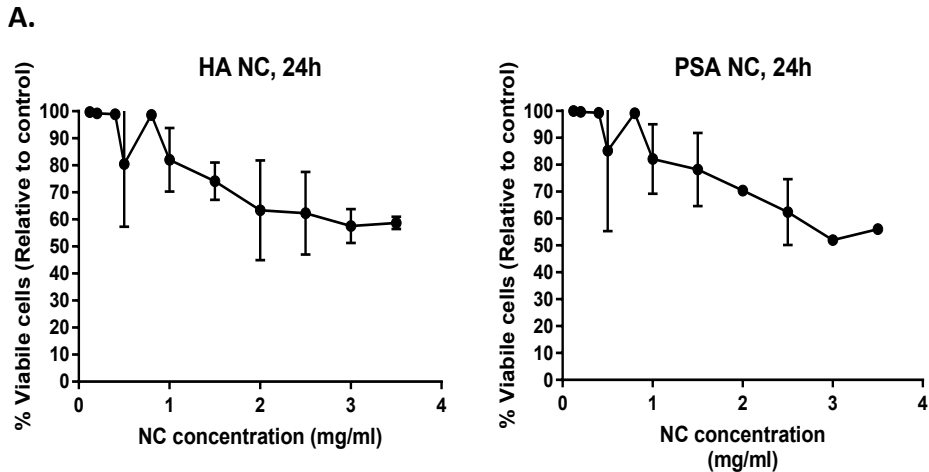


Fig 6. Treatment of CAFs with NC. **A)** 781T CAFs were cultured with α MEM+10% FCS for 96 hours followed by treatment with 0.12-1 mg/mL of HA-NCs/PSA-NCs for 24 hours. Cell viability was measured using the CCK-8 kit. Error bars represent standard deviation of biological repeats (2-4 replicate wells per repeat). HA, Hyaluronic acid. PSA, Polysialic acid. NC, Nanocapsules. **B)** Confocal microscopy images of 781T CAFs treated for 2 hours with 1 mg/mL of NC. Representative images show intracellular localization of labeled HA-NCs (left panel) and the largely extracellular location of labeled PSA-NCs (right panel). For each field, a cross-section is presented below. Red-NC, Blue-nuclei, Green-Actin.

AIM 3. Induce activated CAF-to-cartilage differentiation.

Since CAF activation is considered a key driver of cancer progression, we hypothesized that terminal differentiation of activated CAFs into cartilage would suppress cancer progression. We have analyzed our data from the mouse tissues that were injected with differentiation agents. Contrary to our hypothesis, Masson's trichrome staining analyses did not show any difference in cartilage/bone formation in the control or experimental groups. A major drawback of our experiments was the low level of fibroblast recruitment to the tumor site. It may be worth re-

visiting this hypothesis using our improved mouse models of cancer progression accompanied by fibrosis.

References:

1. Naora H. Heterotypic cellular interactions in the ovarian tumor microenvironment: biological significance and therapeutic implications. *Front Oncol.* 2014;4:18.
2. Loeffler M, Kruger JA, Niethammer AG, and Reisfeld RA. Targeting tumor-associated fibroblasts improves cancer chemotherapy by increasing intratumoral drug uptake. *J Clin Invest.* 2006;116(7):1955-62.
3. Provenzano PP, Cuevas C, Chang AE, Goel VK, Von Hoff DD, and Hingorani SR. Enzymatic targeting of the stroma ablates physical barriers to treatment of pancreatic ductal adenocarcinoma. *Cancer cell.* 2012;21(3):418-29.
4. Liu J, Liao S, Diop-Frimpong B, Chen W, Goel S, Naxerova K, et al. TGF-beta blockade improves the distribution and efficacy of therapeutics in breast carcinoma by normalizing the tumor stroma. *Proc Natl Acad Sci U S A.* 2012;109(41):16618-23.
5. Liao D, Luo Y, Markowitz D, Xiang R, and Reisfeld RA. Cancer associated fibroblasts promote tumor growth and metastasis by modulating the tumor immune microenvironment in a 4T1 murine breast cancer model. *PloS one.* 2009;4(11):e7965.
6. LeBeau AM, Brennen WN, Aggarwal S, and Denmeade SR. Targeting the cancer stroma with a fibroblast activation protein-activated promelittin protoxin. *Mol Cancer Ther.* 2009;8(5):1378-86.
7. Feig C, Jones JO, Kraman M, Wells RJ, Deonarine A, Chan DS, et al. Targeting CXCL12 from FAP-expressing cancer-associated fibroblasts synergizes with anti-PD-L1 immunotherapy in pancreatic cancer. *Proc Natl Acad Sci U S A.* 2013;110(50):20212-7.
8. Jacobetz MA, Chan DS, Neesse A, Bapiro TE, Cook N, Frese KK, et al. Hyaluronan impairs vascular function and drug delivery in a mouse model of pancreatic cancer. *Gut.* 2013;62(1):112-20.
9. Kraman M, Bambrough PJ, Arnold JN, Roberts EW, Magiera L, Jones JO, et al. Suppression of antitumor immunity by stromal cells expressing fibroblast activation protein-alpha. *Science.* 2010;330(6005):827-30.
10. Wang LC, Lo A, Scholler J, Sun J, Majumdar RS, Kapoor V, et al. Targeting fibroblast activation protein in tumor stroma with chimeric antigen receptor T cells can inhibit tumor growth and augment host immunity without severe toxicity. *Cancer Immunol Res.* 2014;2(2):154-66.
11. Lo A, Wang LC, Scholler J, Monslow J, Avery D, Newick K, et al. Tumor-Promoting Desmoplasia Is Disrupted by Depleting FAP-Expressing Stromal Cells. *Cancer research.* 2015;75(14):2800-10.
12. Arnold JN, Magiera L, Kraman M, and Fearon DT. Tumoral immune suppression by macrophages expressing fibroblast activation protein-alpha and heme oxygenase-1. *Cancer Immunol Res.* 2014;2(2):121-6.
13. Kasturi KN, Shibata S, Muryoi T, and Bona CA. Tight-skin mouse an experimental model for scleroderma. *International reviews of immunology.* 1994;11(3):253-71.
14. Kielty CM, Raghunath M, Siracusa LD, Sherratt MJ, Peters R, Shuttleworth CA, et al. The Tight skin mouse: demonstration of mutant fibrillin-1 production and assembly into abnormal microfibrils. *The Journal of cell biology.* 1998;140(5):1159-66.

15. Gayraud B, Keene DR, Sakai LY, and Ramirez F. New insights into the assembly of extracellular microfibrils from the analysis of the fibrillin 1 mutation in the tight skin mouse. *The Journal of cell biology*. 2000;150(3):667-80.
16. Ito S, Bartolak-Suki E, Shipley JM, Parameswaran H, Majumdar A, and Suki B. Early emphysema in the tight skin and pallid mice: roles of microfibril-associated glycoproteins, collagen, and mechanical forces. *American journal of respiratory cell and molecular biology*. 2006;34(6):688-94.
17. Lemaire R, Farina G, Kissin E, Shipley JM, Bona C, Korn JH, et al. Mutant fibrillin 1 from tight skin mice increases extracellular matrix incorporation of microfibril-associated glycoprotein 2 and type I collagen. *Arthritis and rheumatism*. 2004;50(3):915-26.
18. Pablos JL, Everett ET, Harley R, LeRoy EC, and Norris JS. Transforming growth factor-beta 1 and collagen gene expression during postnatal skin development and fibrosis in the tight-skin mouse. *Laboratory investigation; a journal of technical methods and pathology*. 1995;72(6):670-8.
19. Kanamori-Katayama M, Kaiho A, Ishizu Y, Okamura-Oho Y, Hino O, Abe M, et al. LRRN4 and UPK3B are markers of primary mesothelial cells. *PloS one*. 2011;6(10):e25391.
20. Gentles AJ, Newman AM, Liu CL, Bratman SV, Feng W, Kim D, et al. The prognostic landscape of genes and infiltrating immune cells across human cancers. *Nature medicine*. 2015;21(8):938-45.
21. Newman AM, Liu CL, Green MR, Gentles AJ, Feng W, Xu Y, et al. Robust enumeration of cell subsets from tissue expression profiles. *Nature methods*. 2015;12(5):453-7.
22. Heng TS, and Painter MW. The Immunological Genome Project: networks of gene expression in immune cells. *Nature immunology*. 2008;9(10):1091-4.
23. Shay T, and Kang J. Immunological Genome Project and systems immunology. *Trends Immunol*. 2013;34(12):602-9.
24. Ng LG, Ostuni R, and Hidalgo A. Heterogeneity of neutrophils. *Nature reviews Immunology*. 2019;19(4):255-65.
25. Lee W, Ko SY, Mohamed MS, Kenny HA, Lengyel E, and Naora H. Neutrophils facilitate ovarian cancer premetastatic niche formation in the omentum. *The Journal of experimental medicine*. 2019;216(1):176-94.
26. Brandau S, Moses K, and Lang S. The kinship of neutrophils and granulocytic myeloid-derived suppressor cells in cancer: cousins, siblings or twins? *Seminars in cancer biology*. 2013;23(3):171-82.
27. Moses K, and Brandau S. Human neutrophils: Their role in cancer and relation to myeloid-derived suppressor cells. *Seminars in immunology*. 2016;28(2):187-96.
28. Doak GR, Schwertfeger KL, and Wood DK. Distant Relations: Macrophage Functions in the Metastatic Niche. *Trends in cancer*. 2018;4(6):445-59.
29. Nielsen SR, and Schmid MC. Macrophages as Key Drivers of Cancer Progression and Metastasis. *Mediators of inflammation*. 2017;2017:9624760.
30. Kim J, and Bae JS. Tumor-Associated Macrophages and Neutrophils in Tumor Microenvironment. *Mediators of inflammation*. 2016;2016:6058147.
31. Fukuda K, Kobayashi A, and Watabe K. The role of tumor-associated macrophage in tumor progression. *Front Biosci (Schol Ed)*. 2012;4:787-98.

32. Asano K, Takahashi N, Ushiki M, Monya M, Aihara F, Kuboki E, et al. Intestinal CD169(+) macrophages initiate mucosal inflammation by secreting CCL8 that recruits inflammatory monocytes. *Nature communications*. 2015;6:7802.
33. Cassetta L, Frangkogianni S, Sims AH, Swierczak A, Forrester LM, Zhang H, et al. Human Tumor-Associated Macrophage and Monocyte Transcriptional Landscapes Reveal Cancer-Specific Reprogramming, Biomarkers, and Therapeutic Targets. *Cancer cell*. 2019;35(4):588-602.e10.
34. Lee JU, Cheong HS, Shim EY, Bae DJ, Chang HS, Uh ST, et al. Gene profile of fibroblasts identify relation of CCL8 with idiopathic pulmonary fibrosis. *Respiratory research*. 2017;18(1):3.
35. Farmaki E, Chatzistamou I, Kaza V, and Kiaris H. A CCL8 gradient drives breast cancer cell dissemination. *Oncogene*. 2016;35(49):6309-18.
36. Hiratsuka S, Watanabe A, Sakurai Y, Akashi-Takamura S, Ishibashi S, Miyake K, et al. The S100A8-serum amyloid A3-TLR4 paracrine cascade establishes a pre-metastatic phase. *Nature cell biology*. 2008;10(11):1349-55.
37. Henderson NC, Mackinnon AC, Farnworth SL, Kipari T, Haslett C, Iredale JP, et al. Galectin-3 expression and secretion links macrophages to the promotion of renal fibrosis. *The American journal of pathology*. 2008;172(2):288-98.
38. Mackinnon AC, Gibbons MA, Farnworth SL, Leffler H, Nilsson UJ, Delaine T, et al. Regulation of transforming growth factor-beta1-driven lung fibrosis by galectin-3. *American journal of respiratory and critical care medicine*. 2012;185(5):537-46.
39. Henderson NC, Mackinnon AC, Farnworth SL, Poirier F, Russo FP, Iredale JP, et al. Galectin-3 regulates myofibroblast activation and hepatic fibrosis. *Proc Natl Acad Sci U S A*. 2006;103(13):5060-5.
40. Chen L, Arbieva ZH, Guo S, Marucha PT, Mustoe TA, and DiPietro LA. Positional differences in the wound transcriptome of skin and oral mucosa. *BMC genomics*. 2010;11:471.

4) other achievements

Nothing to report.

a. What opportunities for training and professional development has the project provided?

Nothing to report.

b. How were the results disseminated to communities of interest?

We have published our results as open access articles in journals *Cancer Letters*, *Scientific Reports* and *Frontiers in Cell and Developmental Biology*.

c. What do you plan to do during the next reporting period to accomplish the goals?

Nothing to report.

3. IMPACT:

a. What was the impact on the development of the principal discipline(s) of the project?

Nothing to report.

b. What was the impact on other disciplines?

Nothing to report.

c. What was the impact on technology transfer?

Nothing to report.

d. What was the impact on society beyond science and technology?

Nothing to report.

4. CHANGES/PROBLEMS:

a. Changes in approach and reasons for change.

Using three different approaches to targeting CAFs in an immunocompetent mouse model of ovarian cancer that was developed in our laboratory, we failed to show any significant benefits of targeting CAFs. We realized that we needed to develop a more fibrotic model of ovarian cancer to demonstrate the efficacy of anti-fibrotic agents. Thus, we generated two new mouse models, both of which exhibit extensive fibrosis and rapid onset of ovarian carcinomatosis. We believe that these new mouse models will transform future studies of the roles of fibrosis in ovarian cancer initiation and progression.

b. Actual or anticipated problems or delays and actions or plans to resolve them.

Nothing to report.

c. Changes that had a significant impact on expenditures. No

d. Significant changes in use or care of human subjects, vertebrate animals, biohazards, and/or select agents. No

e. Significant changes in use or care of human subjects. No

f. Significant changes in use or care of vertebrate animals. No

g. Significant changes in use of biohazards and/or select agents. No

5. PRODUCTS:

Nothing to report.

a. Publications, conference papers, and presentations

i. Journal publications.

Jia D, Liu Z, Deng N, Tan TZ, Huang R Y-J, Taylor-Harding B, Cheon DJ, Lawrenson K, Wiedemeyer WR, Walts AE, Karlan BY, **Orsulic S.** A COL11A1-correlated pan-cancer gene signature of activated fibroblasts for the prioritization of therapeutic targets. *Cancer Letters* 2016; 382:203-214. (Published, acknowledged grant funding)

Jia D, Kamata Y, Katsumata M, **Orsulic S.** Inflammation is a key contributor to ovarian cancer cell seeding. *Scientific Reports*, 2018, 8:12394. (Published, acknowledged grant funding)

Haro M and **Orsulic S.** A Paradoxical Correlation of Cancer-Associated Fibroblasts with Survival Outcomes in B-Cell Lymphomas and Carcinomas. *Frontiers in Cell and Developmental Biology*, 2018. (Published, acknowledged grant funding)

Hu Y, Taylor-Harding B, Haro, M, Raz Y, Recouvreux M, Taylan E, Walts AE, Karlan BY, **Orsulic S.** Are epithelial ovarian cancers of the mesenchymal subtype actually intraperitoneal metastases to the ovary? (submitted, acknowledged grant funding)

ii. Books or other non-periodical, one-time publications. N/A

iii. Other publications, conference papers, and presentations.

Oral presentation (acknowledged grant funding):

Sandra Orsulic: Tumor Microenvironment. Molecular and Cellular Biology Wednesday Seminar Series, Baylor College of Medicine. Houston, TX. January 6, 2016.

Sandra Orsulic: Signatures of Stromal Activation in Cancer. Molecular Pathology Seminar Series. Johns Hopkins University School of Medicine. Baltimore, MD. November 16, 2016.

Sandra Orsulic. Tumor Microenvironment. Cancer Biology Seminar, Mayo Clinic, Jacksonville, FL. February 23, 2018.

b. Website(s) or other Internet site(s). N/A

c. Technologies or techniques. N/A

d. Inventions, patent applications, and/or licenses. N/A

e. Other Products. N/A

6. PARTICIPANTS & OTHER COLLABORATING ORGANIZATIONS

a. What individuals have worked on the project?

Name:	Sandra Orsulic
Project Role:	PI
Nearest person month worked:	2.00
Contribution to Project:	Dr. Orsulic oversaw projects for all three specific aims, including experimental design, execution, and data analysis and interpretation. She wrote the manuscripts (Jia et al, Scientific Reports, 2018; Haro and Orsulic, Frontiers in Cell and Developmental Biology, 2018) and prepared presentations as well as the progress report.

Name:	Beth Karlan
Project Role:	Collaborator
Nearest person month worked:	0.12
Contribution to Project:	Dr. Karlan advised on the translational aspects of the proposal and participated in experimental design.

Name:	Dongyu Jia, PhD
Project Role:	Postdoctoral Fellow
Nearest person month worked:	0.60
Contribution to Project:	Dr. Jia conducted all experiments that involved testing different combinations of treatments in the immunocompetent mouse model of ovarian cancer and assisted in data acquisition, analysis, and interpretation as well as in the writing of the published manuscripts (Jia et al., Cancer Letters 2016; Jia et al., Scientific Reports 2018).

Name:	Marcela Haro, PhD
Project Role:	Postdoctoral Fellow
Nearest person month worked:	4.50
Contribution to Project:	Dr. Haro conducted all experiments that involved testing different combinations of treatments in the immunocompetent mouse model of ovarian cancer and assisted in data acquisition and analysis. She assisted in the writing of the manuscript (Haro and Orsulic, Frontiers in Cell and Developmental Biology 2018).

Name:	Sandra Billet, PhD
Project Role:	Postdoctoral Fellow
Nearest person month worked:	3.00
Contribution to Project:	Dr. Billet conducted all experiments that involved testing different combinations of treatments in the immunocompetent mouse model of ovarian cancer and assisted in data acquisition and analysis.

Name:	Barbie Taylor-Harding, PhD
Project Role:	Research Associate
Nearest person month worked:	3.00
Contribution to Project:	Dr. Taylor-Harding conducted all experiments that involved testing different combinations of treatments in the immunocompetent mouse model of ovarian cancer and assisted in data acquisition and analysis.

- b. **Has there been a change in the active other support of the PD/PI(s) or senior/key personnel since the last reporting period?** No
- c. **What other organizations were involved as partners?** None

7. SPECIAL REPORTING REQUIREMENTS

- a. **COLLABORATIVE AWARDS:** N/A
- b. **QUAD CHARTS:** N/A

8. APPENDICES:

Reprints and preprints of publications associated with the grant funding:

Jia D, Liu Z, Deng N, Tan TZ, Huang R Y-J, Taylor-Harding B, Cheon DJ, Lawrenson K, Wiedemeyer WR, Walts AE, Karlan BY, **Orsulic S.** A COL11A1-correlated pan-cancer gene signature of activated fibroblasts for the prioritization of therapeutic targets. *Cancer Letters* 2016; 382:203-214.

Jia D, Kamata Y, Katsumata M, **Orsulic S.** Inflammation is a key contributor to ovarian cancer cell seeding. *Scientific Reports*, 2018, 8:12394.

Haro M and **Orsulic S.** A Paradoxical Correlation of Cancer-Associated Fibroblasts with Survival Outcomes in B-Cell Lymphomas and Carcinomas. *Frontiers in Cell and Developmental Biology*, 2018.

Hu Y, Taylor-Harding B, Haro, M, Raz Y, Recouvreux M, Taylan E, Walts AE, Karlan BY, **Orsulic S.** Are epithelial ovarian cancers of the mesenchymal subtype actually intraperitoneal metastases to the ovary? submitted



Original Articles

A COL11A1-correlated pan-cancer gene signature of activated fibroblasts for the prioritization of therapeutic targets

Dongyu Jia ^a, Zhenqiu Liu ^b, Nan Deng ^b, Tuan Zea Tan ^c, Ruby Yun-Ju Huang ^c, Barbie Taylor-Harding ^a, Dong-Joo Cheon ^d, Kate Lawrenson ^a, Wolf R. Wiedemeyer ^a, Ann E. Walts ^e, Beth Y. Karlan ^{a,f}, Sandra Orsulic ^{a,f,*}



^a Women's Cancer Program, Samuel Oschin Comprehensive Cancer Institute, Cedars-Sinai Medical Center, Los Angeles, CA, USA

^b Biostatistics and Bioinformatics Research Center, Cedars-Sinai Medical Center, Los Angeles, CA, USA

^c Cancer Science Institute of Singapore, Center for Translational Medicine, National University of Singapore, Singapore

^d Center for Cell Biology and Cancer Research, Albany Medical College, Albany, NY, USA

^e Department of Pathology and Laboratory Medicine, Cedars-Sinai Medical Center, Los Angeles, CA, USA

^f Department of Obstetrics and Gynecology, David Geffen School of Medicine, University of California at Los Angeles, Los Angeles, CA, USA

ARTICLE INFO

Article history:

Received 10 July 2016

Received in revised form 30 August 2016

Accepted 1 September 2016

Keywords:

Cancer-associated fibroblasts

Myofibroblasts

Pan-cancer

Therapeutic targets

Tumor microenvironment

ABSTRACT

Although cancer-associated fibroblasts (CAFs) are viewed as a promising therapeutic target, the design of rational therapy has been hampered by two key obstacles. First, attempts to ablate CAFs have resulted in significant toxicity because currently used biomarkers cannot effectively distinguish activated CAFs from non-cancer associated fibroblasts and mesenchymal progenitor cells. Second, it is unclear whether CAFs in different organs have different molecular and functional properties that necessitate organ-specific therapeutic designs. Our analyses uncovered COL11A1 as a highly specific biomarker of activated CAFs. Using COL11A1 as a 'seed', we identified co-expressed genes in 13 types of primary carcinoma in The Cancer Genome Atlas. We demonstrated that a molecular signature of activated CAFs is conserved in epithelial cancers regardless of organ site and transforming events within cancer cells, suggesting that targeting fibroblast activation should be effective in multiple cancers. We prioritized several potential pan-cancer therapeutic targets that are likely to have high specificity for activated CAFs and minimal toxicity in normal tissues.

© 2016 The Author(s). Published by Elsevier Ireland Ltd. This is an open access article under the CC BY-NC-ND license (<http://creativecommons.org/licenses/by-nc-nd/4.0/>).

Introduction

Under normal physiological conditions, collagen-rich fibroblasts maintain tissue architecture and serve as a barrier to epithelial cell migration. However, cancer cells have the ability to convert the surrounding fibroblasts into activated CAFs, which secrete specific collagens, growth factors, and enzymes that promote cancer growth, angiogenesis, invasion, and metastasis [1–3]. At the same time, these CAFs suppress anticancer immunity, confer drug resistance and/or limit the access of chemotherapies, anti-angiogenic therapies, and immunotherapies [1–3]. Although the exact mecha-

nisms by which activated CAFs contribute to such diverse aspects of cancer progression are unclear, it is thought that fibroblasts together with increased collagen deposition and altered extracellular matrix (ECM) remodeling serve as a rich depot of cancer-promoting growth factors, cytokines, and chemokines [1,2]. Additionally, altered levels of enzymes responsible for collagen cross-link formation, such as lysyl oxidase (LOX) [4], increase tissue stiffness and modify mechanotransduction resulting in the reorganization of loose connective tissue into tense linear tracks of fibers that serve as highways to promote chemotaxis of cancer cells [5,6].

Recognizing the crucial role of CAFs in most aspects of cancer progression, it has been proposed that rational anticancer therapy design should not only target the cancer cells but also the CAFs [7,8]. Unlike cancer cells, CAFs are genetically stable [9], which reduce the risk of therapy-induced clonal selection, resistance, and cancer recurrence. Furthermore, targeting CAFs could potentially affect multiple biochemical pathways to prevent cancer progression and recurrence. CAF-targeting therapeutic approaches in different experimental mouse cancer models have been shown to improve

Abbreviations: α SMA, α -smooth muscle actin; CAFs, cancer-associated fibroblasts; CSPG4, chondroitin sulfate proteoglycan 4; ECM, extracellular matrix; LOX, lysyl oxidase; EMT, epithelial–mesenchymal transition; FAP, fibroblast activation protein; PALLD, palladin; PDGFR α , platelet-derived growth factor receptor α ; PDPN, podoplanin; TGF β , transforming growth factor β ; TNC, tenascin-C; PRECOG, Prediction of Clinical Outcomes from Genomic Profiles.

* Corresponding author. Fax: +1 310 423 9537.

E-mail address: Sandra.Orsulic@cshs.org (S. Orsulic).

<http://dx.doi.org/10.1016/j.canlet.2016.09.001>

0304-3835/© 2016 The Author(s). Published by Elsevier Ireland Ltd. This is an open access article under the CC BY-NC-ND license (<http://creativecommons.org/licenses/by-nc-nd/4.0/>).

tumoral immune response, intratumoral drug delivery, and therapeutic efficacy [10–15]. These studies confirm the key role of CAFs in cancer progression and demonstrate their effectiveness as a therapeutic target. However, targeting CAFs in some cancer models actually promoted cancer progression. For example, depletion of α SMA+ stroma in a mouse pancreatic cancer model resulted in increased cancer aggressiveness, enhanced hypoxia and epithelial–mesenchymal transition (EMT), suppressed anticancer immunity, and reduced survival [16].

The contradictory results in different cancer models could be explained by different roles of CAFs in different cancer types, i.e. CAFs could be promoting breast cancer and inhibiting pancreatic cancer. Alternatively, in all cancer types CAFs prevent cancer progression until they receive activating signals from cancer cells and convert into ‘activated CAFs’, which in turn confer invasive and metastatic abilities upon cancer cells [7]. Therapies that target all CAFs are counterproductive and likely to result in the death of normal fibroblasts and significant toxicity. Preferential targeting of activated CAFs has been challenging because activated CAFs are poorly understood at the molecular level. During activation, CAFs exhibit phenotypic changes that partially overlap with myofibroblastic changes during wound healing, inflammation, and fibrosis, including secretion of specific ECM components, cytokines and growth factors [1,17]. Several markers have been used to distinguish activated from non-activated CAFs: α -smooth muscle actin (α SMA, encoded by gene ACTA2) [3], fibroblast activation protein (FAP) [12], podoplanin (PDPN) [18], palladin (PALLD) [19,20], tenascin-C (TNC) [21], platelet-derived growth factor receptor α (PDGFR α) [22,23], and chondroitin sulfate proteoglycan 4 (CSPG4) [24]. However, these markers are frequently expressed in other cells within the cancer stroma, such as vascular smooth muscle cells, pericytes, and mesenchymal stem cells. This lack of specificity could pose problems in therapeutic targeting and underscores the need to better understand the molecular characteristics of activated CAFs in order to develop more precise and less toxic targeted therapies.

COL11A1 encodes the α 1 chain of collagen XI, a minor fibrillar collagen expressed by chondrocytes and osteoblasts but not quiescent fibroblasts [25,26]. The absence of functional collagen XI leads to abnormally thickened cartilage and tendon fibrils, suggesting the role of collagen XI in maintaining proper fibril diameter [27,28]. Studies have demonstrated that COL11A1 mRNA is markedly elevated in cancers of the oral cavity/pharynx, head and neck, breast, lung, esophagus, stomach, pancreas, colon, and ovary, but not in matched normal tissues (reviewed in [25,26]). COL11A1 has been identified as part of gene signatures associated with adverse clinical outcomes including resistance to neoadjuvant therapy in breast cancer [29], time to recurrence in glioblastoma [30], poor survival in kidney cancer [31], and time to recurrence and overall survival in ovarian cancer [32,33]. *In situ* hybridization in ovarian cancer and immunohistochemistry in pancreatic cancer revealed that COL11A1 mRNA and pro-protein are primarily expressed in CAFs [25,32]. The restricted expression of COL11A1 in normal tissues and its enrichment in CAFs during cancer progression combined with its association with adverse clinical outcomes in multiple types of cancer support its candidacy as a specific marker of fibroblast activation in diverse cancers. Here, we explore the suitability of COL11A1 as a pan-cancer marker of activated CAFs and use it as a ‘seed’ to identify the transcription signature of activated CAFs in 13 epithelial cancer types. We show that the COL11A1-coexpressed gene set is highly conserved in these 13 cancer types, indicating that the fibroblast reaction to cancer cells is independent of the organ site-of-origin and of the transforming events within cancer cells. Finally, by combining drug target databases with cancer vs. normal tissue expression databases, we identify several potential therapeutic targets that should have high specificity for activated CAFs and minimal toxicity in normal tissues.

Materials and methods

Human tissues

Studies involving human tissue samples were approved by the Cedars-Sinai Institutional Review Board (IRB 15425). The samples included a tissue microarray from 42 patients with matched primary, metastatic, and recurrent ovarian cancer.

In situ hybridization

The RNA hybridization kit (RNAscope 2.0 FFPE Assay) and probes for COL11A1, the bacterial gene *dapB* (negative control), and the housekeeping gene *HPRT* (positive control), were from Advanced Cell Diagnostics, Inc. Formalin-fixed, paraffin-embedded tissue section slides were processed by the Cedars-Sinai Biobank and Translational Research Core following the protocol provided with the RNAscope In Situ Hybridization kit from Advanced Cell Diagnostics, Inc. The slides were counterstained with Mayer’s hematoxylin.

Immunohistochemistry

Immunohistochemical detection of α SMA was performed on formalin-fixed, paraffin-embedded tissue sections using the protocol provided with the pre-diluted asm-1 clone antibody from Leica Microsystems. Staining was done by the Cedars-Sinai Pathology Service on the Ventana Benchmark Ultra automated slide stainer. The staining was visualized using the Ventana OptiView DAB Detection System. The slides were counterstained with Mayer’s hematoxylin.

In vitro co-culture experiments

The ovarian cancer cell lines OVCAR3-GFP, KURAMOCHI-GFP and OVSAHO-GFP were maintained in RPMI-1640 (Corning) supplemented with 10% fetal bovine serum (FBS) and 1x penicillin/streptomycin (Corning). Cell line authenticity was confirmed by Laragen using the short tandem repeat (STR) method. The immortalized normal ovarian fibroblasts INOF-tdTomato cell lines [34] were maintained in a 1:1 ratio of MCDB 105 (Sigma-Aldrich) and Medium 199 (GIBCO) with 10% FBS, 50 U/ml penicillin and 50 μ g/ml streptomycin. Immortalized normal ovarian fibroblasts and ovarian cancer cells were co-cultured in 1% FBS supplemented media (1:1:2 ratio of MCDB 105, Medium 199 and RPMI-1640) using 6-well plates, either by directly plating ovarian cancer cells (10^5 cells/well) onto a 70% confluent layer of normal ovarian fibroblasts or onto a 0.4 μ m Transwell membrane. Media were replaced every 2 days. After 4 days of co-culture, GFP-labeled ovarian cancer cells and tdTomato-labeled fibroblasts were separated by FACS in PBS with 0.5% FBS. RNA extraction from fibroblasts and ovarian cancer cell lines was performed using the RNeasy Mini Kit (Qiagen) and reverse transcribed to cDNA using the Quantitect Reverse Transcription Kit (Qiagen). For qRT-PCR, 50 ng of cDNA was mixed with COL11A1 primers (Forward: 5’-GACTATCCCTCTTCAGAACTGTTAAC-3’; Reverse: 5’-CTTCTATCAAGTGGTTTCGTGGTIT-3’) and the iQ SYBR-Green Supermix (BioRad) and run on the CFX96 Real-Time System (BioRad). Data were analyzed using the $2^{-\Delta\Delta CT}$ method and normalized to INOF-tdTomato control to present the fold change ratios. All mRNA data were normalized to RPL32 expression (Forward: 5’-ACAAAGCATGCTGCCCATG-3’; Reverse: 5’-TTCCACGATGGCTTTGCGGTTC-3’). The statistical analyses were performed using GraphPad Prism (version 6.0; GraphPad Software). The unpaired t test was used for data analyses.

Public database portals and dataset analyses

Data from public portals were used as provided by individual portals without additional processing or normalization, unless otherwise indicated. Box plots of COL11A1 expression in normal tissues and cancers were generated using the Gene Expression across Normal and Tumor tissue (GENT) portal (medical-genome.kribb.re.kr/GENT) in which data from multiple datasets were processed and normalized as previously described [35]. COL11A1 expression level diagrams for inflammatory bowel disease, lung fibrosis, and cancers of the colon and lung were generated using the R2 MegaSampler public portal (hgserver1.amc.nl/cgi-bin/r2/main.cgi). A description of the methods used for data processing and normalization is available through the portal. Survival z-scores for individual genes and cancer types were obtained from the PREDiction of CLinical Outcomes from Genomic Profiles (PRECOG) portal (precog.stanford.edu). Methods for calculating PRECOG z-scores have been published [36]. Ranking of the COL11A1-correlated genes in 13 TCGA carcinoma types was determined using data from individual cancer datasets that were processed by cBio Portal (cbioportal.org) as previously described [37]. Kaplan–Meier survival plots and plots of COL11A1 expression in individual molecular subtypes of ovarian carcinoma were generated using the ovarian cancer microarray gene expression database CSIOVDB (csibio.nus.edu.sg/CSIOVDB/CSIOVDB.html), which has been previously described [38]. The dataset for fibroblast and ovarian epithelial cell co-culture was imported from the Gene Expression Omnibus (ncbi.nlm.nih.gov/geo). The Euclidean distance clustering analysis heatmap for the e-mtab-991 [39] and GSE40595 [40] datasets was generated using the public R2 GeneSet Clustering Analysis portal (hgserver1.amc.nl/cgi-bin/r2/main.cgi), which also describes methods that were used to process and normalize data from datasets included in the portal.

Results

COL11A1 is expressed in a subset of α SMA-positive CAFs and can be induced in normal fibroblasts by the presence of cancer cells

To determine if *COL11A1* expression is associated with fibroblast activation, we used α SMA as a marker of activated CAFs [3]. Comparison of α SMA immunohistochemistry and *COL11A1* *in situ* hybridization in a tissue microarray consisting of primary, metastatic and recurrent ovarian cancers from 42 patients showed that *COL11A1* is expressed in a subset of α SMA+ CAFs (Fig. 1A). Unlike α SMA, *COL11A1* was not expressed in blood vessels (red arrows) or in fibroblasts surrounding the cancer (blue arrows) (Fig. 1A).

In sections of metastatic ovarian cancer, we observed that *COL11A1*-positive cells are confined to the intratumoral and immediate peritumoral CAFs (Fig. 1B), suggesting that *COL11A1* expression may be induced by cues received from epithelial cancer cells. To test if cancer cells can induce *COL11A1* expression in fibroblasts, we co-cultured immortalized normal ovarian fibroblasts (INOFs) with three different ovarian cancer cell lines (OVSAHO, OVCAR3, and KURAMOCHI). *COL11A1* expression in INOFs was most strongly induced by direct co-culture with ovarian cancer cell lines although weak induction occurred by indirect co-culture on a Transwell membrane (Fig. 1C). The induction of *COL11A1* in fibroblasts in the presence of cancer cells was confirmed by analysis of the public expression dataset GSE52104 in which two types of

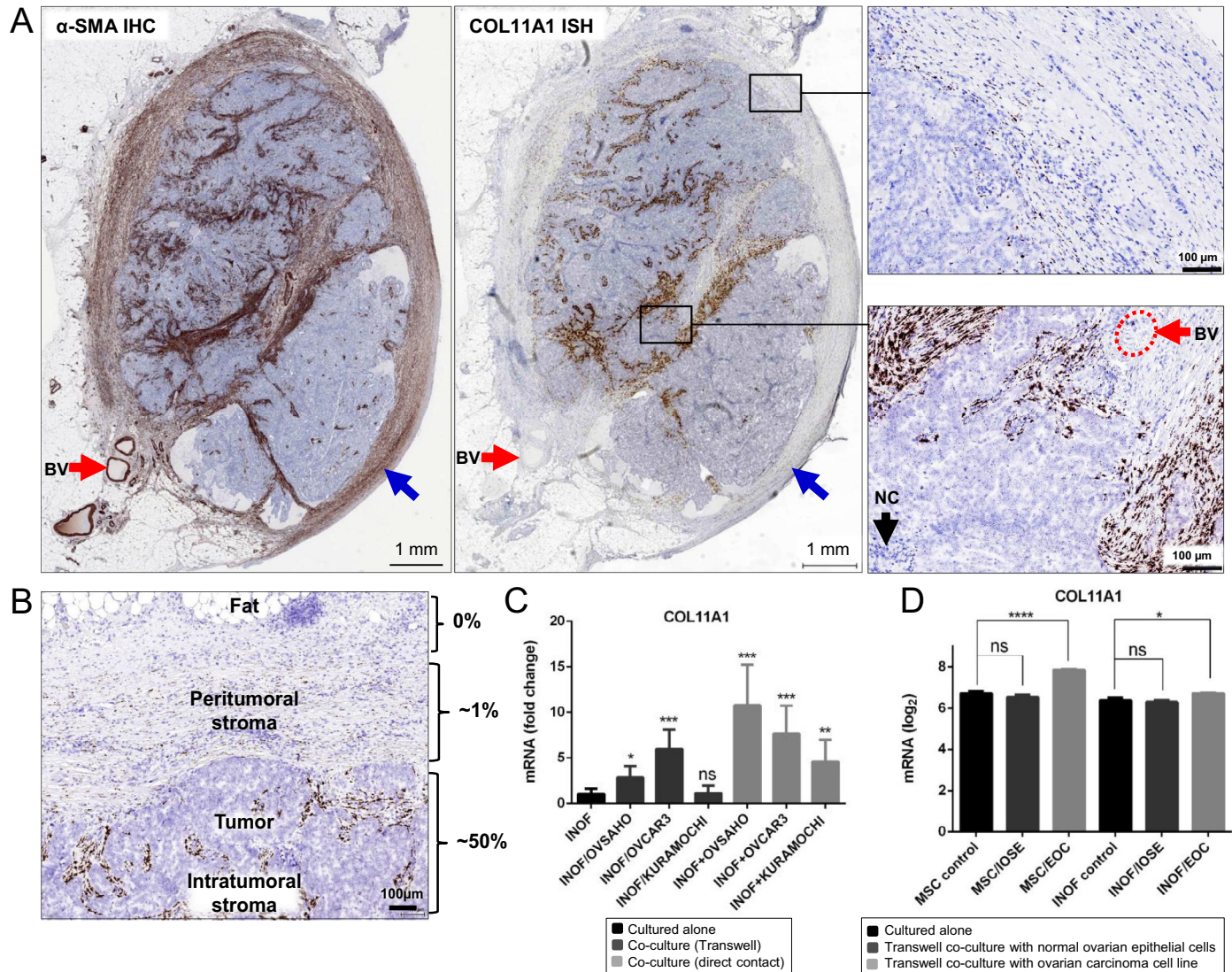


Fig. 1. *COL11A1* is expressed in CAFs. (A) Comparison of α SMA immunohistochemistry and *COL11A1* *in situ* hybridization in a metastatic ovarian cancer sample. Red arrows indicate blood vessels. Blue arrows indicate fibroblasts surrounding the tumor nodule. A high magnification of peritumoral and intratumoral regions in the black rectangles is shown in panels on the left. IHC, immunohistochemistry; ISH, *in situ* hybridization; BV, blood vessel; NC, necrosis. (B) Distribution of *in situ* hybridization *COL11A1*-positive CAFs in relation to cancer cells. The estimated percent of *COL11A1*-positive CAFs is shown on the right. The image is representative of metastatic and recurrent ovarian cancer samples, which typically express higher levels of *COL11A1* than primary ovarian cancers. (C) Quantitative RT-PCR levels of *COL11A1* in sorted (FACS) immortalized normal ovarian fibroblasts (INOFs) grown alone or co-cultured with ovarian cancer cell lines (OVSAHO, OVCAR3, KURAMOCHI) that were either separated from INOFs by a Transwell membrane or directly mixed with INOFs. Statistical analyses were performed between INOFs grown alone and INOFs co-cultured with ovarian cancer cells (* $p < 0.05$; ** $p < 0.01$; *** $p < 0.001$; ns, not significant). Error bars indicate standard deviation. (D) Levels of *COL11A1* in the GSE52104 expression dataset in which mesenchymal stem cells (MSCs) or immortalized normal ovarian fibroblasts (INOFs) were either cultured alone or co-cultured with IOSE4 normal epithelial cells (IOSE) or HEYA8 epithelial ovarian cancer cells (EOC) using a Transwell membrane. Inverse- \log_2 values of the Robust Multi-array Average (RMA) scores from different *COL11A1* probes were averaged, then \log_2 -transformed. The data were extracted for statistical analyses using GraphPad Prism 6. Data are represented as the mean \pm SEM. Intergroup differences were assessed by the Student's t-test. * $p < 0.05$; **** $p < 0.0001$. (For interpretation of the references to color in this figure legend, the reader is referred to the web version of this article.)

presumptive cancer-associated fibroblast precursor cells, mesenchymal stem cells (MSCs) and immortalized normal ovarian fibroblasts (INOFs), were either cultured alone or co-cultured with normal ovarian surface epithelial cells (IOSE) or epithelial ovarian cancer cells (EOC) using a Transwell membrane [41]. *COL11A1* mRNA was statistically significantly upregulated when MSCs and INOFs were co-cultured with EOC but not IOSE (Fig. 1D), indicating that cancer cells have a greater capacity than normal cells to induce *COL11A1* expression in fibroblasts.

COL11A1 is associated with cancer progression and poor survival

COL11A1 mRNA expression has been associated with poor survival in ovarian cancer [32,33] and kidney cancer [31]. To elucidate the underlying biology that could result in poor survival, we investigated its expression in ovarian and colon cancers. Using a comprehensively annotated microarray database for 3431 human ovarian cancers [38], we show that increased expression of *COL11A1* mRNA is associated with overall survival and disease-free survival (Fig. 2A) as well as with clinical and molecular parameters such as increased cancer stage and grade and mesenchymal molecular subtype (Fig. 2B). The association of *COL11A1* expression with poor survival is unlikely to be a manifestation of the total amount of stromal fibroblasts because a general marker of fibroblasts, vimentin (*VIM*), is not associated with poor survival in the same cohort of ovarian cancer patients (Table S1). The association of *COL11A1* with

adverse outcomes is also not restricted to ovarian cancer. We show that in 1820 colon cancers [42], increased expression of *COL11A1* mRNA is associated with poor disease-specific and disease-free survival as well as with clinical and molecular parameters, such as increased cancer stage and microsatellite instability and CMS4 (mesenchymal) molecular subtype (Fig. S1A, B).

To systematically investigate an association between *COL11A1* mRNA expression and survival in various solid and liquid cancers, we plotted *COL11A1* z-score values as determined by the pan-cancer PREdiction of CLinical Outcomes from GeNomic Profiles (PRECOG) analysis of ~18000 cases in 166 cancer datasets [36]. In most epithelial cancers, *COL11A1* expression was associated with poor survival (Fig. 3A). Associations between expression of 43 collagen genes and survival z-scores in 12 common epithelial cancer types revealed that for the majority of collagens, increased expressions of mRNA were associated with poor survival, with *COL11A1* having the strongest association (Fig. 3B).

COL11A1 is among the most differentially expressed genes between cancers and corresponding benign tissues

In the Genotype-Tissue Expression (GTEx) project database [43], *COL11A1* mRNA is expressed at appreciable levels in transformed skin fibroblasts but not in non-transformed skin fibroblasts or other normal tissues (Fig. S2). Additional analyses of various expression datasets containing normal adult mouse and human tissues

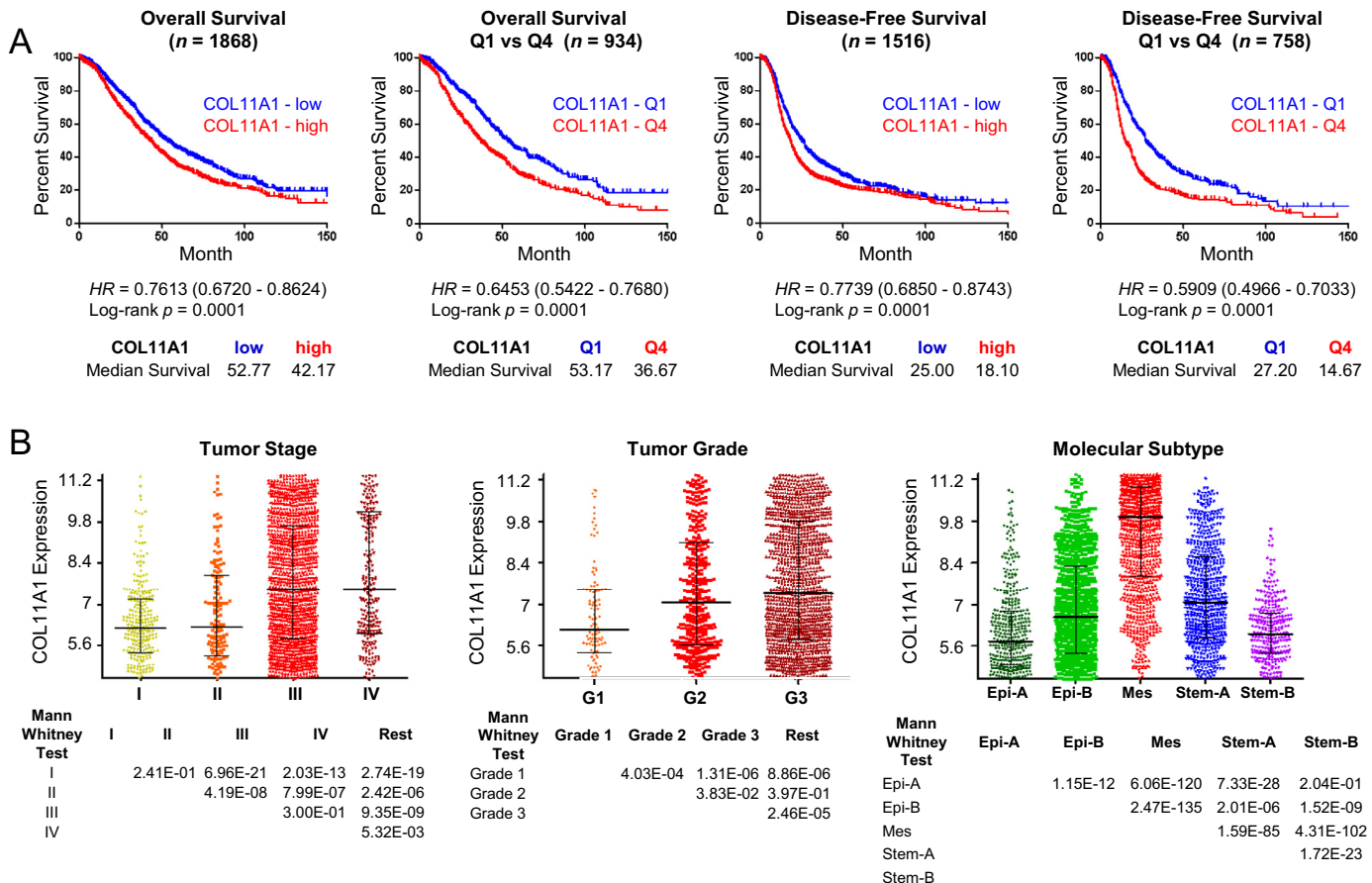
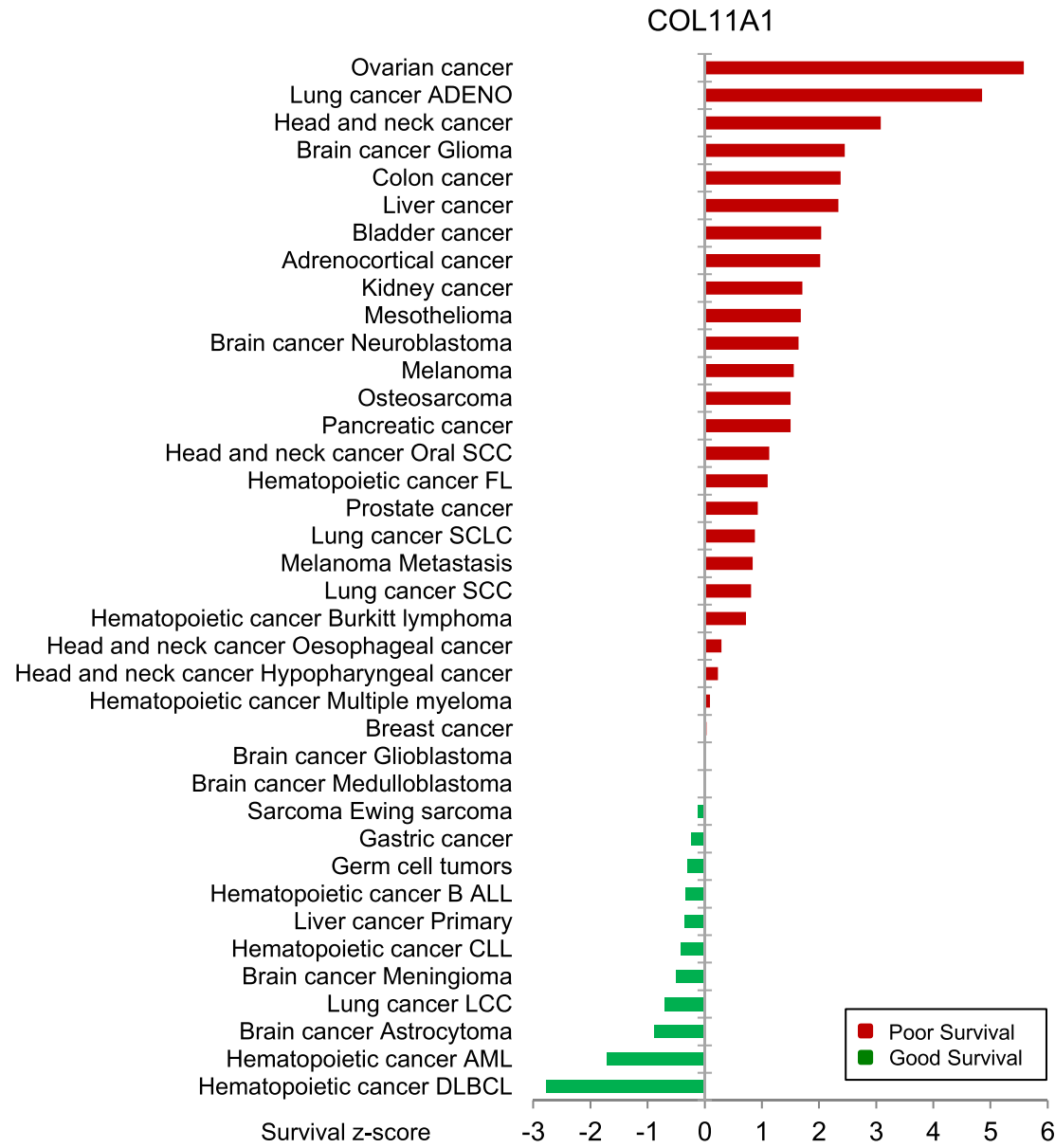
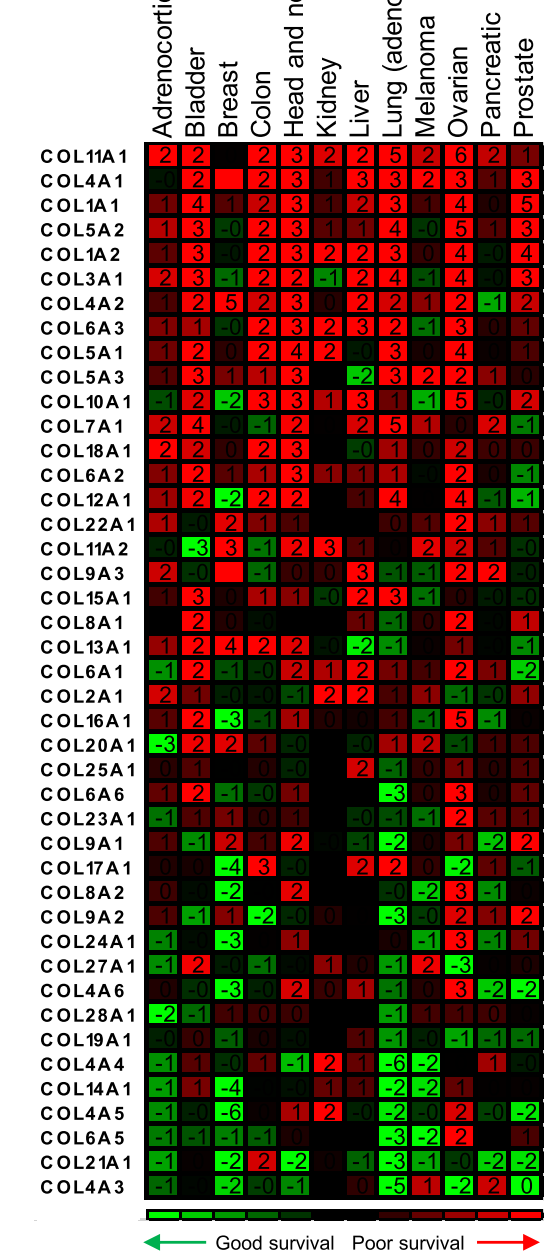


Fig. 2. *COL11A1* expression is associated with adverse clinical parameters. (A) Kaplan–Meier analyses of overall survival (left two panels) and disease-free survival (right two panels) based on *COL11A1* expression in ovarian carcinoma. Disease-free survival includes progression- and recurrence-free survival. Patients were stratified to *COL11A1*-high (red) or *COL11A1*-low (blue) based on the median expression of *COL11A1*, and to *COL11A1*-Q4 (highest 25% expression; red) or *COL11A1*-Q1 (lowest 25% expression; blue). (B) *COL11A1* expression profiles were stratified by FIGO stage (left), FIGO grade (middle), and molecular subtype (right). Data were obtained from the ovarian microarray gene expression database CSIOVDB (csbio.nus.edu.sg/CSIOVDB/CSIOVDB.html). HR, hazard ratio. (For interpretation of the references to color in this figure legend, the reader is referred to the web version of this article.)

A



B



D. Jia et al./Cancer Letters 382 (2016) 203–214

Fig. 3. COL11A1 expression in cancer is associated with poor survival in multiple cancer types. (A) Survival z-scores in different cancer types associated with expression of COL11A1 mRNA. (B) Survival z-scores associated with mRNA expression of different collagen genes. The data were obtained from the PREdiction of CLinical Outcomes from GeNomic Profiles (PRECOG) database (precog.stanford.edu).

revealed that *COL11A1* is expressed in cartilage and collagen-producing cells in the eye and brain, with negligible levels in most other tissues that have been profiled including mesenchymal stem cells in the bone marrow, muscle, and fat (data not shown).

Comparison of *COL11A1* expression in 17931 cancers and 3503 normal tissues (U133Plus2 platform) and 9258 cancers and 4087 normal tissues (U133A platform) using the Gene Expression across Normal and Tumor tissue (GENT) portal [35] revealed that *COL11A1* mRNA is elevated in most cancers in comparison to their corresponding normal tissues (Fig. 4A). In some cancers, *COL11A1* was ranked among the most statistically significant differentially expressed genes when cancer and its corresponding normal tissue were compared. For example, comparison of cancer and normal tissues in The Cancer Genome Atlas (TCGA) datasets for colon cancer and invasive breast cancer ranked *COL11A1* as the first and third most differentially expressed gene, respectively (Fig. S3).

As many collagens and collagen-remodeling genes are frequently upregulated in fibroblast activation associated with inflammation and fibrosis in the absence of cancer, use of these genes as therapeutic targets in cancer could be problematic. Analysis of expression profile datasets show that levels of *COL11A1* mRNA in inflamed colonic tissue from inflammatory bowel disease and fibrotic lung tissues are not significantly different from those in corresponding unaffected colon and lung and that *COL11A1* levels associated with colon inflammation and lung fibrosis are minimal and markedly different from those associated with colon and lung cancers (Fig. 4B). In contrast, levels of *ACTA2*, the gene encoding the prototypical marker of myofibroblast differentiation, α SMA, is expressed at similar levels in cancers and inflamed or fibrotic tissues (Fig. 4B).

A consistent set of genes is co-expressed with COL11A1 across different cancers

To better understand the biology of cancers with high levels of *COL11A1*, we identified genes that most closely correlate with *COL11A1* mRNA expression in 13 TCGA datasets representing different cancer types. Spearman's rank correlations between *COL11A1* and its co-expressed genes for each cancer type were calculated. The genes were then ranked based on the average correlation of each gene across the 13 cancer types. The top 195 correlated genes were selected based on an average correlation of >0.4 *COL11A1*-correlated genes were then ranked based on the average of the absolute correlation values (Table 1 and Table S2). The top 10% most highly correlated genes in each cancer type are highlighted in pink (Table 1). Notably, *COL11A1*-correlated genes with high average correlation scores also tended to be among the top 10% highest scored genes in each cancer type (indicated in pink in Table 1). In contrast, the top 10% *COL11A1*-anticorrelated genes were not conserved across these cancer types (Table S3). Some of the top ranked *COL11A1*-anticorrelated genes in individual cancer types were associated with normal functions of these organs suggesting that they may represent normal tissue or a noninvasive tumor component. For example, the ovarian cancer top 100 *COL11A1*-anticorrelated genes (Table S3) present in the GSE12172 ovarian cancer dataset were primarily expressed in ovarian tumors of low malignant potential (Fig. S4).

Pan-cancer COL11A1-correlated genes are induced in CAFs

Consistent with the induced expression of *COL11A1* in the *in vitro* co-culture model (Fig. 1D), the average expression of the pan-cancer *COL11A1*-correlated gene set was significantly induced in mesenchymal stem cells and normal ovarian fibroblasts co-cultured with ovarian cancer cells but not with normal ovarian epithelial cells (Fig. S5). Since epithelial cells were not profiled in this experiment, it is unknown if fibroblasts also induce expression of the pan-

cancer *COL11A1*-correlated genes in epithelial cells. This is relevant because several of the 195 pan-cancer *COL11A1*-correlated genes have been shown to play a role in EMT [42] and malignant cells undergoing EMT have been proposed as one possible source of CAFs [44]. To determine if the pan-cancer *COL11A1*-correlated gene set is preferentially expressed in cancer cells undergoing EMT or in host-derived fibroblasts, we used the e-mtab-991 public transcription profile dataset of primary patient-derived colon cancers and their patient-derived xenografts (PDX) in nude mice [39]. Presumably, in PDX samples, fast-proliferating human cancer cells continued to grow in mice while slow-proliferating human CAFs were lost and eventually replaced by mouse fibroblasts, which can be distinguished from human cells by species-specific gene probes [39]. GeneSet clustering analysis showed that most of the pan-cancer *COL11A1*-correlated genes had diminished levels in PDX samples in comparison to primary cancers (Fig. 5A), suggesting that the genes are enriched in the CAFs rather than in the cancer cells. However, it is also possible that the pan-cancer *COL11A1*-correlated genes are expressed in epithelial cells in primary colon tumors but become silenced upon adaptation of human cancer cells to the mouse microenvironment. Thus, we conducted GeneSet clustering analysis of the primary ovarian cancer dataset GSE40595 in which ovarian CAFs and epithelial cancer cells were isolated by laser-capture microdissection [40]. The pan-cancer *COL11A1*-correlated genes were preferentially expressed in CAFs in this dataset (Fig. 5B).

In addition to CAFs, immune cells are a major component of the tissue microenvironment. To exclude the possibility that the pan-cancer *COL11A1*-correlated gene set represents immune cells in the tumor microenvironment, we used the expression profile of 230 mouse hematopoietic cell types generated by the Immunological Genome Project (ImmGen) compendium [45]. In addition to hematopoietic cell lineages, the dataset contains expression profiles of skin fibroblasts and fibroblasts residing in the thymus, lymph nodes, and spleen. The pan-cancer *COL11A1*-correlated gene set was highly represented in fibroblasts but not in hematopoietic cell lineages (Fig. 5C).

CAFs have a different expression profile than normal fibroblasts. Moffitt and colleagues defined a 23-gene signature of 'normal stroma' and a 25-gene signature of 'activated stroma' [46] using non-negative matrix factorization for virtual microdissection of primary and metastatic pancreatic ductal cancer samples into cell subsets with prognostic and biologic relevance. None of the 23 (0%) 'normal stroma' genes in contrast to 18 of 25 (72%) 'activated stroma' genes were present in the *COL11A1*-correlated gene set, respectively (Fig. 5D), suggesting that the *COL11A1*-correlated gene set represents CAFs.

Biological processes associated with fibroblast activation in cancer

The remarkable uniformity of *COL11A1*-correlated genes across 13 different cancer types suggests involvement of these genes in common biological processes that are independent of the organ site and of the phenotypic and genetic diversity observed in individual cancer types. To gain insight into the biology of this conserved gene set, we conducted several analyses that identified overlap between the 195 pan-cancer *COL11A1*-correlated genes and genes in various datasets with characterized biological features. The Gene Ontology (GO) Biological Process (BP) analysis revealed that the pan-cancer *COL11A1*-correlated genes are primarily involved in extracellular matrix modification and collagen remodeling (Table S4). Additionally, we used SABiosciences array gene tables, which consist of literature-based curated molecular pathways where each pathway was represented by 84 genes. Analysis of gene overlap between the pan-cancer *COL11A1*-correlated gene set and genes representative of 67 different pathways in SABiosciences arrays showed the largest overlap for pathways associated with extracellular matrix,

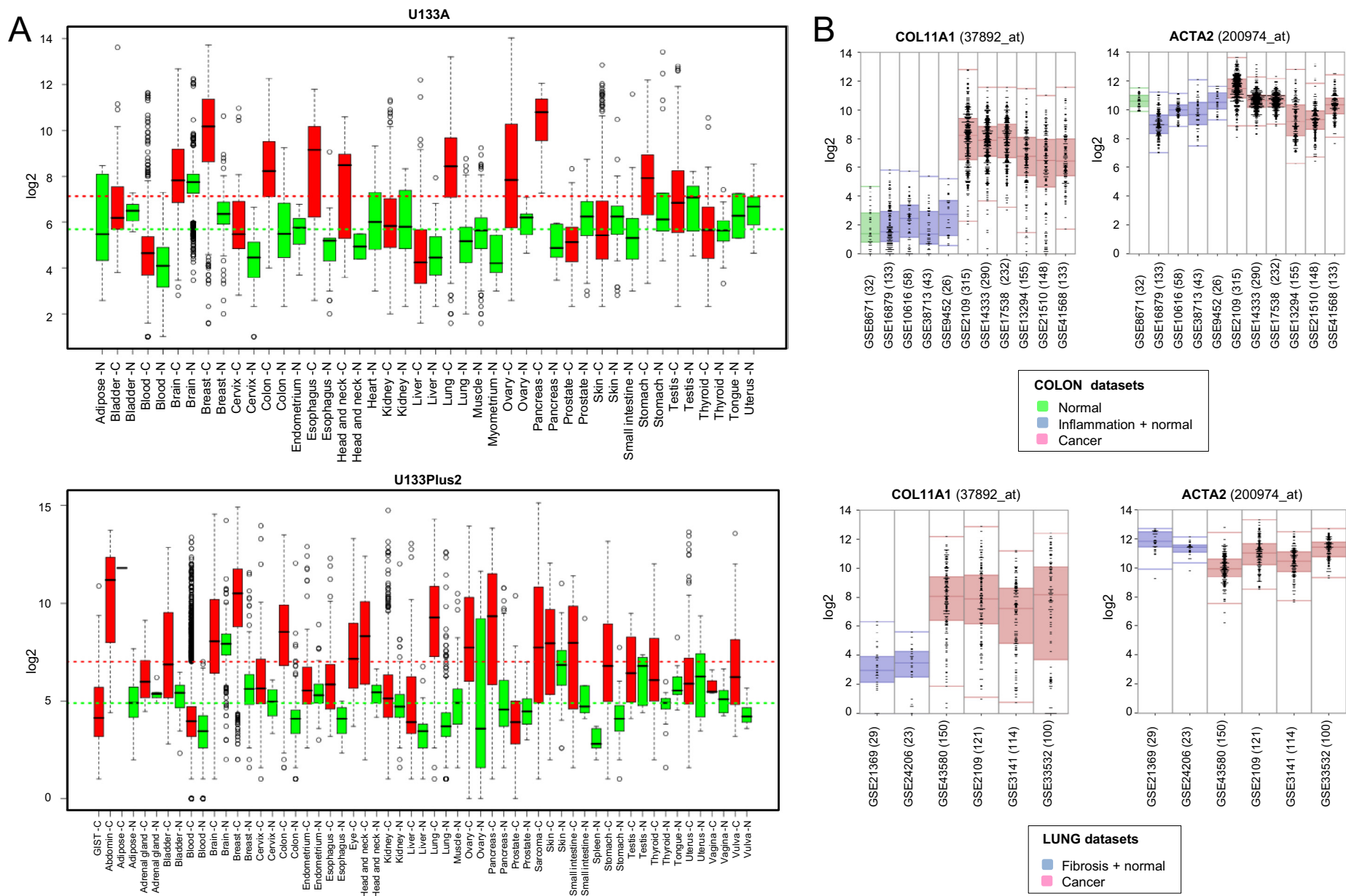


Fig. 4. Increased expression of *COL11A1* in cancer and low expression in normal tissues, inflammation and fibrosis. (A) Comparison of *COL11A1* mRNA expression in normal tissues and corresponding cancers. Box plots for two different platforms (U133Plus2 and U133A) were generated using datasets and software available through the Gene Expression across Normal and Tumor tissue (GENT) portal (medical-genome.kribb.re.kr/GENT). The y axis shows log₂ mRNA levels. Average expression levels in normal tissues and cancer tissues are indicated by vertical dotted green and red lines, respectively. (B) *COL11A1* and *ACTA2* mRNA expression in normal, inflammatory and fibrotic conditions in comparison to cancer. The graphs were generated using the public R2 MegaSampler software (hgserver1.1mc.ncl/cgi-bin/r2/main.cgi) for the processing and normalization of individual datasets imported from the Gene Expression Omnibus (u133p2, MAS5.0 platform). The number of samples in each GSE dataset is indicated in parentheses. (For interpretation of the references to color in this figure legend, the reader is referred to the web version of this article.)

Table 1 COL11A1-correlated genes (Spearman's rank correlation) across 13 different TCGA carcinoma types, each represented by >100 primary tumors from therapy-naive patients. Pink denotes the top 10% COL11A1-correlated genes in each individual carcinoma type. Rectangles denote genes frequently used as markers of activated CAFs.

Table with columns: Rank, Gene Symbol, Bladder, Breast, Colorectal, Cervical, Head and Neck, Kidney Clear Cell, Kidney Papillary, Lung Adeno, Lung Squamous, Ovarian, Prostate, Stomach, Thyroid, Average Correlation. The table is split into 'Pan-cancer COL11A1-correlated genes' and 'Continued'. It lists 100 genes with their Spearman's rank correlation values across 13 cancer types. Pink shading highlights the top 10% correlated genes in each type. Rectangles highlight genes used as markers of activated CAFs.

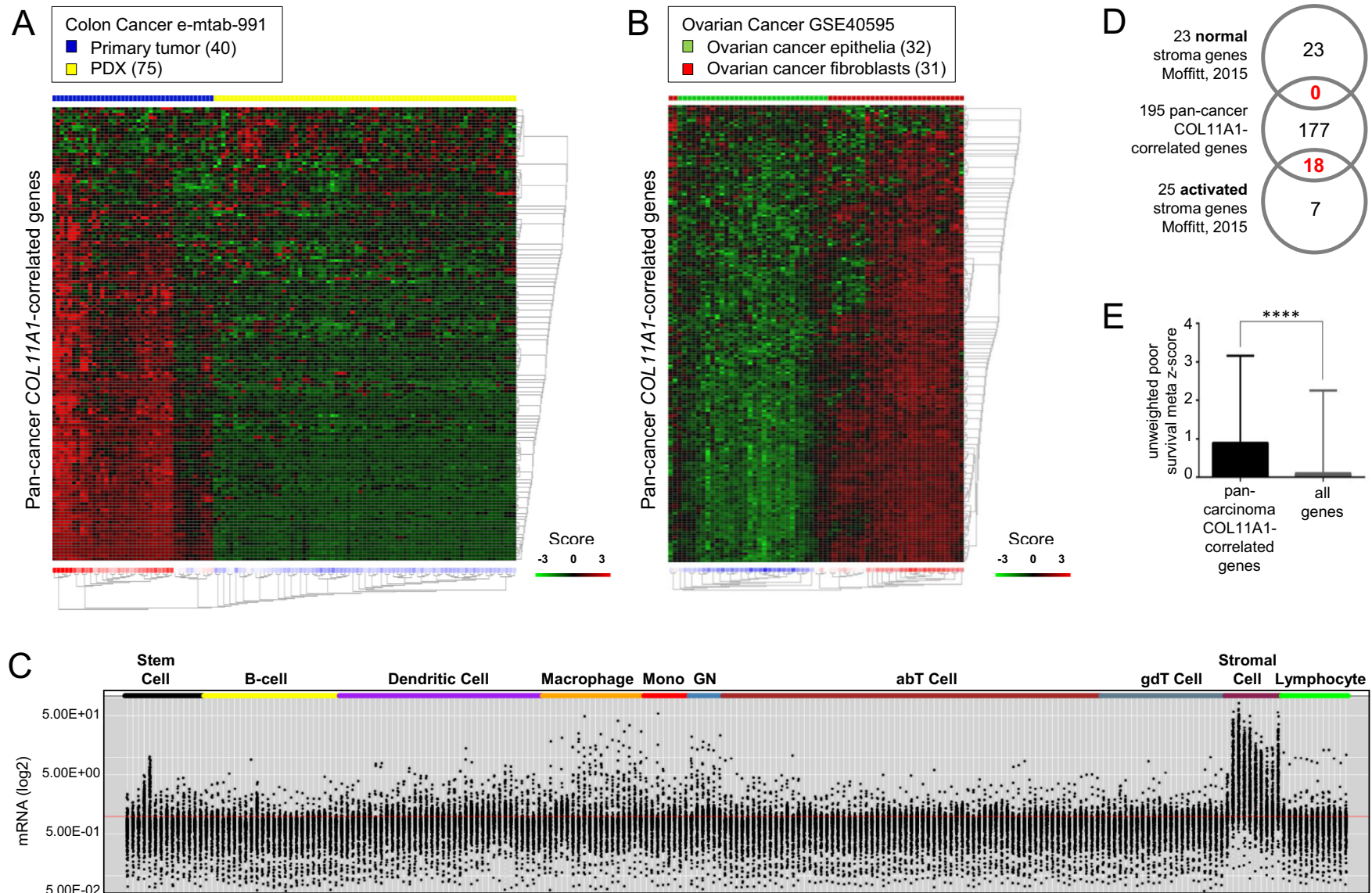


Fig. 5. The pan-cancer *COL11A1*-correlated gene set is expressed in CAFs and associated with poor patient survival in multiple cancer types. (A) GeneSet expression clustering analysis of 40 primary colon cancer samples and 75 patient-derived xenograft (PDX) samples in the e-mtab-991 dataset using the pan-cancer *COL11A1*-correlated genes. (B) GeneSet expression clustering analysis of laser-microdissected ovarian cancer epithelial cells (32 samples) and CAFs (31 samples) in high grade serous ovarian cancer in the GSE40595 dataset using the pan-cancer *COL11A1*-correlated genes. The Euclidean distance clustering analysis heatmaps in (A) and (B) were generated using the public R2 GeneSet Clustering Analysis tool (hgserver1.amc.nl/cgi-bin/r2/main.cgi). (C) Expression of the pan-cancer *COL11A1*-correlated genes mapped on the transcriptome of individual murine hematopoietic and stromal cell types in the ImmGene project (immgen.com). The plot was generated using MyGeneSet tool (rstats.immgen.org/MyGeneSet). Black dots represent mRNA levels (y axis) of 186 pan-cancer *COL11A1*-correlated genes (9 genes were not present in the database) across 230 individual cell types (X axis) grouped into 10 main groups. (D) Overlap of the 195 pan-cancer *COL11A1*-correlated genes with 23 'normal stroma' and 25 'activated stroma' genes defined by Moffitt et al. (E) Unweighted meta z-scores of 191 *COL11A1*-correlated genes (4 genes were not available in the PRECOG database) were compared with those of all genes (total 23,287 genes) in the PRECOG database using unpaired t test. The plot was generated using GraphPad Prism software version 6.0. Intergroup differences were assessed by the Student's t-test. Mean \pm SEM of pan-cancer *COL11A1*-correlated genes (0.8916 \pm 0.1641 N = 191); mean \pm SEM of all genes (0.09918 \pm 0.01416 N = 23287); ****p < 0.0001.

fibrosis, osteogenesis, wound healing, EMT, cardiovascular disease, and transforming growth factor β (TGF β) signaling (Table S5). *COL11A1*-correlated gene set enrichment analysis of chemical and genetic perturbations (CGP) showed the most significant overlap with genes up-regulated in association with cancer invasiveness, advanced stage, stromal cell stemness, and epithelial-mesenchymal transition (EMT) (Table S6). The uniformity of the *COL11A1*-correlated genes across different cancers might also indicate that these genes are regulated by a common mechanism. Ingenuity Pathway Analysis showed that transforming growth factor beta 1 (TGF β 1) is the most strongly associated upstream regulator of the pan-cancer *COL11A1*-correlated genes (Table S7).

COL11A1-correlated genes are associated with poor patient survival and represent potential therapeutic targets

To determine whether the pan-cancer *COL11A1*-correlated gene set is associated with patient survival in the ~18,000 cases of liquid and solid malignancies in the PRECOG dataset [36], we compared survival z-scores for the 195 pan-cancer *COL11A1*-correlated genes with the survival z-scores for all genes in the dataset. This analysis showed that expression of the pan-cancer *COL11A1*-correlated gene set is significantly associated with poor survival (Fig. 5E).

Expression profile analyses have identified a mesenchymal molecular subtype of cancer associated with poor survival in multiple cancers including ovarian [47], pancreatic [46], gastric [48] and colon [49]. In colon cancer, it has been shown that the mesenchymal molecular subtype, which constitutes approximately 23% of colon cancers, has no significant enrichment for targetable mutations or copy number changes in candidate driver genes [49]. Even if future research identifies targetable events in cancer cells of the mesenchymal subtype, it is predicted that enrichment in CAFs and excessive ECM deposition will reduce therapeutic efficacy by creating a physical barrier for drug transport. Thus, simultaneous targeting of CAFs and cancer cells may be necessary for chemotherapeutic accessibility.

To identify therapies that preferentially target activated CAFs and spare normal tissues, we combined drug target searches with expression profile datasets in cancers and normal tissues. Ingenuity Pathway Analysis and searches of the ClinicalTrials.gov (clinicaltrials.gov) and ChEMBL [50] (ebi.ac.uk/chembl) databases revealed that, of the 195 pan-cancer *COL11A1*-correlated genes, 16 are targets of drugs used in clinical trials (Table S8) and 30 are targets of bioactive compounds (Table S9).

To test whether any of the drug/bioactive compound target genes in Tables S8 and S9 are exclusively expressed in activated CAFs, we determined the expression levels of each gene in normal tissues in the GTEx database [43] and in normal vs. cancer tissues in the GENT database [35]. Additionally, to test whether selected genes were exclusively overexpressed in cancer tissues and not in non-cancer associated pathologies such as inflammation and fibrosis, we compared expression of these genes in normal tissues, inflamed/fibrotic tissues and cancer tissues of the colon and lung. Unlike *COL11A1*, which has restricted expression in normal tissues (Fig. S2) and is highly elevated in cancer vs. normal tissues (Fig. 4A) and in cancer vs. inflamed/fibrotic tissues (Fig. 4B) most of the target genes were expressed at high levels in at least one normal tissue and/or exhibited equivalent expression levels in cancers vs. normal tissues, and cancers vs. inflamed/fibrotic tissues. One example of this pattern of expression is *CTGF* (Figs. S6 and S7). However, *FN1*, *MMP13*, *MMP14*, *FAP*, *LOX* and *COL1A2* exhibited restricted expression in normal tissues and elevated expression in cancer vs. normal tissues. One example of this pattern of expression is *FAP* (Figs. S8 and S9). Among *FN1*, *MMP13*, *MMP14*, *FAP*, *LOX* and *COL1A2*, *FAP* was also differentially expressed between inflamed/fibrotic tissues and cancer tissues although this difference in expression was not as prominent as for *COL11A1* (compare Fig. S9B and Fig. 4B).

Discussion

Whereas in the past most therapeutic approaches have focused on the cancer cell and its genetic alterations, it is becoming apparent that the microenvironment plays an equally important role in cancer evolution. We now recognize that the cancer stroma not only serves as a scaffold for tissue organization and integrity but also provides key biomechanical and molecular signals that can affect various aspects of cancer growth and biology, including proliferation, survival, metabolism, stem cell fate, and response to chemotherapy [51,52]. As the genetically stable subpopulations of the cancer microenvironment are increasingly recognized as potentially effective therapeutic targets, a comprehensive definition of their molecular characteristics will be a prerequisite for the development of more precise and less toxic therapies. Currently, there are no reliable methods to distinguish activated CAFs from non-activated CAFs, which although frequently abundant within cancers do not necessarily contribute to adverse outcome. We identified *COL11A1* among the top differentially expressed genes in multiple cancer types when cancer tissues and their corresponding normal tissues were compared. We showed that an increase in *COL11A1* expression is associated with progression and poor survival in most cancer types. *COL11A1* is a particularly attractive therapeutic target because of its restricted expression in normal tissues and non-cancer conditions, such as inflammation and fibrosis.

The identification of a highly conserved set of genes associated with *COL11A1* expression in breast, lung, pancreas, stomach, urinary bladder, colon, thyroid, cervix, head and neck, thyroid, ovary, and prostate cancers was somewhat surprising in light of the genetic and phenotypic diversity among these cancer types. The conserved expression signature indicates that the reaction of stromal tissues to invading epithelial cancer cells may be similar regardless of the organ of origin or genetic alterations. This has significant implications for the development of pan-cancer therapeutic strategies. Our analysis of potential upstream regulators of the pan-cancer *COL11A1*-correlated genes revealed TGF β 1 as the most likely candidate. Dysregulation of TGF β signaling is recognized as the main driver of fibroblast activation and represents the most logical therapeutic target [53]. In immortalized normal ovary fibroblast cell culture, recombinant TGF β 1 has been shown to upregulate expression of *COL11A1* and several other *COL11A1*-correlated genes; this effect was abrogated by the TGF β receptor inhibitor A83-01 [32]. However, the pleiotropic nature of TGF β signaling carries the risk of adverse effects in patients [54]. In order to abrogate fibroblast activation without the negative effects of pan-TGF β therapy, it will be necessary to design therapies for more specific targets.

Sixteen of the 195 pan-cancer *COL11A1*-correlated genes are targets of drugs in clinical trials. These targets include CTGF, a matricellular protein involved in myofibroblast formation in cancer as a binding factor of fibronectin and a downstream mediator of TGF β . A clinical trial (clinicaltrials.gov; NCT02210559) is currently enrolling patients with unresectable pancreatic cancer to test a combination of conventional chemotherapy and FG-3019, the human monoclonal antibody that interferes with the action of CTGF. Our expression analyses, consistent with the published literature (reviewed in Ref. [55]), show that *CTGF* is expressed at similar levels in normal tissues and cancers and therefore unlikely to be a safe therapeutic target for cancer treatment. In contrast, targets such as *FN1*, *FAP*, *MMP13*, *LOX* and *COL2A1* are markedly increased in cancer/inflammation/fibrosis compared to normal tissues and are thus predicted to have a better safety profile than agents targeting CTGF. Our assessment is consistent with the published moderate and reversible toxicity of the FN1-targeting monoclonal antibody-cytokine fusion protein L19-IL2, which is in a phase I/II study for patients with solid cancers (clinicaltrials.gov; NCT01058538) [56,57]. Our expression analyses show that one of the targets of bioactive

compounds, FAP, has low expression in normal tissues and also lower expression in inflamed/fibrotic tissues than in cancer. Yet, this difference in expression may not be sufficient for specific targeting of activated CAFs as studies in mouse models have shown that depletion of the FAP+ stroma can induce toxicity due to expression of FAP in the mesenchymal cells of bone marrow, muscle and adipose tissue [58,59]. Future efforts to specifically target activated CAFs can be improved by designing novel therapies to target genes that exhibit restricted expression in nonmalignant tissues. When considering *COL11A1* as a cancer-specific biomarker and therapeutic target, it is important to note that several normal tissues express *COL11A1*. The potential side effects of *COL11A1* targeting can be predicted based on the phenotypes of mice and humans expressing mutant nonfunctional forms of *COL11A1*. A homozygous truncating mutation of *COL11A1* in mice results in poorly formed cartilage [60], while human *COL11A1* mutations are associated with articular hypermobility, dermal hyperelasticity and widespread tissue fragility [61]. Of note, these collagenopathies are associated with the absence of *COL11A1* function throughout development and are unlikely to manifest upon transient targeting of *COL11A1* in adults. Additionally, since *COL11A1* and many of the pan-cancer *COL11A1*-coexpressed genes have multiple tissue-specific mRNA splicing isoforms, it will be valuable for future targeting purposes to determine if any mRNA isoforms are specifically expressed in activated CAFs [62].

Acknowledgments

We thank S. Swartwood (Biobank and Translational Research Core) for *in situ* hybridization; F. Chung (Pathology Service) for immunohistochemistry; G. Martins (Flow Cytometry Core) for assistance with FACS analysis; and K. Daniels for assistance with manuscript preparation. SO is supported by the Office of the Assistant Secretary of Defense for Health Affairs through the Ovarian Cancer Research Program Award No. W81XWH-14-1-0107 and W81XWH-16-1-0190, the National Cancer Institute grants R21CA194626-01 and 1R01CA208753-01, and the Cantor-UCLA Women's Health Center Executive Advisory Board & NCATS UCLA Clinical and Translational Science Institute grant UL1TR000124. BYK is supported by the American Cancer Society Early Detection Professorship Grant (SIOP-06-258-01-COUN). BYK, SO, KL and WRW are supported by the Ovarian Cancer Research Fund Program Project Development Award and DJC is supported by the Ovarian Cancer Research Fund Ann Shreiber Mentored Investigator Award. Opinions, interpretations, conclusions and recommendations are those of the authors and are not necessarily endorsed by the funding agencies.

Conflict of interest

The authors declare no conflict of interest.

Appendix: Supplementary material

Supplementary data to this article can be found online at doi:10.1016/j.canlet.2016.09.001.

References

- [1] R. Kalluri, M. Zeisberg, Fibroblasts in cancer, *Nat. Rev. Cancer* 6 (2006) 392–401.
- [2] B. Hinz, S.H. Phan, V.J. Thannickal, M. Prunotto, A. Desmouliere, J. Varga, et al., Recent developments in myofibroblast biology: paradigms for connective tissue remodeling, *Am. J. Pathol.* 180 (2012) 1340–1355.
- [3] A. Desmouliere, C. Guyot, G. Gabbiani, The stroma reaction myofibroblast: a key player in the control of tumor cell behavior, *Int. J. Dev. Biol.* 48 (2004) 509–517.
- [4] H.E. Barker, T.R. Cox, J.T. Eler, The rationale for targeting the LOX family in cancer, *Nat. Rev. Cancer* 12 (2012) 540–552.
- [5] M.J. Paszek, N. Zahir, K.R. Johnson, J.N. Lakins, G.I. Rozenberg, A. Gefen, et al., Tensional homeostasis and the malignant phenotype, *Cancer Cell* 8 (2005) 241–254.
- [6] P.P. Provenzano, D.R. Inman, K.W. Eliceiri, J.G. Knittel, L. Yan, C.T. Rueden, et al., Collagen density promotes mammary tumor initiation and progression, *BMC Med.* 6 (2008) 11.
- [7] D.F. Quail, J.A. Joyce, Microenvironmental regulation of tumor progression and metastasis, *Nat. Med.* 19 (2013) 1423–1437.
- [8] R.K. Jain, Normalizing tumor microenvironment to treat cancer: bench to bedside to biomarkers, *J. Clin. Oncol.* 31 (2013) 2205–2218.
- [9] W. Qiu, M. Hu, A. Sridhar, K. Opeskin, S. Fox, M. Shipitsin, et al., No evidence of clonal somatic genetic alterations in cancer-associated fibroblasts from human breast and ovarian carcinomas, *Nat. Genet.* 40 (2008) 650–655.
- [10] J.N. Arnold, L. Magiera, M. Kraman, D.T. Fearon, Tumoral immune suppression by macrophages expressing fibroblast activation protein-alpha and heme oxygenase-1, *Cancer Immunol. Res.* 2 (2014) 121–126.
- [11] C. Feig, J.O. Jones, M. Kraman, R.J. Wells, A. Deonarine, D.S. Chan, et al., Targeting CXCL12 from FAP-expressing carcinoma-associated fibroblasts synergizes with anti-PD-L1 immunotherapy in pancreatic cancer, *Proc. Natl. Acad. Sci. U.S.A.* 110 (2013) 20212–20217.
- [12] M. Kraman, P.J. Bambrough, J.N. Arnold, E.W. Roberts, L. Magiera, J.O. Jones, et al., Suppression of antitumor immunity by stromal cells expressing fibroblast activation protein-alpha, *Science* 330 (2010) 827–830.
- [13] A. Lo, L.C. Wang, J. Scholler, J. Monslow, D. Avery, K. Newick, et al., Tumor-promoting desmoplasia is disrupted by depleting FAP-expressing stromal cells, *Cancer Res.* 75 (2015) 2800–2810.
- [14] M. Loeffler, J.A. Kruger, A.G. Niethammer, R.A. Reisfeld, Targeting tumor-associated fibroblasts improves cancer chemotherapy by increasing intratumoral drug uptake, *J. Clin. Invest.* 116 (2006) 1955–1962.
- [15] P.P. Provenzano, C. Cuevas, A.E. Chang, V.K. Goel, D.D. Von Hoff, S.R. Hingorani, Enzymatic targeting of the stroma ablates physical barriers to treatment of pancreatic ductal adenocarcinoma, *Cancer Cell* 21 (2012) 418–429.
- [16] B.C. Ozdemir, T. Pentcheva-Hoang, J.L. Carstens, X. Zheng, C.C. Wu, T.R. Simpson, et al., Depletion of carcinoma-associated fibroblasts and fibrosis induces immunosuppression and accelerates pancreas cancer with reduced survival, *Cancer Cell* 25 (2014) 719–734.
- [17] M.R. Junttila, F.J. de Sauvage, Influence of tumour micro-environment heterogeneity on therapeutic response, *Nature* 501 (2013) 346–354.
- [18] A. Kawase, G. Ishii, K. Nagai, T. Ito, T. Nagano, Y. Murata, et al., Podoplanin expression by cancer associated fibroblasts predicts poor prognosis of lung adenocarcinoma, *Int. J. Cancer* 123 (2008) 1053–1059.
- [19] M.J. Ronty, S.K. Leivonen, B. Hinz, A. Rachlin, C.A. Otey, V.M. Kahari, et al., Isoform-specific regulation of the actin-organizing protein plectin during TGF-beta1-induced myofibroblast differentiation, *J. Invest. Dermatol.* 126 (2006) 2387–2396.
- [20] T.A. Brentnall, L.A. Lai, J. Coleman, M.P. Bronner, S. Pan, R. Chen, Arousal of cancer-associated stroma: overexpression of plectin activates fibroblasts to promote tumor invasion, *PLoS ONE* 7 (2012) e30219.
- [21] O. De Wever, Q.D. Nguyen, L. Van Hoorde, M. Bracke, E. Bruyneel, C. Gespach, et al., Tenascin-C and SF/HGF produced by myofibroblasts in vitro provide convergent pro-invasive signals to human colon cancer cells through RhoA and Rac, *FASEB J.* 18 (2004) 1016–1018.
- [22] K. Pietras, J. Pahler, G. Bergers, D. Hanahan, Functions of paracrine PDGF signaling in the proangiogenic tumor stroma revealed by pharmacological targeting, *PLoS Med.* 5 (2008) e19.
- [23] N. Erez, M. Truitt, P. Olson, S.T. Arron, D. Hanahan, Cancer-associated fibroblasts are activated in incipient neoplasia to orchestrate tumor-promoting inflammation in an NF-kappaB-dependent manner, *Cancer Cell* 17 (2010) 135–147.
- [24] H. Sugimoto, T.M. Mundel, M.W. Kieran, R. Kalluri, Identification of fibroblast heterogeneity in the tumor microenvironment, *Cancer Biol. Ther.* 5 (2006) 1640–1646.
- [25] F. Vazquez-Villa, M. Garcia-Ocana, J.A. Galvan, J. Garcia-Martinez, C. Garcia-Pravia, P. Menendez-Rodriguez, et al., COL11A1/(pro)collagen 11A1 expression is a remarkable biomarker of human invasive carcinoma-associated stromal cells and carcinoma progression, *Tumor Biol.* 36 (2015) 2213–2222.
- [26] Z. Raglow, S.M. Thomas, Tumor matrix protein collagen XIalpha1 in cancer, *Cancer Lett.* 357 (2015) 448–453.
- [27] R.J. Wenstrup, S.M. Smith, J.B. Florer, G. Zhang, D.P. Beason, R.E. Seegmiller, et al., Regulation of collagen fibril nucleation and initial fibril assembly involves coordinate interactions with collagens V and XI in developing tendon, *J. Biol. Chem.* 286 (2011) 20455–20465.
- [28] S.M. Smith, D.E. Birk, Focus on molecules: collagens V and XI, *Exp. Eye Res.* 98 (2012) 105–106.
- [29] P. Farmer, H. Bonnefoi, P. Anderle, D. Cameron, P. Wirapati, V. Becette, et al., A stroma-related gene signature predicts resistance to neoadjuvant chemotherapy in breast cancer, *Nat. Med.* 15 (2009) 68–74.
- [30] W.Y. Cheng, J.J. Kandel, D.J. Yamashiro, P. Canoll, D. Anastassiou, A multi-cancer mesenchymal transition gene expression signature is associated with prolonged time to recurrence in glioblastoma, *PLoS ONE* 7 (2012) e34705.
- [31] J. Boguslawska, H. Kedzierska, P. Poplawski, B. Rybicka, Z. Tanski, A. Piekietko-Witkowska, Expression of genes involved in cellular adhesion and ECM-remodelling correlates with poor survival of renal cancer patients, *J. Urol.* 195 (2016) 1892–1902.
- [32] D.J. Cheon, Y. Tong, M.S. Sim, J. Dering, D. Berel, X. Cui, et al., A collagen-remodeling gene signature regulated by TGF-beta signaling is associated with

- metastasis and poor survival in serous ovarian cancer, *Clin. Cancer Res.* 20 (2014) 711–723.
- [33] Y.H. Wu, T.H. Chang, Y.F. Huang, H.D. Huang, C.Y. Chou, COL11A1 promotes tumor progression and predicts poor clinical outcome in ovarian cancer, *Oncogene* 33 (2014) 3432–3440.
- [34] J.A. Beach, P.J. Aspuria, D.J. Cheon, K. Lawrenson, H. Agadjanian, C.S. Walsh, et al., Sphingosine kinase 1 is required for TGF-beta mediated fibroblast-to-myofibroblast differentiation in ovarian cancer, *Oncotarget* 7 (2016) 4167–4182.
- [35] G. Shin, T.W. Kang, S. Yang, S.J. Baek, Y.S. Jeong, S.Y. Kim, GENT: gene expression database of normal and tumor tissues, *Cancer Inform.* 10 (2011) 149–157.
- [36] A.J. Gentles, S.V. Bratman, L.J. Lee, J.P. Harris, W. Feng, R.V. Nair, et al., Integrating tumor and stromal gene expression signatures with clinical indices for survival stratification of early-stage non-small cell lung cancer, *J. Natl. Cancer Inst.* 107 (2015).
- [37] E. Cerami, J. Gao, U. Dogrusoz, B.E. Gross, S.O. Sumer, B.A. Aksoy, et al., The cBio cancer genomics portal: an open platform for exploring multidimensional cancer genomics data, *Cancer Discov.* 2 (2012) 401–404.
- [38] T.Z. Tan, H. Yang, J.R. Ye, J. Low, M. Choolani, D.S.P. Tan, et al., CSIOVDB: a microarray gene expression database of epithelial ovarian cancer subtype, *Oncotarget* 6 (2015) 43843–43852.
- [39] S. Julien, A. Merino-Trigo, L. Lacroix, M. Pocard, D. Goere, P. Mariani, et al., Characterization of a large panel of patient-derived tumor xenografts representing the clinical heterogeneity of human colorectal cancer, *Clin. Cancer Res.* 18 (2012) 5314–5328.
- [40] T.L. Yeung, C.S. Leung, K.K. Wong, G. Samimi, M.S. Thompson, J. Liu, et al., TGF-beta modulates ovarian cancer invasion by upregulating CAF-derived versican in the tumor microenvironment, *Cancer Res.* 73 (2013) 5016–5028.
- [41] K. Lawrenson, B. Grun, N. Lee, P. Mhawech-Fauceglia, J. Kan, S. Swenson, et al., NPPB is a novel candidate biomarker expressed by cancer-associated fibroblasts in epithelial ovarian cancer, *Int. J. Cancer* 136 (2015) 1390–1401.
- [42] T.Z. Tan, Q.H. Miow, Y. Miki, T. Noda, S. Mori, R.Y. Huang, et al., Epithelial-mesenchymal transition spectrum quantification and its efficacy in deciphering survival and drug responses of cancer patients, *EMBO Mol. Med.* 6 (2014) 1279–1293.
- [43] G. Consortium, The Genotype-Tissue Expression (GTEx) project, *Nat. Genet.* 45 (2013) 580–585.
- [44] R. Kalluri, R.A. Weinberg, The basics of epithelial-mesenchymal transition, *J. Clin. Invest.* 119 (2009) 1420–1428.
- [45] T. Shay, J. Kang, Immunological Genome Project and systems immunology, *Trends Immunol.* 34 (2013) 602–609.
- [46] R.A. Moffitt, R. Marayati, E.L. Flate, K.E. Volmar, S.G. Loeza, K.A. Hoadley, et al., Virtual microdissection identifies distinct tumor- and stroma-specific subtypes of pancreatic ductal adenocarcinoma, *Nat. Genet.* 47 (2015) 1168–1178.
- [47] R.G. Verhaak, P. Tamayo, J.Y. Yang, D. Hubbard, H. Zhang, C.J. Creighton, et al., Prognostically relevant gene signatures of high-grade serous ovarian carcinoma, *J. Clin. Invest.* 123 (2013) 517–525.
- [48] R. Cristescu, J. Lee, M. Nebozhyn, K.M. Kim, J.C. Ting, S.S. Wong, et al., Molecular analysis of gastric cancer identifies subtypes associated with distinct clinical outcomes, *Nat. Med.* 21 (2015) 449–456.
- [49] J. Guinney, R. Dienstmann, X. Wang, A. de Reynies, A. Schlicker, C. Soneson, et al., The consensus molecular subtypes of colorectal cancer, *Nat. Med.* 21 (2015) 1350–1356.
- [50] A.P. Bento, A. Gaulton, A. Hersey, L.J. Bellis, J. Chambers, M. Davies, et al., The ChEMBL bioactivity database: an update, *Nucleic Acids Res.* 42 (2014) D1083–D1090.
- [51] M. Egeblad, M.G. Rasch, V.M. Weaver, Dynamic interplay between the collagen scaffold and tumor evolution, *Curr. Opin. Cell Biol.* 22 (2010) 697–706.
- [52] I. Malanchi, A. Santamaria-Martinez, E. Susanto, H. Peng, H.A. Lehr, J.F. Delafoye, et al., Interactions between cancer stem cells and their niche govern metastatic colonization, *Nature* 481 (2012) 85–89.
- [53] J. Massague, TGFbeta signalling in context, *Nat. Rev. Mol. Cell Biol.* 13 (2012) 616–630.
- [54] E.C. Connolly, J. Freimuth, R.J. Akhurst, Complexities of TGF-beta targeted cancer therapy, *Int. J. Biol. Sci.* 8 (2012) 964–978.
- [55] S. Kubota, M. Takigawa, Cellular and molecular actions of CCN2/CTGF and its role under physiological and pathological conditions, *Clin. Sci.* 128 (2015) 181–196.
- [56] M. Johannsen, G. Spitaleri, G. Curigliano, J. Roigas, S. Weikert, C. Kempkensteffen, et al., The tumour-targeting human L19-IL2 immunocytokine: preclinical safety studies, phase I clinical trial in patients with solid tumours and expansion into patients with advanced renal cell carcinoma, *Eur. J. Cancer* 46 (2010) 2926–2935.
- [57] T.K. Eigentler, B. Weide, F. de Braud, G. Spitaleri, A. Romanini, A. Pflugfelder, et al., A dose-escalation and signal-generating study of the immunocytokine L19-IL2 in combination with dacarbazine for the therapy of patients with metastatic melanoma, *Clin. Cancer Res.* 17 (2011) 7732–7742.
- [58] E. Tran, D. Chinnasamy, Z. Yu, R.A. Morgan, C.C. Lee, N.P. Restifo, et al., Immune targeting of fibroblast activation protein triggers recognition of multipotent bone marrow stromal cells and cachexia, *J. Exp. Med.* 210 (2013) 1125–1135.
- [59] E.W. Roberts, A. Deonarine, J.O. Jones, A.E. Denton, C. Feig, S.K. Lyons, et al., Depletion of stromal cells expressing fibroblast activation protein-alpha from skeletal muscle and bone marrow results in cachexia and anemia, *J. Exp. Med.* 210 (2013) 1137–1151.
- [60] Y. Li, D.A. Lacerda, M.L. Warman, D.R. Beier, H. Yoshioka, Y. Ninomiya, et al., A fibrillar collagen gene, Col11a1, is essential for skeletal morphogenesis, *Cell* 80 (1995) 423–430.
- [61] J. Spranger, The type XI collagenopathies, *Pediatr. Radiol.* 28 (1998) 745–750.
- [62] U.H. Weidle, D. Maisel, S. Klostermann, E.H. Weiss, M. Schmitt, Differential splicing generates new transmembrane receptor and extracellular matrix-related targets for antibody-based therapy of cancer, *Cancer Genomics Proteomics* 8 (2011) 211–226.



A Paradoxical Correlation of Cancer-Associated Fibroblasts With Survival Outcomes in B-Cell Lymphomas and Carcinomas

Marcela Haro¹ and Sandra Orsulic^{1,2,3*}

¹ Women's Cancer Program at the Samuel Oschin Comprehensive Cancer Institute, Cedars-Sinai Medical Center, Los Angeles, CA, United States, ² Department of Biomedical Sciences, Cedars-Sinai Medical Center, Los Angeles, CA, United States, ³ Department of Obstetrics and Gynecology, David Geffen School of Medicine, University of California, Los Angeles, Los Angeles, CA, United States

OPEN ACCESS

Edited by:

Lucio Miele,
LSU Health Sciences Center New
Orleans, United States

Reviewed by:

Deyin Xing,
Johns Hopkins University,
United States
Lasse Dahl Ejby Jensen,
Linköping University, Sweden

*Correspondence:

Sandra Orsulic
Sandra.Orsulic@cshs.org

Specialty section:

This article was submitted to
Molecular Medicine,
a section of the journal
Frontiers in Cell and Developmental
Biology

Received: 28 May 2018

Accepted: 09 August 2018

Published: 28 August 2018

Citation:

Haro M and Orsulic S (2018) A
Paradoxical Correlation
of Cancer-Associated Fibroblasts
With Survival Outcomes in B-Cell
Lymphomas and Carcinomas.
Front. Cell Dev. Biol. 6:98.
doi: 10.3389/fcell.2018.00098

The tumor microenvironment is increasingly recognized as an active participant in tumor progression. A recent pan-cancer genomic profile analysis has revealed that gene signatures representing components of the tumor microenvironment are robust predictors of survival. A stromal gene signature representing fibroblasts and extracellular matrix components has been associated with good survival in diffuse large B-cell lymphoma (DLBCL). Paradoxically, a closely related gene signature has been shown to correlate with poor survival in carcinomas, including breast, ovarian, pancreatic, and colorectal cancer. To date, there has been no explanation for this paradoxical inverse correlation with survival outcomes in DLBCL and carcinomas. Using public gene data sets, we confirm that the DLBCL stromal gene signature is associated with good survival in DLBCL and several other B-cell lymphomas while it is associated with poor survival in ovarian cancer and several other solid tumors. We show that the DLBCL stromal gene signature is enriched in lymphoid fibroblasts in normal lymph nodes and in cancer-associated fibroblasts (CAFs) in ovarian cancer. Based on these findings, we propose several possible mechanisms by which CAFs may contribute to opposite survival outcomes in B-cell lymphomas and carcinomas.

Keywords: B cells, B-cell lymphoma, CAFs, cancer-associated fibroblasts, DLBCL, gene signature, ovarian cancer, tumor microenvironment

INTRODUCTION

During the past decade, gene expression profile analyses of frozen tumor pieces have been widely used to quantify various biological characteristics of malignant tumor cells and the microenvironment in which they reside. Individual biological characteristics and dominant molecular pathways in tumors are frequently associated with expression of a defined set of genes,

Abbreviations: CAF, cancer-associated fibroblast; CD, cluster of differentiation; CXCL, C-X-C motif chemokine ligand; DC, dendritic cells; DLBCL, diffuse large B-cell lymphoma; ECM, extracellular matrix; FDC, follicular dendritic cells; FRC, fibroblastic reticular cells; GC, germinal center; Ig, immunoglobulin; ImmGen, immunological genome project; IPA, ingenuity pathway analysis; MRC, marginal reticular cells; NK, natural killer; PDGFR α , platelet-derived growth factor receptor α ; PDPN, podoplanin; PRECOG, PREDiction of Clinical Outcomes from genomic profiles; TCGA, the Cancer genome atlas project; TGF β , transforming growth factor β ; TIL, tumor infiltrating lymphocyte; TLS, tertiary lymphoid structure.

known as a gene expression signature. Since phenotypic features represented by gene expression signatures are sometimes associated with clinical features, such as the length of survival of cancer patients or their response to therapy, gene expression signatures can be used as quantitative predictors of clinical outcomes. A recent pan-cancer PREdiction of Clinical Outcomes from Genomic Profiles (PRECOG) analysis revealed that genes in the tumor microenvironment are better predictors of survival than genes expressed in malignant tumor cells (Gentles et al., 2015). The two most prominent components in the microenvironment of solid tumors are fibroblasts and immune cells (Aran et al., 2017). Generally, in carcinomas, genes expressed in fibroblasts are associated with poor survival while genes expressed in immune cells, particularly leukocytes, are associated with good survival (Gentles et al., 2015). Tumor infiltrating lymphocytes (TILs) and tertiary lymphoid structures (TLS) are generally associated with improved clinical outcomes as evidenced by the improved overall survival and disease-free survival in various types of tumors (Fridman et al., 2012; Dieu-Nosjean et al., 2014; Barnes and Amir, 2017). However, depending on the type of tumor, tumor stage, and location of TILs within the tumor (tumor bed, invasive margin and stroma), different types of TILs have been associated with both positive and negative prognosis. For example, cytotoxic CD8+ T cells, memory T cells, and CD4+ T helper cells are generally associated with a better prognosis, whereas T regulatory cells, tumor associated macrophages, and myeloid-derived suppressor cells are associated with poor prognosis and can promote tumor progression (Fridman et al., 2012; Kitamura et al., 2015; Barnes and Amir, 2017). Furthermore, fibroblasts in the tumor microenvironment are phenotypically heterogeneous and may exhibit both a pro- and anti-tumorigenic phenotype (Augsten, 2014). Thus, the tumor microenvironment is a complex network of interaction between tumor cells and components of the stroma, including the extracellular matrix (ECM), and it is currently unclear which factors in the tumor microenvironment control the quantity and distribution of different immune cell subtypes. Specifically, it is unknown if fibroblasts and immune cells affect prognosis independently or through an interdependent interaction.

The functional interaction between fibroblasts and immune cells has been most thoroughly studied in normal lymph nodes and the spleen, where specialized fibroblasts produce ECM to form a network that allows for lymphocyte movement along the matrix in response to chemokine signaling. The presence of lymphoid fibroblasts is necessary for functional attraction, retention, compartmentalization, and survival of immune cells (Koning and Mebius, 2012). Lymphoid fibroblasts are crucial for lymphocyte homeostasis as well as controlling and expanding the lymphocyte pool (Mueller and Germain, 2009). Lymphoid fibroblasts are also key players in mediating functional immune cell interactions in the lymph nodes through direct contact or via secreted molecules (Chang and Turley, 2015). Follicular dendritic cells (FDC) attract B cells to the germinal center (GC) by secreting C-X-C motif chemokine

ligand 13 (CXCL13), while marginal reticular cells (MRC) use a network of follicular conduits to deliver antigens to cognate B cells (Chang and Turley, 2015). By secreting C-C motif chemokine ligands 19 and 21 (CCL19 and CCL21), fibroblastic reticular cells (FRC) recruit mature dendritic cells (DC) and naïve B and T cells to promote cell-cell interactions within the T cell zone (Mueller and Germain, 2009; Brown and Turley, 2015; Fletcher et al., 2015). Recent studies have shown that FRC are important for B-cell homeostasis (Cremasco et al., 2014). This function has been previously ascribed to FDC, however, cell-specific depletion experiments demonstrated that only FRC are crucial for B-cell survival. The mechanism by which FRC support B-cell survival is not entirely clear, but it is thought to involve crosstalk with B cells to control the boundaries of primary B-cell follicles (Cyster, 2010; Mionnet et al., 2013; Cremasco et al., 2014).

Similar to lymphoid fibroblasts in normal lymph nodes, cancer-associated fibroblasts (CAFs) are stromal cells that produce ECM, provide scaffolding, and exert regulatory functions through growth factors, cytokines, and chemokines that can promote tumor growth, angiogenesis, invasion, and metastasis (Kalluri and Zeisberg, 2006; Levental et al., 2009; Lu et al., 2012; Spano and Zollo, 2012; Harper and Sainson, 2014). Recent studies provide evidence that CAFs can also directly or indirectly contribute to immune cell fate and survival (Harper and Sainson, 2014; Costa et al., 2018; Mariathasan et al., 2018; Tauriello et al., 2018). It has recently been shown that a gene signature representing activated CAFs is present in most epithelial tumors (Jia et al., 2016) despite the diversity of resident fibroblasts in different organs and the presence of multiple fibroblast populations within a single tumor type (Costa et al., 2018). Activated CAFs in breast cancer, and possibly in other carcinomas, are associated with immunosuppressive populations of T lymphocytes (Costa et al., 2018). It is unclear if activated CAFs in carcinomas are also associated with immunosuppressive populations of B cells due to poorly defined markers for such cells (Sarvaria et al., 2017). Moreover, studies investigating the associations of B cell subsets with tumor progression using defined B-cell markers have produced conflicting results even within the same tumor type (Guy et al., 2016). An insufficient understanding of the roles of B cells in carcinomas has hindered the development of rational clinical trials targeting B-cells in carcinomas. The remarkable success of B-cell depletion with the cluster of differentiation 20 (CD20) monoclonal antibody, rituximab, in lymphomas and rheumatoid arthritis has sparked interest in rituximab and other B-cell targeted antibodies as possible therapies in carcinomas (Gundersen and Coussens, 2013). Although many carcinomas have significant B cell infiltration (Germain et al., 2014), clinical trials have shown limited benefits of B-cell depletion in carcinomas (Barbera-Guillem et al., 2000; Aklilu et al., 2004), possibly because B cells can have pro-tumorigenic or anti-tumorigenic properties depending on their maturation stage and other conditions that have not yet been defined (Sarvaria et al., 2017).

TABLE 1 | DLBCL “stromal-1” signature genes are inversely correlated with survival outcomes in B-cell lymphomas and other malignancies.

Gene	B-cell lymphoma						Solid tumor					
	BL	CLL	DLBCL	FL	MCL	MM	Bladder	Astrocytoma	Glioma	Colon	Head and neck	Ovarian
ACTN1	-0.928	-3.216	-6.211	-1.901	-0.94	0.658	3.312	3.22	4.557	2.36	1.988	1.552
ADAM12	0.746	-0.084	-7.809	-1.749	-0.866	-0.395	0.537	1.653	4.405	1.675	2.051	2.99
BGN	0.842	1.309	-4.115	-1.775	0	-2.627	1.438	2.341	3.643	2.33	3.559	3.09
CEBPA	-1.516	-3.127	-5.644	-1.639	0	-0.977	1.001	-0.041	2.652	-2.664	-1.578	-1.442
COL13A1	-0.313	-1.513	-2.402	0.332	0	-0.001	2.23	2.006	1.613	2.164	1.74	0.893
COL16A1	-0.481	0.252	-3.89	-0.6	0.333	-0.477	2.214	2.49	5.005	-0.546	1.263	4.542
COL1A1	0.349	-1.476	-4.621	-1.581	0	-1.951	3.592	3.326	3.77	1.544	3.354	3.929
COL1A2	-0.097	-0.879	-6.264	-1.605	0	-0.573	2.745	4.432	4.391	2.42	2.634	3.771
COL5A1	0.715	-0.675	-3.366	0.127	0	-0.467	1.957	3.528	4.438	2.328	3.686	3.65
COL5A2	0.969	1.124	-3.962	-1.597	0	-0.777	3.47	3.588	7.322	2.437	3.26	5.256
COL6A2	0.677	-1.368	-3.719	-0.749	-1.415	0.14	2.369	4.591	5.693	1.301	3.12	2.11
COL6A3	1.194	-0.129	-4.502	-1.442	1.37	2.684	1.282	3.005	3.071	2.403	3.141	3.178
COL8A2	-0.212	-0.894	-3.046	0.069	0	-0.905	-0.085	2.942	3.077	-0.007	1.779	2.908
CSF2RA	-1.84	0	-2.861	0	0	-2.39	-0.046	0.193	0	0	0	-1.959
CTGF	-0.5	0.796	-5.525	-0.73	-1.387	-0.775	1.651	1.676	-1.132	2.024	2.381	2.974
CYR61	1.159	0.092	-1.865	0.074	1.837	-0.123	3.342	1.159	3.807	1.678	1.757	3.607
DCN	0.819	0.185	-3.731	-0.026	0	-0.794	0.472	1.113	2.414	1.303	0.917	4.604
EFEMP2	1.823	1.113	-2.797	0.307	0	-5.014	2.112	4.044	7.62	1.684	3.53	2.576
EMP2	-0.057	0.044	-4.122	0.147	0	-0.579	-1.125	4.55	2.985	-0.368	0.452	-1.446
FAP	-1.551	0.374	-7.496	-0.76	-1.266	-0.536	3.522	2.321	3.736	2.366	2.874	4.814
FBN1	1.125	1.079	-4.907	-1.854	0	-0.044	2.151	1.518	2.239	2.311	1.906	4.676
FN1	-1.025	-0.496	-5.638	-1.852	-1.352	2.973	3.251	2.852	5.499	2.628	2.46	4.439
GNPMB	-1.638	-0.153	-6.899	0.513	0	1.112	1.281	3.946	5.214	1.74	-2.745	1.476
HSPG2	-0.267	2.244	-2.792	-1.63	0	0.845	-0.02	4.261	2.989	1.313	2.108	2.396
IL1R1	-1.566	-2.791	-4.858	-0.432	0.804	-1.789	-0.186	1.194	1.217	1.275	0.897	-0.137
ITGAV	0.897	-2.698	-6.933	0.614	-2.033	-0.212	0.402	0.945	0.226	2.253	1.503	1.792
ITGB2	-1.522	-2.053	-5.68	0.558	0.343	-1.803	0.886	0.4	4.299	-0.086	-2.064	-2.339
KITLG	0.896	-0.172	-1.923	1.04	-1.197	0.454	1.113	-0.331	1.091	1.164	-0.721	-0.504
LAMA4	0.445	2.207	-3.683	0.453	0	-3.155	2.474	0.028	3.397	2.415	2.021	2.168
LAMB2	-0.635	0.504	-1.974	-1.052	0	-0.728	0.926	1.686	5.906	0.913	1.836	2.326
LAMB3	1.291	-1.315	-2.703	0.256	0	0.265	-0.927	1.977	3.542	1.516	2.039	-1.966
LOXL1	-1.453	-1.007	-4.202	-1.287	0	-1.92	0.711	3.9	6.299	1.697	0.751	3.664
LTBP2	0.219	-1.562	-7.565	-0.187	0	-1.848	2.849	1.197	3.314	0.542	2.718	1.541
LUM	-0.357	-1.043	-5.663	-0.089	0	-1.859	1.442	3.796	3.723	1.447	1.428	4.841
MFAP2	0.862	0.01	-2.835	0.608	0	-0.68	3.151	3.543	3.011	0.874	1.666	5.462
MMP14	-1.105	2.746	-3.319	0.69	0.681	-1.647	2.046	1.787	4.691	1.786	1.168	2.297
MMP2	-1.227	-0.269	-5.709	-1.128	0.014	-0.545	0.66	1.792	3.631	1.567	3.12	3.084
MMP9	-0.819	-1.238	-7.734	-0.401	-0.12	-0.892	1.8	2.739	5.06	-0.723	0.039	-3.208
PDGFC	0.62	-3.08	-4.268	0.632	0	-0.486	2.788	-3.419	3.639	1.987	2.096	-0.167
PLAU	-1.723	-1.701	-7.712	0.205	0.528	-0.749	2.515	2.302	4.592	0.627	1.521	2.334
POSTN	1.565	0.675	-5.031	-1.266	-0.77	-1.157	3.246	2.76	5.46	2.632	2.092	4.696
SDC2	-0.209	-1.963	-3.763	-0.47	-0.383	-0.664	-1.091	1.405	5.736	2.239	1.659	1.424
SERPINH1	-1.173	2.067	-2.912	-1.224	0	1.565	1.422	3.846	5.397	3.044	2.065	2.07
SPARC	0.487	-3.125	-7.236	-1.599	1.012	-2.767	2.24	-1.998	-0.074	2.412	2.933	4.188
TGFB11	-0.842	-1.479	-2.367	0.662	0	-1.787	1.518	2.783	4.58	1.523	3.557	4.265
THBS1	1.462	-3.212	-2.038	-1.38	0.238	-1.674	1.673	2.947	3.122	0.799	2.328	3.565
TIMP2	-0.677	-2.448	-1.399	1.006	0.343	0.83	2.608	1.584	1.251	2.73	2.271	2.495
VCAN	1.459	-3.803	-3.177	-0.588	0	-2.078	3.133	-3.546	-3.171	2.264	2.238	4.277

Analysis of the DLBCL “stromal-1” geneset in the PREDiction of Clinical Outcomes from Genomic Profiles (PRECOG) public dataset (<https://precog.stanford.edu>). Each gene is assigned z scores associated with survival in different cancer types. Scores less than or equal to zero (red) are associated with good survival while positive scores (blue) are associated with poor survival. BL, Burkitt lymphoma; CLL, chronic lymphocytic leukemia; DLBCL, diffuse large B-cell lymphoma; FL, follicular lymphoma; MCL, mantle cell lymphoma; MM, multiple myeloma.

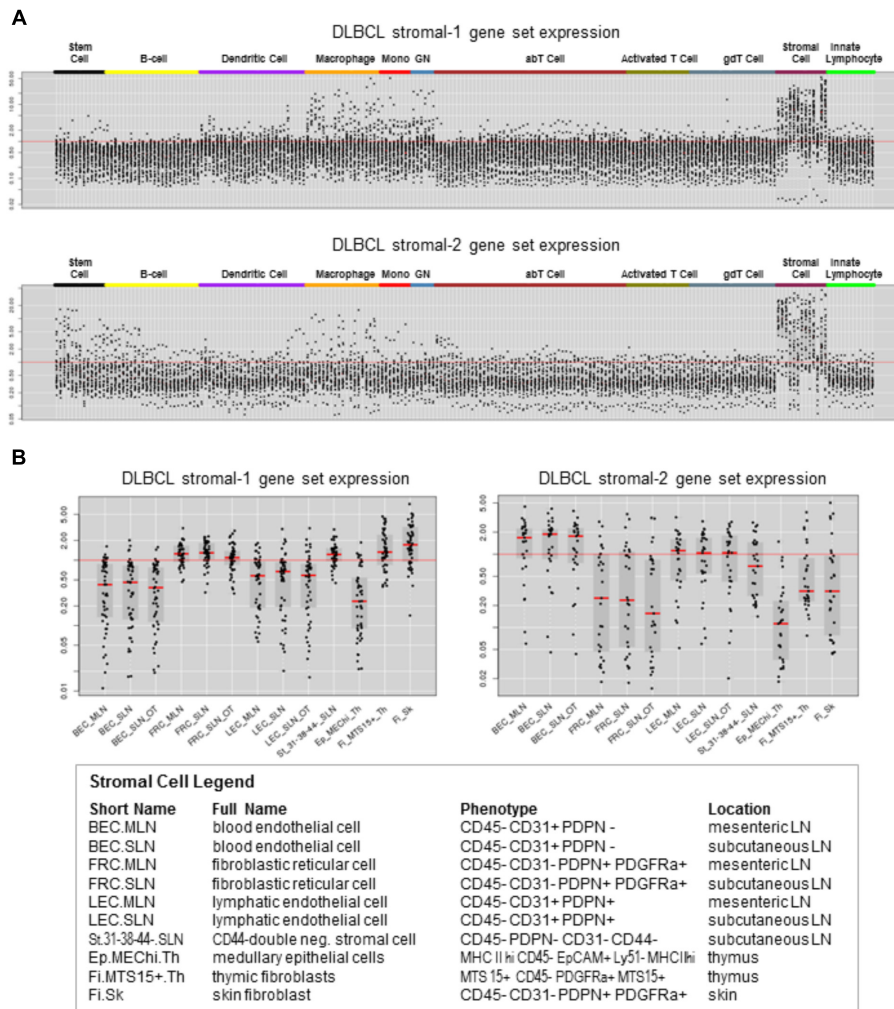


FIGURE 1 | DLBCL stromal-1 and stromal-2 signature genes are enriched in different stromal cell types. Expression of the DLBCL stromal-1 and stromal-2 signature genes in the Immunological Genome Project (ImmGen) data set. **(A)** Gene expression values normalized across 249 mouse immunological cell types. **(B)** Detailed view of gene expression values normalized to the stromal cell types shown in the legend. The graphs were generated using data from ImmGen (<http://www.immgen.org>).

THE DLBCL STROMAL-1 GENE SIGNATURE IS INVERSELY CORRELATED WITH SURVIVAL OUTCOMES IN B-CELL LYMPHOMAS AND OTHER SOLID TUMORS

Using expression profile analysis of DLBCL biopsy samples from treatment-naïve newly diagnosed patients, Lenz et al. identified two stromal gene signatures, stromal-1 and stromal-2, of which the stromal-1 gene signature was found to be associated with good survival in DLBCL patients (Lenz et al., 2008). However, gene signatures similar to the DLBCL stromal-1 gene signatures have been associated with poor survival in carcinomas, including ovarian cancer (Cheon et al., 2014), breast cancer (Farmer et al., 2009), colorectal cancer (Calon et al., 2015; Isella et al., 2015), and pancreatic cancer (Moffitt et al., 2015).

To systematically explore the association of the DLBCL stromal-1 gene signature with survival in cancer patients, we used PRECOG, a pan-cancer database of expression signatures in which each tumor type is represented by multiple independent expression profile data sets and associated survival data. This extensive database is ideal for multi-data set validation of prognostic signatures that have been identified in individual data sets. Using the DLBCL stromal-1 gene signature represented by 50 genes (Lenz et al., 2008), we confirmed that the signature is associated with poor survival in carcinomas and brain tumors and good survival in DLBCL and several other B-cell lymphomas (Table 1). This pattern of inverse association with survival between B-cell lymphomas and carcinomas/brain tumors was specific to the DLBCL stromal-1 gene signature, and was not associated with the DLBCL stromal-2 gene signature represented by 34 genes (Lenz et al., 2008) (data not shown).

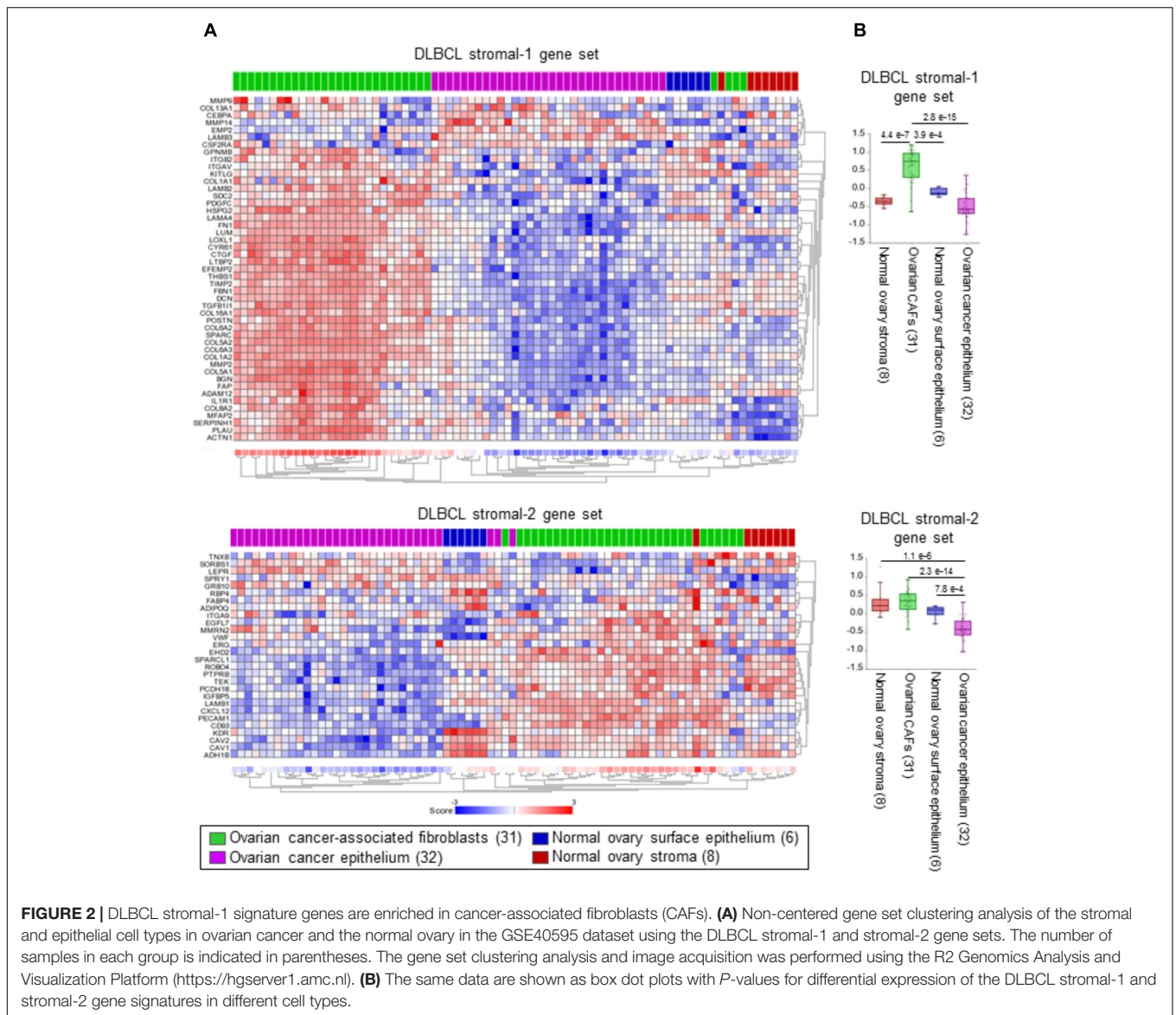


FIGURE 2 | DLBCL stromal-1 signature genes are enriched in cancer-associated fibroblasts (CAFs). **(A)** Non-centered gene set clustering analysis of the stromal and epithelial cell types in ovarian cancer and the normal ovary in the GSE40595 dataset using the DLBCL stromal-1 and stromal-2 gene sets. The number of samples in each group is indicated in parentheses. The gene set clustering analysis and image acquisition was performed using the R2 Genomics Analysis and Visualization Platform (<https://hgserver1.amc.nl>). **(B)** The same data are shown as box dot plots with *P*-values for differential expression of the DLBCL stromal-1 and stromal-2 gene signatures in different cell types.

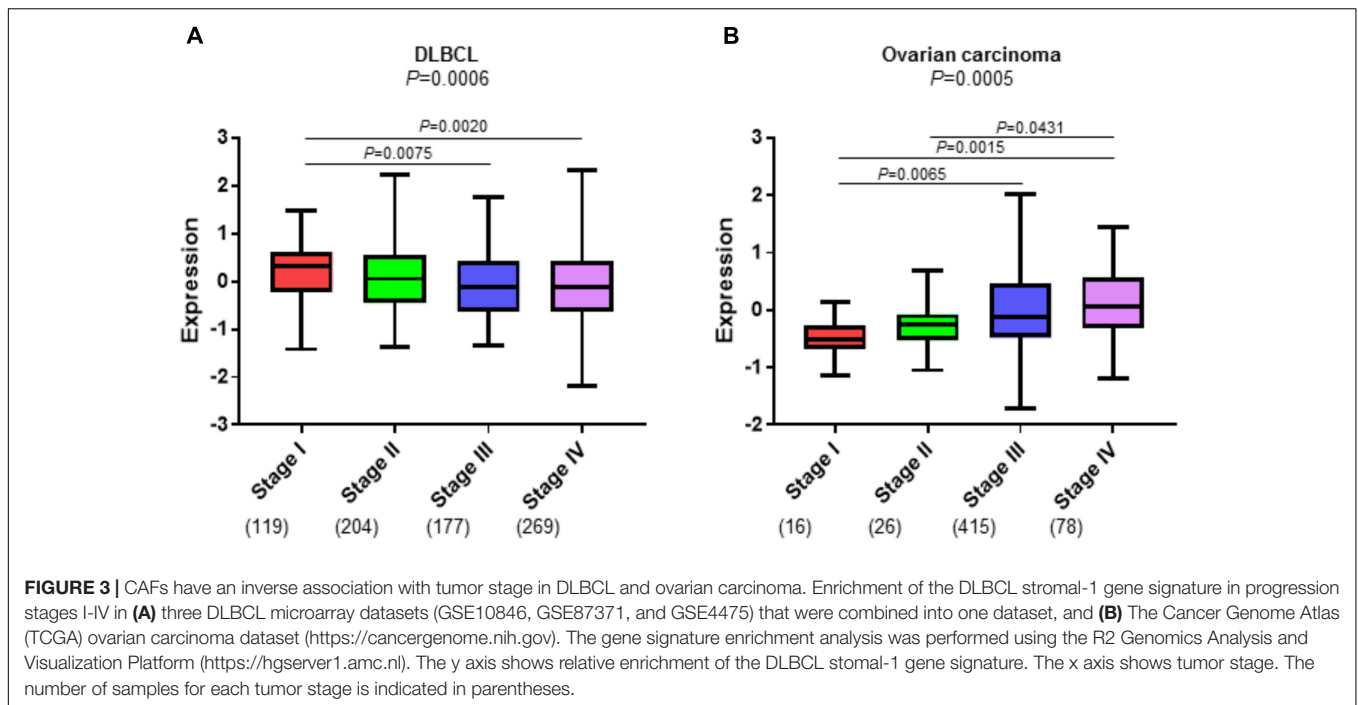
IN NORMAL LYMPH NODES, DLBCL STROMAL-1 AND STROMAL-2 GENE SIGNATURES ARE ENRICHED IN STROMAL FIBROBLASTS AND ENDOTHELIAL CELLS, RESPECTIVELY

To identify immune cell types that express the DLBCL stromal-1 and stromal-2 signature genes, we looked for enrichment of these genes in the transcriptomes of 249 normal immunological cell types that had been isolated from mice and characterized by the Immunological Genome Project (ImmGen) (Heng and Painter, 2008; Shay and Kang, 2013). This analysis identified stromal cells as the most likely source of both gene signatures, although some of the genes were also expressed in macrophages, monocytes, granulocytes, and stem cells (Figure 1A). Closer examination of the stromal cell subtypes revealed that the DLBCL

stromal-1 and stromal-2 signature genes were preferentially expressed in different types of stromal cells. DLBCL stromal-1 signature genes were particularly enriched in cells characterized by expression of podoplanin (PDPN) and platelet-derived growth factor receptor α (PDGFR α), including FRC from mesenteric and subcutaneous lymph nodes and the so-called double-negative stromal cells, while stromal-2 signature genes were enriched in blood and lymphatic endothelial cells (Figure 1B).

THE DLBCL STROMAL-1 GENE SIGNATURE IS ENRICHED IN OVARIAN CAFs

To identify cells that express the DLBCL stromal-1 and stromal-2 signature genes in an epithelial tumor, we selected



ovarian cancer because of the existing microarray data set (GSE40595) in which a large number of ovarian cancers have been laser capture microdissected into epithelial and stromal components (Yeung et al., 2013). For comparison with normal tissue, a small number of samples in this data set were microdissected from the normal ovary epithelium and stroma (Yeung et al., 2013). Our gene signature enrichment analysis revealed strong enrichment of the DLBCL stromal-1 gene signature in CAFs in comparison to cancer cells, normal ovary fibroblasts, and normal ovary epithelial cells (Figure 2). The DLBCL stromal-2 gene signature was enriched in CAFs but also in the normal ovary stroma (Figure 2).

POSSIBLE MECHANISMS BY WHICH CAFs CONTRIBUTE TO INVERSE SURVIVAL OUTCOMES IN B-CELL LYMPHOMAS AND CARCINOMAS

It is unusual for a gene signature to be associated with inverse survival outcomes in B-cell lymphomas and carcinomas. This is unlikely to be a technical error related to microarray technology as several individual genes from the DLBCL stromal-1 signature have been validated as predictors of good survival in DLBCL by independent technologies, such as immunohistochemistry and qPCR in formalin-fixed paraffin-embedded tissues (Lossos et al., 2004; Meyer et al., 2011; Tekin et al., 2016). Similarly, various technologies have been used to validate many of the signature genes as predictors of poor survival in carcinomas (Farmer et al., 2009; Cheon et al., 2014; Calon et al., 2015; Isella et al., 2015;

TABLE 2 | Upstream regulators of genes in the DLBCL stromal gene signature-1 and stromal gene signature-2.

Upstream regulator	Molecule type	p-value of overlap
DLBCL stromal-1 gene signature		
TGFB1	Growth factor	4.78E-31
COLQ	Other	2.70E-20
Bleomycin	Chemical drug	1.97E-18
SPDEF	Transcription regulator	2.73E-18
Tgf beta	Group	3.95E-18
TGFB3	Growth factor	8.04E-18
TNF	Cytokine	1.53E-17
DLBCL stromal-2 gene signature		
KLF2	Transcription regulator	1.89E-09
Rosiglitazone	Chemical drug	5.82E-09
VEGFA	Growth factor	5.90E-09
PPARG	Ligand-dependent nuclear receptor	1.36E-08
10E,12Z-octadecadienoic acid	Chemical – endogenous Mammalian	4.98E-08
WNT3A	Cytokine	6.02E-08
MGEA5	Enzyme	1.08E-07

The identification of upstream regulators was done using Ingenuity Pathway Analysis (www.qiagenbioinformatics.com/products/ingenuity-pathway-analysis/).

Moffitt et al., 2015; Jia et al., 2016). While the mechanism by which the DLBCL stromal-1 signature genes could contribute to good survival in DLBCL is still unclear, multiple mechanisms by which CAFs contribute to poor outcomes in carcinomas

have been proposed, including the promotion of tumor growth, angiogenesis, invasion and metastasis, the provision of protective niches for cancer stem cells, and the obstruction of access of chemotherapies and immunotherapies (Jain, 2013; Kalluri, 2016). Here, we will specifically focus on the possible direct or indirect roles of CAFs that could contribute to inverse survival outcomes in DLBCL and carcinomas.

Cancer-associated fibroblasts share structural and molecular features with the reticular fiber networks of secondary lymphoid organs, which are known to guide and compartmentalize specific immune cell types and play key roles in mediating functional immune cell interactions (Acton et al., 2012; Astarita et al., 2012; Cremasco et al., 2014; Chang and Turley, 2015; Fletcher et al., 2015; Turley et al., 2015). However, in addition to being sites in which immune responses are initiated, secondary lymphoid organs are also sites that foster immune privilege that prevents autoimmunity by inducing tolerance and deleting autoreactive T cells, suppressing effector T cell proliferation, and supporting regulatory T cells (Fletcher et al., 2011, 2014, 2015; Brown and Turley, 2015). Currently, lymph node fibroblasts are being explored for their therapeutic potential to circumvent unwanted inflammation in autoimmune diseases, sepsis, and graft rejection after organ transplantation (Fletcher et al., 2011, 2014, 2015). Based on the molecular similarity between CAFs and lymph node fibroblasts, we propose that CAFs primarily play an immunosuppressive role in tumors using similar molecular mechanisms to those used by lymph node fibroblasts in regulating immune cell tolerance and homeostasis. In support of this hypothesis, CAF-derived factors have been shown to contribute to immune editing *in vivo* to avoid tumor detection and rejection by the host immune system (Stover et al., 2007; Kraman et al., 2010). Specific to B cells, several *in vitro* models have shown the ability of different types of fibroblasts to modulate B cell differentiation, activation, and function. Adipose tissue-derived fibroblasts have been shown to suppress plasmablast formation and induce formation of regulatory B cells (Franquesa et al., 2015) while rheumatoid synovial fibroblasts have been shown to induce immunoglobulin (Ig) class-switch recombination and IgG/IgA production in IgD⁺ B cells (Bombardieri et al., 2011). We envision that the immunoregulatory functions of CAFs may lead to improved survival in DLBCL and other B-cell lymphomas where malignant cells themselves are subject to functional alteration. In contrast, immunosuppression by CAFs in carcinomas may lead to an ineffective immune defense against malignant cells, which is associated with poor survival.

Cancer-associated fibroblasts are also capable of modifying the immune landscape by selective attraction, recruitment, retention, activation, and suppression of different immune cell types (Karin, 2010; Raz and Erez, 2013; Harper and Sainson, 2014). Recent studies provide evidence that CAFs can directly contribute to immune cell fate and survival (Harper and Sainson, 2014). In mouse models, CAFs have been shown to attract macrophages, neutrophils, and subsets

of T cells that promote tumor progression (Silzle et al., 2003; Grum-Schwensen et al., 2010; Elkabets et al., 2011). One possible underlying mechanism for the association of the DLBCL stromal-1 gene signature with good survival in patients with DLBCL is that fibroblasts and the associated ECM attract and trap malignant B cells thereby impeding their spread to new anatomical locations. We show a small but consistent inverse association of the DLBCL stromal-1 gene signature expression with DLBCL tumor stage (a measure of lymph node groups and extranodal sites to which malignant cells have metastasized) (**Figure 3A**). The decrease in stromal gene signature expression in the later stages of DLBCL may indicate that the stroma plays a role in localizing the lymphoma cells to the lymph nodes during the earlier stages of the disease. In contrast, DLBCL stromal-1 gene signature expression is typically increased with increased tumor stage in epithelial carcinomas, such as ovarian cancer (**Figure 3B**). The increase in CAFs in the later stages of carcinomas may prevent immune cells from reaching the tumor parenchyma by trapping the immune cells in the stroma thereby preventing an anti-tumor response. A recent study of immune cell infiltration in metastatic urothelial carcinomas showed that patients whose tumors were classified as immune-excluded (immune cells localized in the CAF-rich stroma) had increased disease progression and decreased response to immunotherapy (Mariathasan et al., 2018). Therefore, we hypothesize that CAFs aid in retaining DLBCL in the lymph node, which is associated with better prognosis, whereas in carcinomas CAFs trap immune cells, which is associated with decreased anti-tumor immune activity and a worse prognosis.

One of the key modulators of the cancer microenvironment is the multifunctional cytokine, transforming growth factor β (TGF β). TGF β induces CAF activation and fibroblast-to-myofibroblast transition with consequent linearization of collagen fibers and stiffening of the ECM. In turn, activated CAFs induce TGF β signaling to perpetually maintain the activated state (Calon et al., 2014; Beach et al., 2016; Erdogan and Webb, 2017). Consistent with the DLBCL stromal-1 signature representing CAFs, our Ingenuity Pathway Analysis (IPA) of the DLBCL gene signatures implicates TGF β signaling as the main upstream regulator of the DLBCL stromal-1 gene signature (**Table 2**). In carcinomas, TGF β has been shown to promote tumor progression by inhibiting immunosurveillance through multiple mechanisms (Flavell et al., 2010; Sheng et al., 2015), including the recruitment of macrophages (Byrne et al., 2008) and limited efficacy of immunotherapy by excluding CD8⁺ T cells from the tumor parenchyma (Mariathasan et al., 2018; Tauriello et al., 2018). It is likely that TGF β also plays an immunosuppressive role in lymphomas. However, TGF β is also a potent negative regulator of B-cell survival, proliferation, activation, and differentiation (Sanjabi et al., 2017). Stroma-derived TGF β has been shown to induce senescence and apoptosis in mouse models of B-cell lymphoma (Reimann et al., 2010; Stelling et al., 2018). Thus, the DLBCL stromal-1 gene signature may be primarily associated with tumor-promoting immunosuppression in carcinomas, while the same immunosuppression may lead to the eradication of

B cells, which represent the malignant component of B-cell lymphoma.

CONCLUSION

Past clinical trials have taught us that successful targeted therapies in one disease do not always yield the desired results in another disease despite the presence of the same target. One example is the poor response of B-cell-infiltrated carcinomas to rituximab, which has shown remarkable success in lymphomas and rheumatoid arthritis. The opposite survival outcomes associated with the presence of stromal cells in B-cell lymphomas and carcinomas should serve as a warning that targeting the tumor microenvironment may produce opposite effects in B-cell lymphomas and carcinomas.

DATABASE LINKS

GEO Data Sets (<https://www.ncbi.nlm.nih.gov/gds>)
 Immunological Genome Project (<https://www.immgen.org>)
 PRECOG – PRediction of Clinical Outcomes from Genomic Profiles (<https://precog.stanford.edu>)
 R2: Genomics Analysis

REFERENCES

- Acton, S. E., Astarita, J. L., Malhotra, D., Lukacs-Kornek, V., Franz, B., Hess, P. R., et al. (2012). Podoplanin-rich stromal networks induce dendritic cell motility via activation of the C-type lectin receptor CLEC-2. *Immunity* 37, 276–289. doi: 10.1016/j.immuni.2012.05.022
- Aklilu, M., Stadler, W. M., Markiewicz, M., Vogelzang, N. J., Mahowald, M., Johnson, M., et al. (2004). Depletion of normal B cells with rituximab as an adjunct to IL-2 therapy for renal cell carcinoma and melanoma. *Ann. Oncol.* 15, 1109–1114. doi: 10.1093/annonc/mdh280
- Aran, D., Hu, Z., and Butte, A. J. (2017). xCell: digitally portraying the tissue cellular heterogeneity landscape. *Genome Biol.* 18:220. doi: 10.1186/s13059-017-1349-1
- Astarita, J. L., Acton, S. E., and Turley, S. J. (2012). Podoplanin: emerging functions in development, the immune system, and cancer. *Front. Immunol.* 3:283. doi: 10.3389/fimmu.2012.00283
- Augsten, M. (2014). Cancer-associated fibroblasts as another polarized cell type of the tumor microenvironment. *Front. Oncol.* 4:62. doi: 10.3389/fonc.2014.00062
- Barbera-Guillem, E., Nelson, M. B., Barr, B., Nyhus, J. K., May, K. F. Jr., Feng, L., et al. (2000). B lymphocyte pathology in human colorectal cancer. Experimental and clinical therapeutic effects of partial B cell depletion. *Cancer Immunol. Immunother.* 48, 541–549. doi: 10.1007/PL00006672
- Barnes, T. A., and Amir, E. (2017). HYPE or HOPE: the prognostic value of infiltrating immune cells in cancer. *Br. J. Cancer* 117, 451–460. doi: 10.1038/bjc.2017.220
- Beach, J. A., Aspuria, P. J., Cheon, D. J., Lawrenson, K., Agadjanian, H., Walsh, C. S., et al. (2016). Sphingosine kinase 1 is required for TGF-beta mediated fibroblast-to-myofibroblast differentiation in ovarian cancer. *Oncotarget* 7, 4167–4182. doi: 10.18632/oncotarget.6703
- Bombardieri, M., Kam, N. W., Brentano, F., Choi, K., Filer, A., Kyburz, D., et al. (2011). A BAFF/APRIL-dependent TLR3-stimulated pathway enhances the capacity of rheumatoid synovial fibroblasts to induce AID expression and Ig class-switching in B cells. *Ann. Rheum. Dis.* 70, 1857–1865. doi: 10.1136/ard.2011.150219
- Brown, F. D., and Turley, S. J. (2015). Fibroblastic reticular cells: organization and regulation of the T lymphocyte life cycle. *J. Immunol.* 194, 1389–1394. doi: 10.4049/jimmunol.1402520

and Visualization Platform (<http://hgserver1.amc.nl>) The Cancer Genome Atlas Project (<https://cancergenome.nih.gov>).

AUTHOR CONTRIBUTIONS

SO analyzed the public data sets. SO and MH wrote the manuscript.

FUNDING

This research was supported by the National Cancer Institute grant R01CA208753 and the Office of the Assistant Secretary of Defense for Health Affairs through the Ovarian Cancer Research Program Awards Nos. W81XWH-17-1-0144 and W81XWH-16-1-0190.

ACKNOWLEDGMENTS

We thank Kristy J. Daniels for assistance in manuscript preparation and members of the Women's Cancer Program for their support.

- Byrne, S. N., Knox, M. C., and Halliday, G. M. (2008). TGFbeta is responsible for skin tumour infiltration by macrophages enabling the tumours to escape immune destruction. *Immunol. Cell Biol.* 86, 92–97. doi: 10.1038/sj.icb.7100116
- Calon, A., Lonardo, E., Berenguer-Llargo, A., Espinet, E., Hernando-Momblona, X., Iglesias, M., et al. (2015). Stromal gene expression defines poor-prognosis subtypes in colorectal cancer. *Nat. Genet.* 47, 320–329. doi: 10.1038/ng.3225
- Calon, A., Tauriello, D. V., and Batlle, E. (2014). TGF-beta in CAF-mediated tumor growth and metastasis. *Semin. Cancer Biol.* 25, 15–22. doi: 10.1016/j.semcancer.2013.12.008
- Chang, J. E., and Turley, S. J. (2015). Stromal infrastructure of the lymph node and coordination of immunity. *Trends Immunol.* 36, 30–39. doi: 10.1016/j.it.2014.11.003
- Cheon, D. J., Tong, Y., Sim, M. S., Dering, J., Berel, D., Cui, X., et al. (2014). A collagen-remodeling gene signature regulated by TGF-beta signaling is associated with metastasis and poor survival in serous ovarian cancer. *Clin. Cancer Res.* 20, 711–723. doi: 10.1158/1078-0432.CCR-13-1256
- Costa, A., Kieffer, Y., Scholer-Dahirel, A., Pelon, F., Bourachot, B., Cardon, M., et al. (2018). Fibroblast heterogeneity and immunosuppressive environment in human breast cancer. *Cancer Cell* 33, 463.e10–479.e10. doi: 10.1016/j.ccell.2018.01.011
- Creмасco, V., Woodruff, M. C., Onder, L., Cupovic, J., Nieves-Bonilla, J. M., Schildberg, F. A., et al. (2014). B cell homeostasis and follicle confines are governed by fibroblastic reticular cells. *Nat. Immunol.* 15, 973–981. doi: 10.1038/ni.2965
- Cyster, J. G. (2010). B cell follicles and antigen encounters of the third kind. *Nat. Immunol.* 11, 989–996. doi: 10.1038/ni.1946
- Dieu-Nosjean, M. C., Goc, J., Giraldo, N. A., Sautes-Fridman, C., and Fridman, W. H. (2014). Tertiary lymphoid structures in cancer and beyond. *Trends Immunol.* 35, 571–580. doi: 10.1016/j.it.2014.09.006
- Elkabets, M., Gifford, A. M., Scheel, C., Nilsson, B., Reinhardt, F., Bray, M. A., et al. (2011). Human tumors instigate granulysin-expressing hematopoietic cells that promote malignancy by activating stromal fibroblasts in mice. *J. Clin. Invest.* 121, 784–799. doi: 10.1172/JCI43757
- Erdogan, B., and Webb, D. J. (2017). Cancer-associated fibroblasts modulate growth factor signaling and extracellular matrix remodeling to regulate tumor metastasis. *Biochem. Soc. Trans.* 45, 229–236. doi: 10.1042/bst20160387

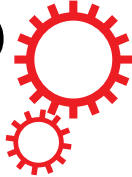
- Farmer, P., Bonnefoi, H., Anderle, P., Cameron, D., Wirapati, P., Becette, V., et al. (2009). A stroma-related gene signature predicts resistance to neoadjuvant chemotherapy in breast cancer. *Nat. Med.* 15, 68–74. doi: 10.1038/nm.1908
- Flavell, R. A., Sanjabi, S., Wrzesinski, S. H., and Licona-Limon, P. (2010). The polarization of immune cells in the tumour environment by TGFbeta. *Nat. Rev. Immunol.* 10, 554–567. doi: 10.1038/nri2808
- Fletcher, A. L., Acton, S. E., and Knoblich, K. (2015). Lymph node fibroblastic reticular cells in health and disease. *Nat. Rev. Immunol.* 15, 350–361. doi: 10.1038/nri3846
- Fletcher, A. L., Elman, J. S., Astarita, J., Murray, R., Saeidi, N., D'Rozario, J., et al. (2014). Lymph node fibroblastic reticular cell transplants show robust therapeutic efficacy in high-mortality murine sepsis. *Sci. Transl. Med.* 6:249ra109. doi: 10.1126/scitranslmed.3009377
- Fletcher, A. L., Malhotra, D., and Turley, S. J. (2011). Lymph node stroma broaden the peripheral tolerance paradigm. *Trends Immunol.* 32, 12–18. doi: 10.1016/j.it.2010.11.002
- Franquesa, M., Mensah, F. K., Huizinga, R., Strini, T., Boon, L., Lombardo, E., et al. (2015). Human adipose tissue-derived mesenchymal stem cells abrogate plasmablast formation and induce regulatory B cells independently of T helper cells. *Stem Cells* 33, 880–891. doi: 10.1002/stem.1881
- Fridman, W. H., Pages, F., Sautes-Fridman, C., and Galon, J. (2012). The immune contexture in human tumours: impact on clinical outcome. *Nat. Rev. Cancer* 12, 298–306. doi: 10.1038/nrc3245
- Gentles, A. J., Newman, A. M., Liu, C. L., Bratman, S. V., Feng, W., Kim, D., et al. (2015). The prognostic landscape of genes and infiltrating immune cells across human cancers. *Nat. Med.* 21, 938–945. doi: 10.1038/nm.3909
- Germain, C., Gnajatic, S., Tamzalit, F., Knockaert, S., Remark, R., Goc, J., et al. (2014). Presence of B cells in tertiary lymphoid structures is associated with a protective immunity in patients with lung cancer. *Am. J. Respir. Crit. Care Med.* 189, 832–844. doi: 10.1164/rccm.201309-1611OC
- Grum-Schwensen, B., Klingelhofer, J., Grigorian, M., Almholt, K., Nielsen, B. S., Lukanidin, E., et al. (2010). Lung metastasis fails in MMTV-PyMT oncomice lacking S100A4 due to a T-cell deficiency in primary tumors. *Cancer Res.* 70, 936–947. doi: 10.1158/0008-5472.CAN-09-3220
- Gundersen, A. J., and Coussens, L. M. (2013). B cells and their mediators as targets for therapy in solid tumors. *Exp. Cell Res.* 319, 1644–1649. doi: 10.1016/j.yexcr.2013.03.005
- Guy, T. V., Terry, A. M., Bolton, H. A., Hancock, D. G., Shklovskaya, E., and Fazekas de St. Groth, B. (2016). Pro- and anti-tumour effects of B cells and antibodies in cancer: a comparison of clinical studies and preclinical models. *Cancer Immunol. Immunother.* 65, 885–896. doi: 10.1007/s00262-016-1848-z
- Harper, J., and Sainson, R. C. (2014). Regulation of the anti-tumour immune response by cancer-associated fibroblasts. *Semin. Cancer Biol.* 25, 69–77. doi: 10.1016/j.semcancer.2013.12.005
- Heng, T. S., and Painter, M. W. (2008). The immunological genome project: networks of gene expression in immune cells. *Nat. Immunol.* 9, 1091–1094. doi: 10.1038/nri1008-1091
- Isella, C., Terrasi, A., Bellomo, S. E., Petti, C., Galatola, G., Muratore, A., et al. (2015). Stromal contribution to the colorectal cancer transcriptome. *Nat. Genet.* 47, 312–319. doi: 10.1038/ng.3224
- Jain, R. K. (2013). Normalizing tumor microenvironment to treat cancer: bench to bedside to biomarkers. *J. Clin. Oncol.* 31, 2205–2218. doi: 10.1200/JCO.2012.46.3653
- Jia, D., Liu, Z., Deng, N., Tan, T. Z., Huang, R. Y., Taylor-Harding, B., et al. (2016). A COL11A1-correlated pan-cancer gene signature of activated fibroblasts for the prioritization of therapeutic targets. *Cancer Lett.* 382, 203–214. doi: 10.1016/j.canlet.2016.09.001
- Kalluri, R. (2016). The biology and function of fibroblasts in cancer. *Nat. Rev. Cancer* 16, 582–598. doi: 10.1038/nrc.2016.73
- Kalluri, R., and Zeisberg, M. (2006). Fibroblasts in cancer. *Nat. Rev. Cancer* 6, 392–401. doi: 10.1038/nrc1877
- Karin, N. (2010). The multiple faces of CXCL12 (SDF-1alpha) in the regulation of immunity during health and disease. *J. Leukoc. Biol.* 88, 463–473. doi: 10.1189/jlb.0909602
- Kitamura, T., Qian, B. Z., and Pollard, J. W. (2015). Immune cell promotion of metastasis. *Nat. Rev. Immunol.* 15, 73–86. doi: 10.1038/nri3789
- Koning, J. J., and Mebius, R. E. (2012). Interdependence of stromal and immune cells for lymph node function. *Trends Immunol.* 33, 264–270. doi: 10.1016/j.it.2011.10.006
- Kraman, M., Bambrough, P. J., Arnold, J. N., Roberts, E. W., Magiera, L., Jones, J. O., et al. (2010). Suppression of antitumor immunity by stromal cells expressing fibroblast activation protein-alpha. *Science* 330, 827–830. doi: 10.1126/science.1195300
- Lenz, G., Wright, G., Dave, S. S., Xiao, W., Powell, J., Zhao, H., et al. (2008). Stromal gene signatures in large-B-cell lymphomas. *N. Engl. J. Med.* 359, 2313–2323. doi: 10.1056/NEJMoa0802885
- Levental, K. R., Yu, H., Kass, L., Lakins, J. N., Egeblad, M., Erler, J. T., et al. (2009). Matrix crosslinking forces tumor progression by enhancing integrin signaling. *Cell* 139, 891–906. doi: 10.1016/j.cell.2009.10.027
- Lossos, I. S., Czerwinski, D. K., Alizadeh, A. A., Wechser, M. A., Tibshirani, R., Botstein, D., et al. (2004). Prediction of survival in diffuse large-B-cell lymphoma based on the expression of six genes. *N. Engl. J. Med.* 350, 1828–1837. doi: 10.1056/NEJMoa032520
- Lu, P., Weaver, V. M., and Werb, Z. (2012). The extracellular matrix: a dynamic niche in cancer progression. *J. Cell Biol.* 196, 395–406. doi: 10.1083/jcb.201102147
- Mariathasan, S., Turley, S. J., Nickles, D., Castiglioni, A., Yuen, K., Wang, Y., et al. (2018). TGFbeta attenuates tumour response to PD-L1 blockade by contributing to exclusion of T cells. *Nature* 554, 544–548. doi: 10.1038/nature25501
- Meyer, P. N., Fu, K., Greiner, T., Smith, L., Delabie, J., Gascoyne, R., et al. (2011). The stromal cell marker SPARC predicts for survival in patients with diffuse large B-cell lymphoma treated with rituximab. *Am. J. Clin. Pathol.* 135, 54–61. doi: 10.1309/ajcpjx4bjv9nlqhy
- Mionnet, C., Mondor, I., Jorquera, A., Loosveld, M., Maurizio, J., Arcangeli, M. L., et al. (2013). Identification of a new stromal cell type involved in the regulation of inflamed B cell follicles. *PLoS Biol.* 11:e1001672. doi: 10.1371/journal.pbio.1001672
- Moffitt, R. A., Marayati, R., Flate, E. L., Volmar, K. E., Loeza, S. G., Hoadley, K. A., et al. (2015). Virtual microdissection identifies distinct tumor- and stroma-specific subtypes of pancreatic ductal adenocarcinoma. *Nat. Genet.* 47, 1168–1178. doi: 10.1038/ng.3398
- Mueller, S. N., and Germain, R. N. (2009). Stromal cell contributions to the homeostasis and functionality of the immune system. *Nat. Rev. Immunol.* 9, 618–629. doi: 10.1038/nri2588
- Raz, Y., and Erez, N. (2013). An inflammatory vicious cycle: fibroblasts and immune cell recruitment in cancer. *Exp. Cell Res.* 319, 1596–1603. doi: 10.1016/j.yexcr.2013.03.022
- Reimann, M., Lee, S., Loddenkemper, C., Dorr, J. R., Tabor, V., Aichele, P., et al. (2010). Tumor stroma-derived TGF-beta limits myc-driven lymphomagenesis via Suv39h1-dependent senescence. *Cancer Cell* 17, 262–272. doi: 10.1016/j.ccr.2009.12.043
- Sanjabi, S., Oh, S. A., and Li, M. O. (2017). Regulation of the immune response by TGF-beta: from conception to autoimmunity and infection. *Cold Spring Harb. Perspect. Biol.* 9:a022236. doi: 10.1101/cshperspect.a022236
- Sarvaria, A., Madrigal, J. A., and Saudemont, A. (2017). B cell regulation in cancer and anti-tumor immunity. *Cell Mol. Immunol.* 14, 662–674. doi: 10.1038/cmi.2017.35
- Shay, T., and Kang, J. (2013). Immunological genome project and systems immunology. *Trends Immunol.* 34, 602–609. doi: 10.1016/j.it.2013.03.004
- Sheng, J., Chen, W., and Zhu, H. J. (2015). The immune suppressive function of transforming growth factor-beta (TGF-beta) in human diseases. *Growth Factors* 33, 92–101. doi: 10.3109/08977194.2015.1010645
- Silzle, T., Kreutz, M., Dobler, M. A., Brockhoff, G., Knuechel, R., and Kunz-Schughart, L. A. (2003). Tumor-associated fibroblasts recruit blood monocytes into tumor tissue. *Eur. J. Immunol.* 33, 1311–1320. doi: 10.1002/eji.200323057
- Spano, D., and Zollo, M. (2012). Tumor microenvironment: a main actor in the metastasis process. *Clin. Exp. Metastasis* 29, 381–395. doi: 10.1007/s10585-012-9457-5
- Stelling, A., Hashwah, H., Bertram, K., Manz, M. G., Tzankov, A., and Muller, A. (2018). The tumor suppressive TGF-beta/SMAD1/S1PR2 signaling axis is recurrently inactivated in diffuse large B-cell lymphoma. *Blood* 131, 2235–2246. doi: 10.1182/blood-2017-10-810630

- Stover, D. G., Bierie, B., and Moses, H. L. (2007). A delicate balance: TGF-beta and the tumor microenvironment. *J. Cell. Biochem.* 101, 851–861. doi: 10.1002/jcb.21149
- Tauriello, D. V. F., Palomo-Ponce, S., Stork, D., Berenguer-Llgero, A., Badia-Ramentol, J., Iglesias, M., et al. (2018). TGFbeta drives immune evasion in genetically reconstituted colon cancer metastasis. *Nature* 554, 538–543. doi: 10.1038/nature25492
- Tekin, N., Omidvar, N., Morris, T. P., Conget, P., Bruna, F., Timar, B., et al. (2016). Protocol for qRT-PCR analysis from formalin fixed paraffin embedded tissue sections from diffuse large b-cell lymphoma: validation of the six-gene predictor score. *Oncotarget* 7, 83319–83329. doi: 10.18632/oncotarget.13066
- Turley, S. J., Cremasco, V., and Astarita, J. L. (2015). Immunological hallmarks of stromal cells in the tumour microenvironment. *Nat. Rev. Immunol.* 15, 669–682. doi: 10.1038/nri3902
- Yeung, T. L., Leung, C. S., Wong, K. K., Samimi, G., Thompson, M. S., Liu, J., et al. (2013). TGF-beta modulates ovarian cancer invasion by upregulating CAF-derived versican in the tumor microenvironment. *Cancer Res.* 73, 5016–5028. doi: 10.1158/0008-5472.can-13-0023

Conflict of Interest Statement: The authors declare that the research was conducted in the absence of any commercial or financial relationships that could be construed as a potential conflict of interest.

Copyright © 2018 Haro and Orsulic. This is an open-access article distributed under the terms of the Creative Commons Attribution License (CC BY). The use, distribution or reproduction in other forums is permitted, provided the original author(s) and the copyright owner(s) are credited and that the original publication in this journal is cited, in accordance with accepted academic practice. No use, distribution or reproduction is permitted which does not comply with these terms.

SCIENTIFIC REPORTS



OPEN

Inflammation is a key contributor to ovarian cancer cell seeding

Dongyu Jia^{1,4}, Yoshiko Nagaoka², Makoto Katsumata² & Sandra Orsulic^{1,2,3} 

The incidence of ovarian cancer dramatically increases in early menopause but the factors contributing to cancer onset are unclear. Most ovarian cancers originate in the fallopian tube with subsequent implantation of malignant cells into the ovary. However, the events and conditions that lead to cancer cell implantation are unknown. To quantify which conditions are conducive to the seeding of cancer cells in an immunocompetent mouse model, we surgically implanted mouse ovarian cancer cells into the oviducts of syngeneic mice and simulated conditions associated with ovulatory wound repair, incessant ovulation, ovarian surface scarring, and aging. We found that the dominant site of cancer cell seeding was not the ovary but the nearby surgical wound site, which was associated with a strong and persistent inflammatory reaction. Conditions in the ovary associated with inflammation, such as acute ovulatory wound repair, active healing of the scarred ovarian surface, and mouse aging, contributed to increased seeding of the cancer cells to the surgical wound site and tissues surrounding the ovary. Changes in the ovary not accompanied by inflammation, such as completed ovulatory cycles and fully-healed scars on the ovarian surface, did not contribute to increased cancer cell seeding. We conclude that inflammation is the most likely mechanism by which ovulation and postmenopausal events contribute to the increased risk of ovarian cancer.

Despite modern day cytoreductive surgical techniques and combination chemotherapies for high-grade ovarian cancer, five-year survival rates remain below 40%¹. However, when found early, the survival rate dramatically rises to 90%^{1,2}. Thus, the ability to detect ovarian cancer in its earliest stages is critical to a cure. It is increasingly accepted that high-grade ovarian cancers actually originate in the fallopian tube with malignant cells shedding to the adjacent ovary^{3–7}. Since the bulk of the tumor typically forms in the ovary, rather than the fallopian tube, ovaries must play a significant role in the early stages of cancer development. Discovering which cellular and molecular processes promote and inhibit the seeding of malignant cells to the ovary could facilitate the development of markers for early detection as well as the identification of rate-limiting events in the early stages of ovarian cancer development. If contextual molecular cues provided by the ovary are required for the clinical development of ovarian cancer, such molecules could serve as novel therapeutic targets to prevent cancer progression in the early stages, when cures are more viable.

Epithelial ovarian cancer is predominantly a disease of postmenopausal women⁸. Many theories of postmenopausal onset of ovarian cancer have been proposed, including incessant ovulation and inflammation, hormonal changes, reduced immunity, increased cell senescence, and uncontrolled production of reactive oxygen species^{9–13}. Epidemiologic data consistently show that the risk of ovarian cancer increases with the number of ovulatory cycles^{14–16}, indicating that ovulation plays a significant role in ovarian cancer etiology. However, the peak incidence of menopause occurs at age 51, while the peak incidence of invasive epithelial ovarian cancer occurs at age 63¹. Thus, most women develop ovarian cancer years after their last ovulatory cycle. Currently, it is unknown which conditions in the ovary promote tumor growth but the fact that more than 80% of ovarian cancer cases occur after menopause suggests that the events associated with menopause and aging are major contributing factors⁸.

During the postmenopausal years, ovarian follicles are largely depleted and much of the remaining ovary is reduced to a collagenous scar tissue¹⁷. If the microenvironment of postmenopausal ovaries is conducive to the implantation of cancer cells, simulating postmenopausal conditions should result in more cancer cell deposits in the ovary. A better understanding of ovarian cancer pathogenesis, specifically the role of the early postmenopausal

¹Women's Cancer Program at the Samuel Oschin Comprehensive Cancer Institute, Cedars-Sinai Medical Center, Los Angeles, CA, USA. ²Department of Biomedical Sciences, Cedars-Sinai Medical Center, Los Angeles, CA, USA. ³Department of Obstetrics and Gynecology, David Geffen School of Medicine, University of California, Los Angeles, Los Angeles, CA, USA. ⁴Present address: Department of Biology, Georgia Southern University, Statesboro, GA, USA. Correspondence and requests for materials should be addressed to S.O. (email: orsulics@cshs.org)

ovarian microenvironment in supporting the seeding and survival of malignant cells in the ovary, is necessary to develop strategies for ovarian cancer prevention and detection. Experiments in mice provide a convenient system in which both the effect and the outcome of specific conditions can be examined and quantified. Previously, we used a mouse model to study events associated with ovulation and ovulatory wound repair, including epithelial cell entrapment and the formation of epithelial inclusion cysts¹⁸. Here, we extended those studies by simulating various postmenopausal conditions in mice and quantifying cancer cell deposits for each condition. The goal of the study was to determine whether conditions associated with ovulation and aging increase the spread of cancer cells from the oviduct to the ovary. To account for a possible role of the immune system in ovarian cancer cell seeding, we used an immunocompetent FVB mouse model with syngeneic ovarian cancer cell aggregates implanted into the fallopian tube. Our data show that premenopausal and postmenopausal conditions contribute to increased cancer cell seeding only in the presence of an inflammatory reaction.

Materials and Methods

Cancer cell line. The FVB-syngeneic mouse ovarian cancer cell line, BR, was engineered with combinations of genetic alterations (p53^{-/-}, Brca1^{-/-}, myc, and Akt) as described¹⁹. We have shown that this ovarian cancer model recapitulates human serous histology, pattern of metastatic spread, and response to standard and targeted therapies^{19–23}. The BR cells were subsequently transduced with luciferase lentiviral plasmid pLenti-CMVPuro-LUC (Addgene, w168-1) to generate BR-luc cells.

Preparation of cell aggregates. BR-luc cells were seeded at a density of 1×10^6 cells per well in Costar ultra-low attachment 6-well plates (Corning). The cells were incubated with 3 ml DMEM media in 5% CO₂ at 37 °C. After 2 days, culture media were collected in 15 ml conical tubes and cells were precipitated at 1000 rpm for 0.5 minutes. After two rounds of washing with phosphate buffered saline (PBS), large cell aggregates were separated into small aggregates by multiple pipetting through a 1 ml pipette tip.

Injection of cell aggregates into oviducts. All procedures in mice were performed in accordance with the approved Cedars-Sinai IACUC protocol (IACUC5318). The procedures were performed in an AAALAC-accredited facility at Cedars-Sinai Medical Center. The surgical procedures were performed according to the method described for embryo transfer into the oviduct (Manipulating the Mouse Embryo: A Laboratory Manual, 3rd Edition, ISBN-978-087969591-0). Under the dissecting microscope, a small incision between the infundibulum and the ampulla of the oviduct (equivalent to human fallopian tube) was created using Vannas scissors (Supplementary Video 1). The transfer pipette loaded with cell aggregates in PBS was inserted into the incision with the tip pointing toward the ovary and approximately 200 cell aggregates in 2 μl volume were injected into each oviduct (Supplementary Video 1).

Simulation of ovulatory and menopausal conditions. Mice were superovulated by intraperitoneal injection of pregnant mare serum (PMS) and human chorionic gonadotropin (hCG) as previously described¹⁸. In the control mice, PBS was injected instead of PMS and hCG. To generate scar tissue, bursa (a thin membrane covering the ovary in mice) was removed (Supplementary Video 2) and the ovarian surface was burned with a hand-held battery-powered cauterizer (Gemini Cautery System) (Supplementary Video 3).

Quantification of cancer cell deposits. Mice were euthanized by CO₂ asphyxiation followed by cervical dislocation prior to harvesting the ovaries and surrounding tissues. To quantify macroscopic tumors, dimensions (length, width, height) were measured by calipers. Tumor volume (mm³) was calculated using the equation $V = (L \times W \times H)/2$, where V is tumor volume, L is tumor length, W is tumor width, and H is tumor height. For the flat, superficial tumors that typically formed on the surgical wounds/scars, tumor area (mm²) was measured using the equation $A = L \times W$, where A is tumor area size, L is tumor length, and W is tumor width. To quantify microscopic cancer cell deposits, the ovaries, oviducts, and surrounding fat tissues were fixed in formalin and embedded in paraffin. One 4 μm-thick section per sample was stained with hematoxylin and eosin (H&E) and evaluated under the light microscope for visible cancer cell deposits.

Statistical analyses. The statistical analyses were performed using GraphPad Prism (version 6.0; GraphPad Software). Intergroup differences were assessed by the Student's *t*-test.

Data availability. No datasets were generated or analyzed during the current study.

Results

Our ability to screen for early stage ovarian cancer is hampered by deficiencies in the understanding of the molecular and morphological steps involved in ovarian carcinogenesis. It is currently unknown why cancer cells in the fallopian tube have the propensity to migrate to the ovary where they tend to form a large tumor mass. To determine which ovarian conditions are most conducive to implantation of detached tubal cells, we simulated in mice conditions associated with ovulatory wound healing, incessant ovulation, atrophy/scarring, and aging.

Inflammatory events associated with ovulatory wound repair contribute to increased cancer cell seeding to tissues surrounding the ovary but are not directly associated with the implantation of cancer cells to the ovary. To simulate cancer cell seeding and entrapment during ovulatory wound healing, superovulation was induced in 4 week-old female FVB mice by intraperitoneal injection of PMS and hCG hormones (superovulated group, N = 6) or PBS (control group, N = 6). This combination of hormones induces ovulation of a large number of follicles to form 10–30 acute ovulatory wounds within one ovulatory cycle¹⁸. Two days after hCG (or control PBS) injection, when ovulatory wound repair is at its peak¹⁸, cancer cell

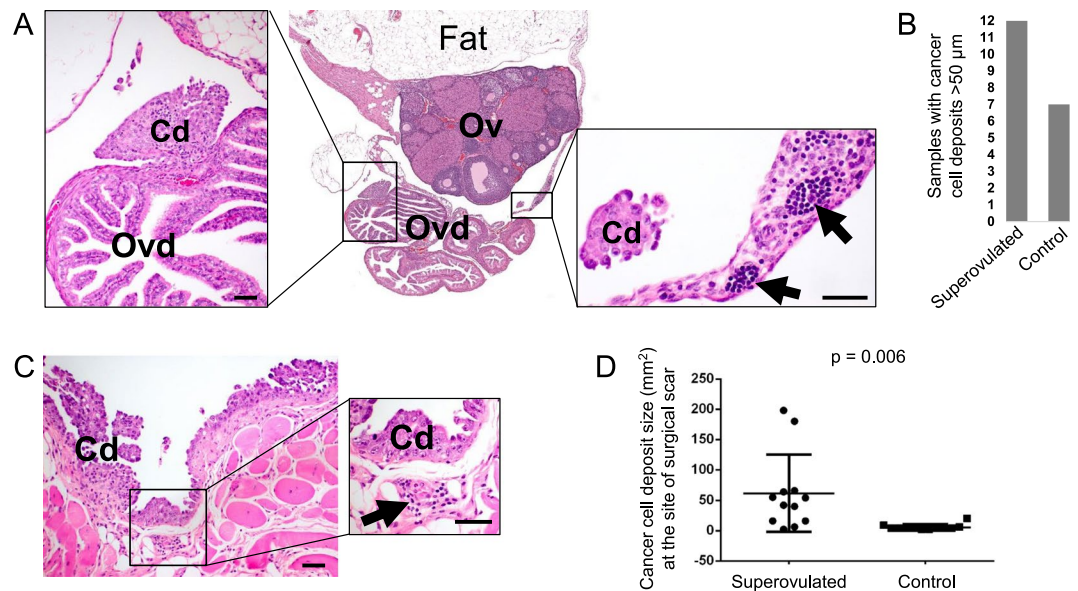


Figure 1. Assessing the effect of ovulatory wound repair on cancer cell seeding from the oviduct to the ovary and adjacent tissues. **(A)** Representative H&E-stained section of cancer cell deposits on the oviduct and ovary. Arrows indicate immune cell infiltrates. Size bars: 50 μm. Cd, cancer cell deposit; Ov, ovary; Ovd, oviduct. **(B)** Graph indicates the number of superovulated and control ovary/oviduct samples containing cancer cell deposits larger than 50 μm in diameter (out of 12 ovaries in each group). **(C)** H&E-stained section representing ‘carpeting’ of cancer cells along the surgical wound/scar site in the peritoneal wall. Arrow indicates an immune cell infiltrate. Size bars: 50 μm. Cd, cancer cell deposit. **(D)** Comparison of cancer cell deposit size at the surgical wound/scar site in superovulated and control mice.

aggregates were bilaterally implanted into the mouse oviduct. Three weeks later, intraperitoneal tumor dissemination was evaluated by recording the presence of ascites and measurable tumor deposits inside of the peritoneal cavity. Macroscopically visible swelling was observed in 4/12 ovaries from the superovulated mice and in 0/12 ovaries from the control mice. Microscopic cancer cell deposits in the oviducts, ovaries, and surrounding fat were quantified by pathologic examination of H&E-stained sections under the 4x objective, and the presence of cancer cells was further verified under higher magnification (Fig. 1A). The deposits in tissues surrounding the ovary were frequently associated with immune cell infiltrates (Fig. 1A). Cancer cell deposits larger than 50 μm were present in tissues surrounding the ovary (oviduct, bursa, and space between the fat and ovarian surface) in 12/12 samples from the superovulated mice and in 7/12 samples from the control mice (Fig. 1B). However, neither group of mice exhibited cell deposits directly on the ovarian surface or as intraovarian inclusions. These results suggest that ovulatory wound healing is not directly associated with the implantation of cancer cells to the ovary. In both groups of mice, the largest cancer cell deposits presented as carpeting of the abdominal wall at the sites of surgical wounds/scar (Fig. 1C). The surgical wound/scar cancer cell deposits were frequently associated with immune cell infiltrates (Fig. 1C) and were significantly larger in superovulated mice than in control mice (Fig. 1D). Taken together, our results indicate that events associated with ovulatory wound healing contributed to increased seeding of cancer cells to the surgical site and tissues surrounding the ovary. The lack of cancer cell deposits attached to the ovarian surface indicates that re-epithelialization of the ovarian surface does not significantly contribute to cancer cell seeding. It is more likely that ovulatory events contributed to increased inflammatory infiltrates, which attracted cancer cells and/or supported their survival and expansion.

Ovarian atrophy resulting from previous incessant ovulation is not associated with increased cancer cell seeding.

To simulate cancer cell seeding in ovaries that endured repeated damage and repair due to multiple cycles of ovulation, six week-old female FVB mice were subjected to nine weeks of weekly intraperitoneal PMS and hCG hormone injections (repeatedly superovulated group, N = 7) or PBS injections (control group, N = 7). To mimic conditions in postmenopausal women whose ovaries have not been actively cycling for years, we waited 12 weeks after the last superovulation to implant BR-luc cell aggregates into the oviducts of the repeatedly superovulated and control mice. Eight weeks after cancer cell implantation, the tumor burden was evaluated in both groups. The majority of tumor deposits were found at the surgical wound/scar tissue, which was frequently fused with the adjacent fat and infiltrated with immune cells (data not shown). There were no macroscopically or microscopically visible cancer cell deposits on the ovaries and oviducts in either group of mice (data not shown). Thus, in the absence of acute inflammation, ovaries that have undergone repetitive superovulations do not appear to attract cancer cells any more than age-matched ovaries with a normal number of ovulatory cycles. One caveat to this experiment is that we did not achieve complete depletion of the oocytes pool despite nine cycles of superovulation, possibly because mice become unresponsive to hormone induction after reaching reproductive maturity²⁴.

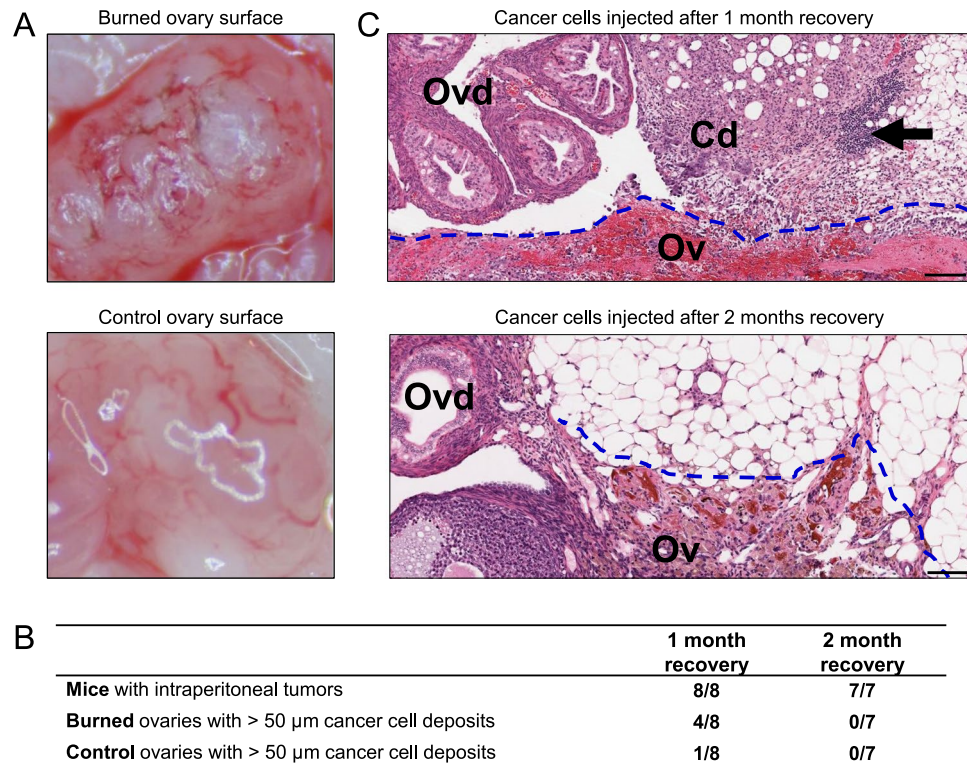


Figure 2. Assessing the effect of burn-induced ovarian scarring on the seeding of intraperitoneally injected cancer cells. **(A)** Representative images of ovarian surface immediately after manipulation. Control ovaries were surgically released from the bursa while burned ovaries were first surgically released from the bursa, then superficially burned with a cauterizer. **(B)** Comparison of seeding efficiency of intraperitoneally injected cancer cells one or two months after surgical ovary manipulation. **(C)** Representative H&E-stained sections of cancer cell deposits on the ovaries and oviducts of mice that were injected one or two months after surgical ovary manipulation and euthanized four weeks later. Arrow indicates an immune cell infiltrate. Size bars: 100 μm. Cd, cancer cell deposit; Ov, ovary; Ovd, oviduct.

Burn-induced scarring of the ovarian surface is associated with increased cancer cell seeding to the ovaries and surrounding tissues only in the presence of active scar wound healing. To simulate events associated with postmenopausal ovary atrophy and connective tissue scarring, burn-induced scars were generated on the ovarian surface of the six week-old female FVB mice. In each mouse, one ovary was surgically released from the ovarian bursa (Supplementary Video 2) and superficially burned with a cauterizer (Fig. 2A and Supplementary Video 3). The contralateral ovary was surgically released from the bursa but not burned (control ovary) (Fig. 2A). Mice were intraperitoneally injected with a single-cell suspension of BR-luc cells ($\sim 1 \times 10^6$ cells) after one month recovery (N = 8) or two months recovery (N = 7). Four weeks after intraperitoneal cell injection, mice were euthanized for tumor burden quantification. Regardless of whether mice were intraperitoneally injected with cancer cells one month or two months after surgery, BR-luc cells formed multiple small tumor nodules on the mesothelial surfaces of the omentum, pancreas, diaphragm, spleen and abdominal lining; however, there were no visible tumor cell deposits on the surface of the burned or control ovaries. Therefore, we assessed microscopic cancer cell deposits in H&E-stained sections of ovaries/oviducts and adjacent fat. For the one month recovery group (N = 8), cancer cell deposits larger than 50 μm were present in the tissues surrounding the ovary (fat, oviduct, and bursa) in 4/8 burned ovaries and in 1/8 control ovaries (Fig. 2B). All ovaries that contained tumor deposits also had abundant immune cell infiltrates (Fig. 2C). For the two months recovery group (N = 7), none of the ovary sections contained cancer cell deposits (Fig. 2B). Although burn-induced scars on the ovarian surface were detectable two months later, the scars were no longer associated with abundant immune cell infiltrates (Fig. 2C). These results suggest that burn-induced scars attract cancer cells but only in the presence of inflammation.

Events associated with aging contribute to increased cancer cell seeding to the ovaries and surrounding tissues. BR-luc cancer cell aggregates were bilaterally implanted into the oviducts of eight week-old (N = 10) and greater than one year-old (age range 14–19 months; N = 10) female FVB mice. Mice were euthanized for analysis four weeks after cancer cell implantation. Both groups of mice developed multiple intraperitoneal metastases with the largest tumor masses present on the omentum and abdominal wall. Omental and abdominal wall masses were more frequent in aged mice (Fig. 3A). Three of the aged mice also exhibited unilateral or bilateral uterine horn hyperplasia (data not shown). H&E-stained sections showed that the ovaries from young mice contained multiple follicles in different phases of maturation (data not shown), while the ovaries from old mice were devoid of follicles (Fig. 3B). Microscopic examination of the ovaries and adjacent tissues (oviduct,

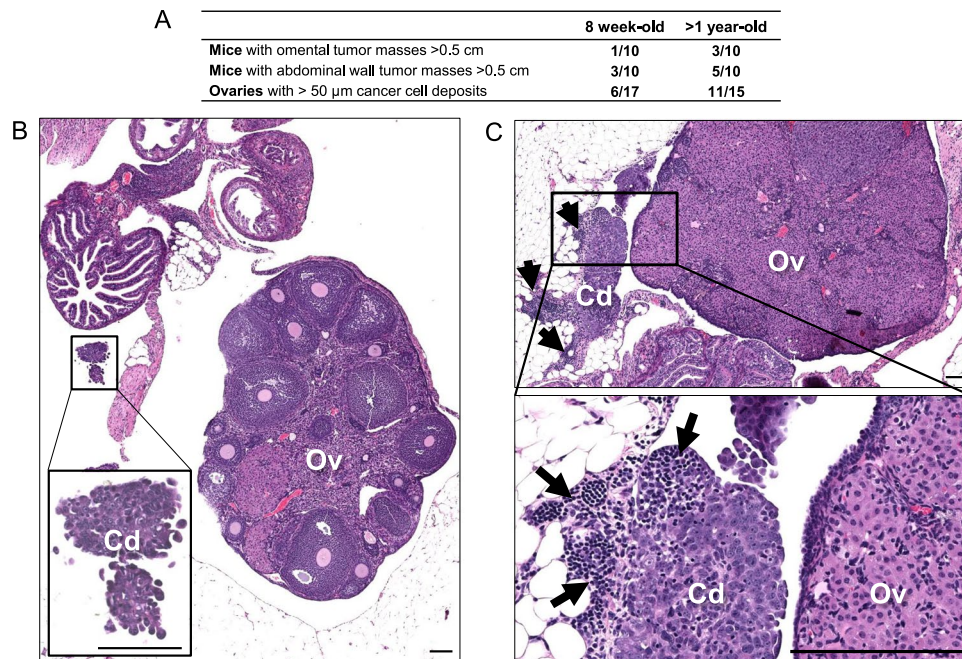


Figure 3. Assessing the effect of aging on cancer cell seeding from the oviduct to the ovary and adjacent tissues. **(A)** Comparison of seeding efficiency of cancer cells implanted into the oviducts of young (8 weeks) and aged (>1 year) mice. In H&E-stained sections, several ovaries were excluded from the analysis because they were either missing from the slide section or the tissue was insufficient for evaluation. **(B,C)** Representative H&E-stained section of cancer cell deposits on ovaries and oviducts four weeks after surgical implantation of cancer cells into the oviducts of **(B)** 8-week-old mice and **(C)** >1-year-old mice. Arrow indicates an immune cell infiltrate. Size bars: 100 μ m. Cd, cancer cell deposit; Ov, ovary.

bursa, and adjacent fat) revealed that tumor cell deposits were more frequent in aged mice (Fig. 3A), which also contained more abundant immune cell infiltrates (Fig. 3B). These results suggest that ovaries from aged mice are more conducive to cancer cell seeding than ovaries from young mice.

Discussion

A poor understanding of the initiating events in ovarian cancer has significantly hampered our efforts towards early ovarian cancer detection and prevention. Most early stage cancers in the tubal fimbria are associated with a dominant mass in the ovary, indicating that the ovarian microenvironment is essential for tumor growth. However, conditions that promote cancer cell seeding and growth in the ovary are still unknown. Recently, Yang-Hartwich and colleagues used a mouse xenograft model to test the role of ovulatory wound repair in the migration of cancer cells from the injection site in the uterus toward the ovary²⁵. Consistent with epidemiologic data that increased ovulation is strongly associated with ovarian cancer^{15,16}, they showed that superovulation in mice enhances the migration and adhesion of malignant cells to the ovary and that this attraction is mediated through the release of cytokines/chemokines from the surface wound created by oocyte release²⁵. Using a syngeneic immunocompetent mouse model with cancer cells surgically implanted into the oviduct, we confirmed that superovulation contributes to ovarian cancer cell seeding. Tumor cell deposits were accompanied by immune infiltrates, indicating that ovulation-induced inflammation may play an important role in cancer cell seeding. It is possible that the inflammatory reaction is the only factor that contributes to increased cancer cell seeding because the largest cancer cell deposits typically formed in the abdominal wall along surgical wounds, which were associated with extensive immune infiltrates. It appears that the wounded surface of the superovulated ovary did not play a direct role in cancer cell attraction as there were no cancer cells attached to the ovarian surface epithelium or inside the ovarian stroma. The importance of the inflammatory reaction, rather than the damaged ovarian surface in cancer cell seeding, was illustrated by the next two sets of experiments in which we repeatedly wounded the ovarian surface by multiple rounds of superovulation or burned the ovarian surface to induce scarring. The wounded/scarred ovarian surface proved to be attractive to cancer cells only if the wounds were ‘fresh’. If ovarian wounds/scars were allowed to recover for two months, cancer cells were no longer attracted to the ovarian surface but were still attracted to other sites in the peritoneal cavity where inflammation persisted. It is well established that aging is characterized by subclinical, chronic inflammation²⁶. Consistent with multiple studies showing that the overall proinflammatory status in older mice is associated with increased tumor burden²⁷, our results show that oviductal implantation of cancer cells in aged mice resulted in increased tumor burden throughout the peritoneal cavity.

Our finding that surgical wounds in mice attract cancer cells is consistent with an observation in clinical practice that wound trauma in patients is associated with cancer recurrence^{28,29}. It has been shown that an early peak of breast cancer recurrence is due to surgery-driven intervention³⁰. The exact reasons for surgery-related cancer

attraction are not fully understood but possible factors include surgery-related acute wound healing process, inflammation, and activation of dormant cancer cells by surgery-driven growth factors^{31–33}. If inflammation is a key factor in cancer cell seeding, what are the contributions of other factors strongly associated with increased cancer incidence, such as ovulation, oocyte depletion and atrophy, and aging? Our data in a mouse model are consistent with the concept that most of the factors implicated in ovarian cancer incidence converge on inflammation as a common denominator. One successful path to ovarian cancer prevention has been controlling factors that induce inflammation, such as the use of oral contraceptives to suppress ovulation³⁴. Epidemiologic data show that aspirin and other nonsteroidal anti-inflammatory drugs (NSAIDs) can be beneficial in the prevention of multiple cancers, including ovarian^{35,36}. Although factors associated with the increased risk of ovarian cancer, such as aging and menopause cannot be prevented, the risk can be reduced by suppressing inflammation. The results of our study in a mouse model confirm previous results that inflammation is a key factor in promoting ovarian cancer cell seeding. An understanding of the mechanisms by which inflammation plays a role in the early stages ovarian cancer will be necessary for effective ovarian cancer prevention.

References

- Torre, L. A. *et al.* Ovarian cancer statistics, 2018. *CA Cancer J Clin* (2018).
- Smith, R. A. *et al.* Cancer screening in the United States, 2018: A review of current American Cancer Society guidelines and current issues in cancer screening. *CA Cancer J Clin* (2018).
- Kurman, R. J. & Shih, I. M. Molecular pathogenesis and extraovarian origin of epithelial ovarian cancer—shifting the paradigm. *Hum Pathol* **42**, 918–931 (2011).
- Medeiros, F. *et al.* The tubal fimbria is a preferred site for early adenocarcinoma in women with familial ovarian cancer syndrome. *Am J Surg Pathol* **30**, 230–236 (2006).
- Crum, C. P. *et al.* Lessons from BRCA: the tubal fimbria emerges as an origin for pelvic serous cancer. *Clin Med Res* **5**, 35–44 (2007).
- Kindelberger, D. W. *et al.* Intraepithelial carcinoma of the fimbria and pelvic serous carcinoma: Evidence for a causal relationship. *Am J Surg Pathol* **31**, 161–169 (2007).
- Przybycin, C. G., Kurman, R. J., Ronnett, B. M., Shih, I. M. & Vang, R. Are all pelvic (nonuterine) serous carcinomas of tubal origin? *Am J Surg Pathol* **34**, 1407–1416 (2010).
- Jayson, G. C., Kohn, E. C., Kitchener, H. C. & Ledermann, J. A. Ovarian cancer. *Lancet* **384**, 1376–1388 (2014).
- Chuffa, L. G., Lupi-Junior, L. A., Costa, A. B., Amorim, J. P. & Seiva, F. R. The role of sex hormones and steroid receptors on female reproductive cancers. *Steroids* **118**, 93–108 (2017).
- Fleming, J. S., Beaugie, C. R., Haviv, I., Chenevix-Trench, G. & Tan, O. L. Incessant ovulation, inflammation and epithelial ovarian carcinogenesis: revisiting old hypotheses. *Mol Cell Endocrinol* **247**, 4–21 (2006).
- Laven, J. S. E., Visser, J. A., Uitterlinden, A. G., Vermeij, W. P. & Hoeymakers, J. H. J. Menopause: Genome stability as new paradigm. *Maturitas* **92**, 15–23 (2016).
- Saed, G. M., Diamond, M. P. & Fletcher, N. M. Updates of the role of oxidative stress in the pathogenesis of ovarian cancer. *Gynecol Oncol* (2017).
- Yang, H. P. *et al.* Lifetime Number of Ovulatory Cycles and Risks of Ovarian and Endometrial Cancer Among Postmenopausal Women. *Am J Epidemiol* **183**, 800–814 (2016).
- Fathalla, M. F. Incessant ovulation—a factor in ovarian neoplasia? *Lancet* **2**, 163 (1971).
- Casagrande, J. T. *et al.* “Incessant ovulation” and ovarian cancer. *Lancet* **2**, 170–173 (1979).
- Purdie, D. M., Bain, C. J., Siskind, V., Webb, P. M. & Green, A. C. Ovulation and risk of epithelial ovarian cancer. *Int J Cancer* **104**, 228–232 (2003).
- Focchi, G. R., Simoes Mde, J., Baracat, E. C., de Lima, G. R. & Evencio Neto, J. Ultrastructural aspects of the remodeling process of the Corpus albicans in the recent postmenopausal period. *Sao Paulo Med J* **114**, 1173–1176 (1996).
- Singavarapu, R., Buchinsky, N., Cheon, D. J. & Orsulic, S. Whole ovary immunohistochemistry for monitoring cell proliferation and ovulatory wound repair in the mouse. *Reprod Biol Endocrinol* **8**, 98 (2010).
- Xing, D. & Orsulic, S. A mouse model for the molecular characterization of brca1-associated ovarian carcinoma. *Cancer Res* **66**, 8949–8953 (2006).
- Goldberg, M. S. *et al.* Nanoparticle-mediated delivery of siRNA targeting Parp1 extends survival of mice bearing tumors derived from Brca1-deficient ovarian cancer cells. *Proc Natl Acad Sci USA* **108**, 745–750 (2011).
- Huang, J. *et al.* The PARP1 inhibitor BMN 673 exhibits immunoregulatory effects in a Brca1(-/-) murine model of ovarian cancer. *Biochem Biophys Res Commun* **463**, 551–556 (2015).
- Mantia-Saldone, G. *et al.* The immunomodulatory effects of pegylated liposomal doxorubicin are amplified in BRCA1-deficient ovarian tumors and can be exploited to improve treatment response in a mouse model. *Gynecol Oncol* **133**, 584–590 (2014).
- Wang, L. *et al.* Decitabine Enhances Lymphocyte Migration and Function and Synergizes with CTLA-4 Blockade in a Murine Ovarian Cancer Model. *Cancer Immunol Res* **3**, 1030–1041 (2015).
- Hoogenkamp, H. & Lewing, P. Superovulation in mice in relation to their age. *Vet Q* **4** (47–48), 44 (1982).
- Yang-Hartwich, Y. *et al.* Ovulation and extra-ovarian origin of ovarian cancer. *Sci Rep* **4**, 6116 (2014).
- Zhang, X., Meng, X., Chen, Y., Leng, S. X. & Zhang, H. The Biology of Aging and Cancer: Frailty, Inflammation, and Immunity. *Cancer J* **23**, 201–205 (2017).
- Myers, C. E., Mirza, N. N. & Lustgarten, J. Immunity, cancer and aging: lessons from mouse models. *Aging Dis* **2**, 512–523 (2011).
- Morihara, K., Takenaka, H., Morihara, T. & Kishimoto, S. Primary cutaneous anaplastic large cell lymphoma associated with vascular endothelial growth factor arising from a burn scar. *J Am Acad Dermatol* **57**, S103–105 (2007).
- Oosterling, S. J., van der Bij, G. J., van Egmond, M. & van der Sijp, J. R. Surgical trauma and peritoneal recurrence of colorectal carcinoma. *Eur J Surg Oncol* **31**, 29–37 (2005).
- Demicheli, R., Retsky, M. W., Hrushesky, W. J. & Baum, M. Tumor dormancy and surgery-driven interruption of dormancy in breast cancer: learning from failures. *Nat Clin Pract Oncol* **4**, 699–710 (2007).
- Castano, Z., Tracy, K. & McAllister, S. S. The tumor microenvironment and systemic regulation of breast cancer progression. *Int J Dev Biol* **55**, 889–897 (2011).
- DeNardo, D., Andreu, P. & Coussens, L. M. Interactions between lymphocytes and myeloid cells regulate pro- versus anti-tumor immunity. *Cancer and Metastasis Reviews* **29**, 309–316 (2010).
- Quail, D. F. & Joyce, J. A. Microenvironmental regulation of tumor progression and metastasis. *Nature Medicine* **19**, 1423–1437 (2013).
- TwoRoger, S. S., Fairfield, K. M., Colditz, G. A., Rosner, B. A. & Hankinson, S. E. Association of oral contraceptive use, other contraceptive methods, and infertility with ovarian cancer risk. *Am J Epidemiol* **166**, 894–901 (2007).
- Trabert, B. *et al.* Aspirin, nonaspirin nonsteroidal anti-inflammatory drug, and acetaminophen use and risk of invasive epithelial ovarian cancer: a pooled analysis in the Ovarian Cancer Association Consortium. *J Natl Cancer Inst* **106**, djt431 (2014).
- Trabert, B. *et al.* Analgesic Use and Ovarian Cancer Risk: An Analysis in the Ovarian Cancer Cohort Consortium. *J Natl Cancer Inst* (2018).

Acknowledgements

We thank Kristy J. Daniels for assistance in manuscript preparation and members of the Women's Cancer Program for their support. This work was supported by the Office of the Assistant Secretary of Defense for Health Affairs through the Ovarian Cancer Research Program Award No. W81XWH-17-1-0144 and W81XWH-16-1-0190; the National Cancer Institute grants R21CA194626 and 1R01CA208753; and the Cantor-UCLA Women's Health Center Executive Advisory Board & NCATS UCLA Clinical and Translational Science Institute grant UL1TR000124.

Author Contributions

D.J. performed all experiments described in this study except mouse surgery, which was performed by Y.N. and M.K. D.J. also participated in data collection, analysis, and interpretation. S.O. conceived and designed the study, participated in data analysis and interpretation, and wrote the manuscript. All authors contributed to manuscript revisions and approved the submitted version.

Additional Information

Supplementary information accompanies this paper at <https://doi.org/10.1038/s41598-018-30261-8>.

Competing Interests: The authors declare no competing interests.

Publisher's note: Springer Nature remains neutral with regard to jurisdictional claims in published maps and institutional affiliations.



Open Access This article is licensed under a Creative Commons Attribution 4.0 International License, which permits use, sharing, adaptation, distribution and reproduction in any medium or format, as long as you give appropriate credit to the original author(s) and the source, provide a link to the Creative Commons license, and indicate if changes were made. The images or other third party material in this article are included in the article's Creative Commons license, unless indicated otherwise in a credit line to the material. If material is not included in the article's Creative Commons license and your intended use is not permitted by statutory regulation or exceeds the permitted use, you will need to obtain permission directly from the copyright holder. To view a copy of this license, visit <http://creativecommons.org/licenses/by/4.0/>.

© The Author(s) 2018

1 **Are epithelial ovarian cancers of the mesenchymal subtype actually intraperitoneal metastases**
2 **to the ovary?**

3
4 Ye Hu¹, Barbie Taylor-Harding¹, Yael Raz¹, Marcela Haro¹, Maria Sol Recouvreux¹, Enes Taylan¹,
5 Jenny Lester², Joshua Millstein³, Ann E. Walts⁴, Beth Y. Karlan^{2,5} and Sandra Orsulic^{1, 2, *}

6
7 ¹Women's Cancer Program at the Samuel Oschin Comprehensive Cancer Institute, Cedars-Sinai Medical
8 Center, Los Angeles, CA, USA

9 ²Department of Obstetrics and Gynecology, David Geffen School of Medicine, University of California Los
10 Angeles, Los Angeles, CA, USA

11 ³Division of Biostatistics, Department of Preventive Medicine, Keck School of Medicine, University of
12 Southern California, Los Angeles, CA, USA

13 ⁴Department of Pathology and Laboratory Medicine, Cedars-Sinai Medical Center, Los Angeles, CA, USA

14 ⁵Jonsson Comprehensive Cancer Center, University of California Los Angeles, Los Angeles, CA, USA

15
16 **Running Title:** Mesenchymal subtype indicates advanced intraperitoneal dissemination

17 **Keywords:** ovarian cancer, mesenchymal, molecular subtype, metastases, desmoplasia

18
19 ***Corresponding Author:** Sandra Orsulic, Cedars-Sinai Medical Center, 8700 Beverly Blvd., Los
20 Angeles, CA, 90048, Tel: 310-423-9546, Email: orsulics@cshs.org

21
22 **Tables:** 0

23 **Figures:** 5

24 **Supplementary tables:** 5

25 **Supplementary figures:** 3

26
27 Note for reviewers: The GSE135712 and GSE133296 data sets have been deposited into GEO.

28
29 To review GEO accession GSE135712:

30 Go to <https://www.ncbi.nlm.nih.gov/geo/query/acc.cgi?acc=GSE135712>

31 Enter token obynqwaujjerda into the box

32
33 To review GEO accession GSE133296:

34 Go to <https://www.ncbi.nlm.nih.gov/geo/query/acc.cgi?acc=GSE133296>

35 Enter token mpgvewiwjbmbrqd into the box

36 **Abstract**

37

38 Primary ovarian high-grade serous carcinoma (HGSC) has been classified into 4 molecular
39 subtypes: Immunoreactive, Proliferative, Differentiated, and Mesenchymal (Mes), of which the
40 Mes subtype (Mes-HGSC) is associated with the worst clinical outcomes. We propose that Mes-
41 HGSC comprise clusters of cancer and associated stromal cells that detached from tumors in the
42 upper abdomen/omentum and disseminated in the peritoneal cavity, including to the ovary. Using
43 comparative analyses of multiple transcriptomic data sets, we provide the following evidence that
44 the phenotype of Mes-HGSC matches the phenotype of tumors in the upper abdomen/omentum:
45 1) irrespective of the primary ovarian HGSC molecular subtype, matched upper
46 abdominal/omental metastases were typically of the Mes subtype, 2) the Mes subtype was present
47 in primary ovarian HGSC only in patients with concurrent upper abdominal/omental metastases
48 and not in those with primary HGSC confined to the ovary, and 3) primary ovarian Mes-HGSC
49 had an expression profile characteristic of stromal cells in the upper abdominal/omental
50 metastases. We suggest that Mes-HGSC signifies advanced intraperitoneal tumor dissemination to
51 the ovary rather than a subtype of primary ovarian HGSC. This is consistent with the presence of
52 upper abdominal/omental disease, suboptimal debulking, and worst survival previously reported
53 in patients with primary ovarian Mes-HGSC compared to other molecular subtypes.

54

55 **Introduction**

56
57 The majority of ovarian cancer patients with HGSC are diagnosed with tumors involving one or both
58 ovaries and various additional intraperitoneal sites including the upper abdomen/omentum (FIGO
59 stage III) (1). HGSC can arise from the fallopian tube, the ovarian surface serous epithelium, or
60 extraovarian peritoneal tissues as primary peritoneal carcinoma (PPC) (**Fig. 1A**). Currently, it is
61 thought that ovarian cancer cells shed from the primary tumor into the peritoneal fluid and disseminate
62 in the peritoneal cavity, typically from the ovary to the upper abdomen/omentum (**Fig. 1A**). However,
63 the model of primarily unidirectional HGSC metastasis from the pelvis to the upper
64 abdomen/omentum seems simplistic within a cavity that lacks internal physical barriers to cancer
65 dissemination. We propose that in stage III HGSC, metastases and PPC in the upper
66 abdomen/omentum shed cancer cell-stroma aggregates into the peritoneal fluid, resulting in
67 intraperitoneal dissemination that includes secondary metastases to the primary tumor in the pelvis
68 (**Fig. 1B**). Patterns of cancer dissemination within the peritoneal cavity have been difficult to discern
69 using genomic data because genomic instability is an early event in HGSC and copy number profiles
70 and mutational patterns are typically shared across different anatomic sites (2-6). However, individual
71 clones have been tracked using whole-genome and single-nucleus sequencing of patient-matched
72 tumor deposits at different anatomic locations. These studies identified evidence of metastases to the
73 ovary or the fallopian tube in 4 of 15 patients, thereby demonstrating that re-seeding of the primary
74 tumor site by clones from peritoneal metastases is not a rare event (2,3).

75
76 Transcriptomic analyses have clustered primary ovarian HGSC into 4 main molecular subtypes:
77 Immunoreactive, Mesenchymal (Mes), Proliferative and Differentiated (7,8). The feature that
78 distinguishes primary ovarian HGSC of the Mes molecular subtype (hereafter referred to as primary
79 ovarian Mes-HGSC) from the other 3 subtypes (non-Mes subtypes) is the elevated expression of
80 myofibroblast/extracellular matrix (ECM) remodeling genes (9-11). In addition to this distinct
81 transcriptome, Mes-HGSC is more frequently associated with the presence of upper
82 abdominal/omental metastases (12,13), suboptimal surgical debulking (presence of residual
83 macroscopic disease after cytoreductive surgery) (13-15), severe postoperative complications (13,16),
84 and reduced overall survival (12-17) in comparison to the non-Mes subtypes. The current theory
85 suggests that cancer cells in primary ovarian Mes-HGSC recruit myofibroblasts or convert the local

86 ovarian stroma into myofibroblasts, which equip cancer cells with greater metastatic ability (11,13,18).
87 However, this theory does not explain why metastases are predominantly of the Mes phenotype even
88 when the primary tumor is Immunoreactive, Proliferative, or Differentiated subtype (19). PPC is also
89 typically of the Mes phenotype (20), suggesting that this phenotype is an inherent feature of peritoneal
90 lesions.

91
92 In this study, we used transcriptomic analyses of tumor samples with annotated presumed sites of
93 tumor origin and sites of sample collection (**Table S1**) to show that the Mes gene signature is
94 expressed in the stromal component of tumors in the upper abdomen/omentum but not in most primary
95 ovarian HGSC. However, if a tumor in the ovary expresses the Mes signature, we propose that this
96 tumor contains the microenvironment from tumors in the upper abdomen/omentum. This can occur by
97 two mechanisms (**Fig. 1B**). The first mechanism involves a primary tumor in the ovary/pelvis that
98 metastasizes to the omentum/upper abdomen, then the metastases, which have now acquired the Mes
99 phenotype, continue to seed the rest of the peritoneal cavity, including the ovary where the tumor
100 initially originated. The second mechanism involves PPC from the upper abdomen/omentum that
101 metastasizes throughout the peritoneal cavity, including to the ovary. If our hypothesis is correct, we
102 predict that stage II primary ovarian HGSC (tumors confined to the pelvis) cannot exhibit the Mes
103 subtype because of the absence of cancer/stroma cell aggregates from the upper abdomen/omentum
104 (**Fig. 1C**).

105

106 **Results**

107

108 **The Mes subtype reflects tumor location**

109 We examined whether the Mes phenotype varies across patient-matched FFPE samples of primary,
110 metastatic, and recurrent HGSC from 24 patients (**Fig. 2A and B**). The Mes phenotype was determined
111 by threshold expression of 15 mesenchymal genes (Materials and Methods, **Table S2**). The 15 genes
112 were among the top 100 genes used by Verhaak *et al.* (7) to define the Mes subtype by expression
113 profile analysis (Mes 100-gene set) (**Table S2**). In the TCGA data set, this 15-gene signature was
114 associated with poor overall and progression-free survival (**Fig. S1**) and was equivalent to the Mes
115 100-gene set in classifying samples of the Mes subtype (**Fig. S2**). All 15 genes were expressed at
116 higher levels in the metastatic and recurrent tumors compared to the matched primary tumors (**Fig.**

117 **2A**). While only 20% of the primary ovarian HGSC were classified as Mes, 19 79% of the metastatic
118 and 58% of the recurrent HGSC were classified as Mes (**Fig. 2B**). The higher percentage of the Mes
119 subtype in the metastatic samples than in the recurrent samples may be attributed to different sites of
120 sample collection; the omentum was the most common collection site for metastases while the serosal
121 aspects of the intestine/colon/rectum were the most common collection sites for recurrent tumors (**Fig.**
122 **2B**). Notably, 15 of 17 metastatic and recurrent samples collected from the omentum were classified as
123 Mes and none of the 4 metastatic and recurrent samples collected from the lymph nodes was classified
124 as Mes (**Fig. 2B**).

125
126 Since most metastases located in the upper abdomen/omentum were classified as Mes (**Fig. 2B**), we
127 hypothesized that primary ovarian HGSC of the Mes subtype are actually metastases from the upper
128 abdomen/omentum to the ovary. If this is correct, HGSC collected from patients with cancer confined
129 to the pelvis (stage I-II) should not exhibit the Mes phenotype because of the absence of upper
130 abdominal/omental disease as a source of metastatic tumor clusters able to seed the ovary (**Fig. 1C**).
131 We tested this hypothesis in 2 public data sets in which samples had been divided into 4 molecular
132 subtypes. In this study, we used the original molecular classifications for the TCGA and GSE9891
133 data sets (8,23). Of note, subsequent studies may have used different classification algorithms, which
134 resulted in different molecular subtype assignments to the same samples; in a recent study, 22% of
135 samples had been reclassified to a different molecular subtype (17).

136
137 In the TCGA data set, samples had been divided into 4 molecular subtypes: Immunoreactive,
138 Mesenchymal (Mes), Proliferative, and Differentiated (8). All of the TCGA tumor samples
139 presumably originated in the ovary and were collected from the ovary (ov-ov) (**Fig. 2C**). Of 26 stage II
140 HGSC samples, only 1 was classified as Mes (**Fig. 2C**). Notably, that sample (TCGA-61-2133) had
141 features of an aggressive malignancy despite its stage II designation: it was annotated as stage IIc,
142 grade 3 with extensive lymphovascular permeation, positive pelvic lymph nodes and the shortest
143 overall survival among patients with stage IIc HGSC who died from the disease (676 days vs 1380
144 days mean survival). In contrast to stage II HGSC, in 325 stage III HGSC and 74 stage IV HGSC, Mes
145 tumors contributed to 23% and 27% of samples, respectively (**Fig. 2C**).

146

147 In the GSE9891 data set, HGSC samples had been clustered into C1/Mesenchymal,
148 C2/Immunoreactive, C4/Proliferative, and C5/Differentiated molecular subtypes (23) and annotated by
149 their presumed tissue of origin and the site of specimen collection as ov-ov, per-ov, ov-per, and per-
150 per (**Fig. 2D**). Due to a small number of stage I and stage IV samples, we grouped stage I and II
151 samples as stage I-II, and stage III and IV samples as stage III-IV. None of the 14 ov-ov stage I-II
152 HGSC was classified as Mes/C1 (**Fig. 2D**). Of the 104 ov-ov stage III-IV HGSC, 23% were classified
153 as C1/Mes. Of the 38 ov-per stage III-IV HGSC, 66% were classified as C1/Mes (**Fig. 2D**). Of the 9
154 per-ov HGSC (including 1 stage II and 8 stage III-IV), 67% were classified as C1/Mes (**Fig. 2D**).
155 According to our hypothesis, all metastases that originated in the upper abdomen/omentum as PPC and
156 then spread to the ovary (per-ov) should be of the C1/Mes subtype. However, it is important to note
157 that these 9 per-ov tumors were reported by pathologists as PPC based only on the impression of
158 disease distribution gathered from the surgeon's description of the intraoperative findings in the
159 operative report and the tissue samples that surgeons had elected to excise. Interestingly, and as noted
160 by pathologists in some of these surgical pathology reports, pathologists were not always certain or in
161 agreement about the origin of the tumor (primary ovarian vs. PPC). Of the 21 per-per stage III-IV
162 HGSCs, 86% were classified as C1/Mes. It is unknown if some of these PPC samples were located in
163 the pelvis.

164
165 Together, we conclude that ov-ov HGSC stage I-II (confined to the pelvis) are almost never of the Mes
166 subtype while 20%-27% of ov-ov HGSC stage III-IV (presence of concurrent upper
167 abdominal/omental metastases) are of the Mes subtype. The Mes subtype is predominant among
168 HGSC samples collected from the peritoneal cavity (ov-per and per-per) as well as samples presumed
169 to be peritoneal metastases to the ovary (per-ov).

170

171 **The Mes molecular subtype is defined by the metastatic microenvironment, not the epithelial** 172 **cancer cells**

173 To determine which cell type expresses the Mes 15-gene signature, we used digital image analysis for
174 the annotation of fibroblasts, epithelial cancer cells, and immune cells in H&E-stained full sections of
175 omental metastases collected during primary debulking surgery from 152 HGSC patients
176 (GSE135712) (**Fig. 3A**). The Mes 15-gene signature z-score was determined for each patient (**Fig.**
177 **S3A**) and correlated with the content of each of the 3 annotated cell types. The two prevalent cell types

178 in omental metastases were epithelial cancer cells and fibroblasts, while the content of immune cells
179 was variable across 152 samples (data not shown). The Mes 15-gene signature correlated with the
180 fibroblast content ($r=0.660$; $p=2.4e-20$), inversely correlated with the epithelial cancer cell content ($r=-$
181 0.619 ; $p=1.8e-17$) and showed no significant correlation with the immune cell content ($r=-0.035$;
182 $p=0.67$) (**Fig. 3B**), suggesting that among these 3 cell types in omental metastases, fibroblasts are the
183 most likely source of the Mes 15-gene signature.

184
185 To study the correlation of the Mes 15-gene signature with fibroblast content in primary and metastatic
186 tumors, we used concurrent primary ovarian HGSC, omental metastases, and non-omental
187 intraperitoneal metastases collected at the time of primary debulking surgery from 10 HGSC patients
188 (GSE133296). The average fibroblast content did not differ significantly between primary ovarian
189 HGSC, omental metastases, and non-omental metastases (**Fig. 3C**). The Mes 15-gene signature z-
190 score (**Fig. S3B**) was significantly correlated with the fibroblast content in omental ($r=0.703$; $p=0.02$)
191 and non-omental intraperitoneal ($r=0.893$; $p=5.0e-4$) metastases but not in primary tumors ($r=0.170$;
192 $p=0.64$) (**Fig. 3D**), suggesting that primary tumor fibroblasts were not expressing high levels of the 15
193 Mes genes. This result is consistent with our prior *in situ* hybridization findings that only a small
194 number of patients (~20%) expressed COL11A1 in cancer-associated fibroblasts (CAFs) in primary
195 ovarian HGSC, while the majority of patient-matched metastases expressed COL11A1 in CAFs (21).

196
197 The Mes 15-gene signature was not enriched in metastases if metastatic epithelial cancer cells were
198 stripped of their microenvironment. EpCAM-positive epithelial cancer cells isolated from matched
199 primary ovarian HGSC, ascites, and metastasis from 5 patients (3 with replicate samples) (GSE73168)
200 (24) exhibited equivalent relative levels of the Mes 15-gene signature z-score (**Fig. S3C, D**). Together,
201 these results show that the Mes phenotype is determined by the metastatic microenvironment rather
202 than by the intrinsic molecular subtype of epithelial cancer cells.

203
204 **Primary ovarian HGSC of the Mes subtype are enriched for a gene signature characteristic of**
205 **stromal cells in metastases located in the upper abdomen/omentum**

206 We were interested to know if the stroma in primary ovarian HGSC differs from the stroma in HGSC
207 metastases located in various tissue sites in the peritoneal cavity. To completely exclude the epithelial
208 cancer cell transcriptome from the analysis, we used published stromal gene signatures derived from

209 proteome data of laser-capture microdissected stromal cells from primary ovarian HGSC and matched
210 omental metastases from 11 HGSC patients (22). We first validated the 2 stromal gene signatures (22)
211 in our own data set (GSE133296) of matched primary ovarian HGSC, omental metastases, and non-
212 omental metastases from 10 HGSC patients. The primary ovarian HGSC stromal gene signature was
213 overexpressed in a subset of primary ovarian HGSC while the omental metastasis stromal gene
214 signature was overexpressed in a subset of omental and non-omental metastases (**Fig. 4A**). Thus,
215 application of the published proteome-derived stromal gene signatures to our data set shows that the 2
216 stromal gene signatures are differentially enriched in primary and metastatic tumors in most, but not
217 all, patients (i.e. all 3 tumors cluster together in the asterisk-marked gray-colored patient and the teal-
218 colored patient) (**Fig. 4A**). To assign a quantitative value to the difference in enrichment of the 2
219 stromal gene signatures, we used an unweighted ratio of the stromal gene signature z-scores (positive
220 value for the omental metastasis gene signature and negative value for the primary ovarian HGSC
221 gene signature). The average ratio of the stromal gene signatures was significantly lower in primary
222 ovarian HGSC compared to patient-matched omental or non-omental metastases in the GSE133296
223 data set (**Fig. 4B**).

224

225 Using 2 large transcriptomic data sets in which subsets of samples have been annotated by the site of
226 sample collection (GSE9891 and GSE2109), we showed that the average ratio of the 2 stromal gene
227 signatures was lower in tumors located retroperitoneally or in the pelvis (ovary, uterus, and fallopian
228 tube) than in tumors located outside of the pelvis (omentum, colon/intestine, abdominal wall,
229 peritoneum, and diaphragm) (**Fig. 4C, D**). Together, these data suggest that intraperitoneal tumors
230 located in the pelvis are enriched for a stromal gene signature of primary ovarian HGSC while tumors
231 outside of the pelvis are enriched for a stromal gene signature of omental metastases.

232

233 To determine whether the 2 stromal gene signatures are associated with molecular subtypes in primary
234 ovarian HGSC, we used the ovarian TCGA data set (8). Overlay of the 2 stromal gene signatures with
235 the ovarian TCGA data set showed strong enrichment of the omental metastasis gene signature in the
236 Mes subtype while the stromal gene signature of primary ovarian HGSC was not significantly
237 enriched in any specific molecular subtype (**Fig. 5A**). The ratio of the 2 stromal gene signatures was
238 significantly enriched in the Mes subtype in comparison to the Immunoreactive, Differentiated, and
239 Proliferative molecular subtypes (**Fig. 5B**). Since the Immunoreactive and Mesenchymal primary

240 ovarian HGSC subtypes have been shown to contain more stroma (less epithelial cancer cells) than the
241 Differentiated and Proliferative subtypes (10,11,25,26), it is possible that the stromal gene signatures
242 are overexpressed in samples with high stromal content and underexpressed in samples with high
243 epithelial cancer cell content. However, we show little correlation between the stromal gene signatures
244 and epithelial cancer cell content in the TCGA data set (**Fig. 5C**), suggesting that the strong
245 enrichment of the stromal gene signature ratio in Mes-HGSC (**Fig. 5B**) reflects a molecularly different
246 type of stroma rather than an increased presence of the stroma in the Mes subtype.

247

248 **Discussion**

249

250 Molecular profiling studies have identified 4 distinct molecular subtypes of primary ovarian HGSC of
251 which the Mes subtype has the lowest rate of optimal surgical debulking and the worst overall survival
252 (7,10,13,15,23,27-29), and is almost always associated with coexisting upper abdominal/omental
253 metastases (13,15). It has been shown that cancer-associated stroma and ECM largely contribute to the
254 Mes gene signature (9-11). Additionally, our analyses showed that the transcriptome of primary
255 ovarian Mes-HGSC is strongly correlated with the stromal gene signature of omental metastasis (22).
256 Considering the phenotypic similarity between primary ovarian Mes-HGSC and peritoneal metastases
257 and the frequent coexistence of primary ovarian Mes-HGSC with upper abdominal/omental
258 metastases, we propose that primary ovarian Mes-HGSC might actually be cancer-stroma aggregates
259 that detached from tumors located in the upper abdomen/omentum. Indeed, whole-genome and single-
260 nucleus sequencing analyses have demonstrated that metastases are not always unidirectional and that
261 the re-seeding of peritoneal metastasis to the fallopian tube or ovary can occur (2,3). Unfortunately,
262 the gene expression based molecular subtypes of such samples cannot be determined as these studies
263 isolated high purity epithelial tumor cells rather than the stroma, which frequently contributes to gene
264 expression signatures that define molecular subtypes.

265

266 Studies in cell co-cultures and in mouse models demonstrated the existence of heterotypic aggregates
267 of cancer cells and stroma, in which stromal cells support epithelial cancer cell survival and guide
268 peritoneal invasion, and can accompany epithelial cancer cells to a new metastatic site and actively
269 reconstitute the tumor stroma in newly formed metastases (24,30). However, it has been shown that
270 HGSC metastases rarely contain CAFs from primary ovarian HGSC (24), suggesting that stromal cells

271 in primary ovarian tumors are not overly efficient in accompanying cancer cells to a new metastatic
272 site and/or are not proficient in re-building the stroma at a new site. It is likely that implantation of
273 cancer cell-stroma aggregates at a new metastatic site requires significant remodeling of the local
274 stroma or recruitment of new stroma. Indeed, stroma in the upper abdominal/omental metastases is
275 frequently enriched for markers of myofibroblasts and ECM remodeling, such as POSTN, COL11A1,
276 LOX, VCAN, TNC, and THBS2 (9,20,22). It is possible that the upper abdominal/omental metastasis
277 stroma is more efficient than primary ovarian cancer stroma in accompanying metastatic cancer cells
278 and reconstituting the stroma at secondary metastatic sites. For example, omental adipocytes have
279 been shown to promote ovarian cancer metastasis and provide energy for rapid tumor growth (31,32).

280
281 Our result that the majority of patient-matched metastatic or recurrent HGSC samples were classified
282 as Mes-HGSC irrespective of the primary cancer subtype is consistent with the results of a recent
283 study in a different cohort of patients (19) as well as a study showing that the majority of PPC are
284 classified as the Mes subtype (20). According to our hypothesis that the Mes signature is a signature of
285 stromal cells in the upper abdominal/omental HGSC, all HGSC in the upper abdomen/omentum
286 should be classified as Mes. Yet in our study, only 86% of PPC and 66% of peritoneal metastases were
287 classified as Mes. It is also expected that all PPC metastases to the ovary are Mes but only 67% were
288 classified as Mes. Multiple technical reasons could explain why some metastases to the ovary did not
289 classify as Mes including imperfections in algorithms that had been used for the Mes subtype
290 classification in the original publications, unknown precise site of sample collection in the peritoneal
291 cavity (pelvis vs upper abdomen/omentum), and/or inclusion of samples that had been annotated as
292 PPC based on the tumor distribution but are actually primary ovarian or fallopian tube HGSC. A
293 biological explanation for the existence of non-Mes-HGSC metastases in the upper abdomen/omentum
294 could be that metastases are initially associated with accompanying stroma from the primary ovarian
295 HGSC until cancer cells can recruit and/or remodel the stroma at the metastatic site.

296
297 We cannot completely exclude the possibility that cancer cells in primary ovarian Mes-HGSC are
298 capable of converting the resident ovarian stromal cells into myofibroblasts or recruiting
299 myofibroblast-like stroma to the ovary. However, if this were true, it would be expected that some of
300 the stage I-II primary ovarian HGSC were of the Mes subtype. Of the 37 stage I-II primary ovarian
301 HGSC samples that satisfied our inclusion criteria in the TCGA and GSE9891 data sets, only 1 was

302 classified as Mes and that tumor exhibited features of a highly aggressive malignancy (stage IIc with
303 lympho-vascular invasion and early death from the disease), suggesting the potential presence of
304 malignant ascites containing microscopic cancer cell-stroma aggregates from the upper
305 abdomen/omentum.

306
307 Although the main purpose of this study was to present a new perspective in the understanding of
308 intraperitoneal HGSC dissemination, our results have clinical relevance. We suggest that the Mes gene
309 signature in primary ovarian HGSC signifies advanced/high-stage intraperitoneal metastatic
310 dissemination that includes metastasis to the ovary by cancer cell-stroma aggregates from the upper
311 abdomen/omentum. From this perspective, stage III Mes-HGSC could be considered “more advanced”
312 than stage III non-Mes-HGSC. Additionally, our results may be relevant to the future clinical use of
313 molecular subtype biomarkers to triage patients to primary cytoreductive surgery or neoadjuvant
314 chemotherapy. Genes associated with the Mes subtype have been associated with suboptimal
315 debulking and increased postoperative morbidity and mortality (13,15,33,34), suggesting that the Mes
316 subtype could be helpful as a biomarker to triage patients toward neoadjuvant chemotherapy (35).
317 Some medical centers are already using preoperative biopsy to assess resectability and triage patients
318 for neoadjuvant chemotherapy (36,37). Our results show that the site of tumor biopsy is important in
319 determining the Mes subtype. Although large omental metastases are most easily accessed (37), they
320 are not reliable for patient stratification by tumor molecular subtype classification because they usually
321 exhibit the Mes subtype. If classification by molecular subtype is to be used to inform clinical
322 management, our findings underscore that biopsies submitted for molecular analysis should be
323 obtained from the ovarian mass, even though it may be more difficult to obtain than an omental
324 biopsy. With the advancement of image-guided core needle biopsy and minimally invasive surgical
325 techniques, diagnostic ovarian sampling to precisely identify molecular characteristics of the tumor
326 could become standard clinical practice in individualizing the treatment approach (38,39).

327

328 **Materials and Methods**

329

330 **Patient samples and gene expression analyses.** Formalin-fixed paraffin-embedded (FFPE) blocks
331 were retrieved from the pathology archives at Cedars-Sinai Medical Center under an approved IRB
332 protocol. FFPE blocks were sectioned onto uncharged glass slides. One 4 µm H&E-stained section

333 was used by a pathologist to circle the tumor areas and delineate them from the adjacent normal tissue.
334 Depending on the tumor size, 1 to 3 unstained 10 μ m sections were macrodissected (removal of non-
335 tumor areas based on the H&E template) with a clean razor blade. Total RNA was isolated using the
336 miRNeasy FFPE kit according to the manufacturer's instructions (Qiagen). For the GSE135712 data
337 set, samples of omental metastases collected from 152 HGSC patients at the time of primary debulking
338 surgery were analyzed for RNA expression of 1067 genes by NanoString nCounter technology
339 (NanoString Technologies). Data were normalized using nSolver software (NanoString Technologies).
340 In a separate NanoString data set, matched primary, metastatic, and recurrent HGSC samples from 29
341 patients were analyzed for RNA expression of 15 genes by NanoString nCounter. Five patients were
342 excluded from the analysis due to missing tissue or missing mRNA data for one of the matched
343 tumors. In 4 patients where more than one matched metastatic or recurrent tumor sample was
344 available, one sample was randomly selected for the study. For the GSE133296 data set, matched
345 HGSC samples collected from the ovary, omental metastasis, and non-omental intraperitoneal
346 metastasis from 10 patients at the time of primary debulking surgery were analyzed for RNA
347 expression by RNA sequencing using the SMARTer Stranded Total RNA-Seq Kit v2 on the Illumina
348 HiSeqX platform (MedGenome). Unwanted sequences (non-polyA tailed RNAs from the sample,
349 mitochondrial genome sequences, ribosomal RNAs, transfer RNAs, adapter sequences and others)
350 were removed using Bowtie2 (version 2.2.4). The paired-end reads were aligned to the reference
351 human genome downloaded from the UCSC database (GRCh37/hg19). STAR (2.4.1) aligner was used
352 for read alignment. Reads mapping to ribosomal and mitochondrial genomes were removed before
353 alignment was performed. The raw read counts were estimated using HTSeq-0.6.1. Read count data
354 were normalized using DESeq2.

355
356 **Expression data sets.** For the ovarian TCGA data set, level 3 data (gene merged) on the
357 AgilentG4502A_07_3 platform was used for analyses. The GSE9891, GSE2109, and GSE73168 data
358 sets were obtained from the Gene Expression Omnibus (GEO) repository. Raw and normalized data
359 for GSE135712 and GSE133296 were deposited into the GEO archive. Datasets used in this study and
360 their associated publications are listed in **Table S1**.

361
362 **Gene signatures distinguishing Mes-HGSC from non-Mes-HGSC.** For the 15-gene Mes signature,
363 matched primary, metastatic, and recurrent FFPE tumor samples from 24 patients with HGSC were

364 profiled with NanoString nCounter for expression of 15 genes (**Table S2**) that we previously found to
365 be associated with poor survival in HGSC (21) and/or belonged to the pan-cancer gene signature of
366 activated cancer-associated fibroblasts (9). A threshold for each of the 15 genes was determined by its
367 median expression level in the primary tumors (**Table S3**). A score of 1 was given if the expression
368 exceeded the threshold, otherwise a score of 0 was given (**Table S3**). Once 15 individual scores
369 corresponding to 15 mesenchymal genes were obtained, they were used to create a Mes score. The
370 Mes score was normalized to a range between 0 and 1, in which 1 indicated Mes-HGSC while all other
371 values indicated non-Mes-HGSC. Application of this 15-gene score algorithm to the TCGA data set
372 correctly classified 96 of 105 (91%) samples annotated as the Mesenchymal subtype and 317 of 355
373 (89%) samples annotated as the non-Mesenchymal subtype (Immunoreactive, Proliferative or
374 Differentiated) (**Table S4**). For the 100-gene set mesenchymal HGSC gene signature, we used the top
375 100 genes that distinguished the Mes subtype from other subtypes, according to the study by Verhaak
376 *et al.* (7) (**Table S2**). The 21-gene stromal signature of primary ovarian HGSC and the 21-gene
377 stromal signature of omental metastasis have been described (22).

378
379 **Data analyses.** The R2: Genomic Analysis and Visualization Platform ([http://hgserver1.amc.nl/cgi-](http://hgserver1.amc.nl/cgi-bin/r2/main.cgi)
380 [bin/r2/main.cgi](http://hgserver1.amc.nl/cgi-bin/r2/main.cgi)) was used for analyses of RNA expression levels and correlation between gene set
381 signatures and sample groups in different data sets. The gene set signature score was defined as the
382 average z-score of a z-score-transformed data set. For digital image data analyses, H&E stained slides
383 were scanned at 20x magnification using Aperio AT Turbo. The image analysis was performed using
384 the QuPath software. The image analysis workflow consisted of cell/nucleus detection, annotation of
385 regions containing 3 different cell types (fibroblast, epithelial cancer cell, immune cell), creating the
386 cell detection classifier, and applying the classifier to all cells in the circled regions of the slide.

387
388
389
390 **Acknowledgments:** We thank Kristy J. Daniels for assistance in manuscript preparation and Elad
391 Yana for assistance with the illustration. We also thank the Australian Ovarian Cancer Study
392 (AOCS) group for providing additional information about the GSE9891 data set.

393

394 **Author Contributions:** SO conceived the hypothesis, analyzed data sets and wrote the manuscript. JL
395 reviewed and categorized clinical information. AEW reviewed the pathology and selected tissue
396 blocks for mRNA isolation. BT-H isolated RNA from FFPE samples and conducted NanoString
397 nCounter analyses. YH, YR, MH, MSR, and ET contributed to data analyses. JM analyzed the
398 NanoString nCounter data for matched primary, metastatic, and recurrent tumor samples. AEW and
399 BYK provided critical input and contributed to the writing of the manuscript. All authors participated
400 in manuscript revisions.

401
402 **Grant Support:** This research was supported by the National Cancer Institute grant R01CA208753
403 and the Office of the Assistant Secretary of Defense for Health Affairs through the Ovarian Cancer
404 Research Program Awards Nos. W81XWH-17-1-0144 and W81XWH-16-1-0190 and the Ovarian
405 Cancer Research Alliance Program Project Grant to SO, the Foundation for Women's Cancer (FWC)
406 Laura Crandall Brown Foundation Ovarian Cancer Early Detection Research Grant and the Rivkin
407 Center Grant to YR, Tina's Wish Rising Star award to MSR, and the Ovarian Cancer Research
408 Alliance Ann and Sol Schreiber Mentored Investigator Awards to YH and MH.

409

410 **Disclosure of Potential Conflicts of Interest:** Authors declare no conflicts of interest.

411

412 **FIGURE LEGENDS**

413

414 **Fig. 1. Diagram of peritoneal dissemination of HGSC.** For graphical purposes, only stages II and III
415 are shown and up to 3 different primary tumors (p1, p2, p3) occurring in individual patients are shown
416 as if they occurred in a single patient. In stage III HGSC, metastases from the ovary to the upper
417 abdomen/omentum (ov-per) and PPC (per-per) usually exhibit the Mes subtype (red). Primary ovarian
418 HGSC are mostly of the non-Mes subtype (blue) but a subset exhibits the Mes subtype (red). **(A)** In
419 the current model of ovarian cancer dissemination, tumors spread in one direction - from the pelvis to
420 the upper abdomen/omentum (ov-per). Primary ovarian HGSC of the non-Mes and Mes subtype form
421 metastases of the Mes subtype. **(B)** In the proposed model of peritoneal metastasis, tumors spread in
422 both directions – from the pelvis to the upper abdomen/omentum (ov-per) and from the upper
423 abdomen/omentum (HGSC metastases or PPC) to the pelvis (per-ov). True primary ovarian HGSC
424 (ov-ov) are of the non-Mes subtype while metastases from the upper abdomen/omentum to the ovary
425 (per-ov) are of the Mes subtype. **(C)** In stage II HGSC, masses in the ovary are of the non-Mes
426 subtype because upper abdominal/omental tumors are absent.

427

428 **Fig. 2. The Mes subtype is characteristic of upper abdominal/omental metastases and PPC while**
429 **HGSC confined to the pelvis does not exhibit the Mes subtype.** **(A)** NanoString expression of 15
430 mesenchymal genes in FFPE samples from primary, metastatic, and recurrent stage III-IV HGSC from
431 24 patients. **(B)** The samples were classified into Mes (red) and non-Mes subtypes using the Mes 15-
432 gene signature z-score. The site of sample collection is indicated for each tumor, with the omentum
433 and lymph nodes indicated in red and blue, respectively. **(C)** Distribution of molecular subtypes by
434 disease stage in the TCGA data set. Excluded from the analysis were 4 samples for which the ovary
435 was not the presumed site of tumor origin or the site of tumor collection (2 fallopian tube and 2
436 omentum samples). Additionally, 81 samples that did not cluster among the 4 molecular subtypes were
437 excluded. **(D)** Distribution of molecular subtypes by disease stage, site of presumed tumor origin, and
438 site of sample collection. Included in the analysis were only tumors annotated as high grade (2 or 3);
439 serous histology; malignant; stage I, II, III or IV; molecular subtype C1/Mesenchymal, C2/Immune,
440 C5/Differentiated or C4/Proliferative; primary site ovary (ov) or peritoneum (per); and collection site
441 ovary (ov) or peritoneum/colon/omentum (per). Due to the small number of stage I and stage IV

442 samples, stage I and II samples were grouped as stage I-II, and stage III and IV samples were grouped
443 as stage III-IV. One stage II per-per sample was grouped with 8 stage III-IV per-per samples.

444

445 **Fig. 3. The Mes gene signature expression correlates with fibroblast content in HGSC metastases**

446 **but not primary ovarian HGSC. (A)** A representative example of cell type (fibroblast, epithelial
447 cancer cell, immune cell) annotation by QuPath analysis of H&E-stained full sections of omental
448 metastases isolated from 152 HGSC patients at the time of primary debulking surgery (GSE135712).

449 **(B)** Correlation of the Mes 15-gene signature score (Y axis) with the content of fibroblasts, cancer
450 cells, and immune cells in omental metastases isolated from 152 HGSC patients (GSE135712). The
451 content of each cell type was determined as the percent of one cell type in the 3 annotated cell types
452 (fibroblasts, cancer cells, immune cells) in each sample (X axis). **(C)** Fibroblast content in matched

453 primary tumors, omental metastases, and non-omental peritoneal metastases isolated at the time of
454 primary debulking surgery from 10 HGSC patients (GSE133296). Fibroblast content was determined
455 as the percent of fibroblasts in the 3 annotated cell types in each sample. **(D)** Correlation of the Mes

456 15-gene signature score (Y axis) with the content of fibroblasts (X axis) individually in matched
457 primary tumors, omental metastases, and non-omental intraperitoneal metastases from 10 HGSC
458 patients (GSE133296).

459

460 **Fig. 4. The stroma in HGSC metastases has different molecular features than the stroma in**

461 **primary ovarian HGSC. (A)** Euclidean clustering heatmap of expression values of 2 public stromal
462 gene signatures (derived from laser-capture microdissected stromal cells in matched primary ovarian
463 HGSC and omental metastases from 11 patients with HGSC) applied to the GSE133296 transcriptome
464 data set of matched primary ovarian HGSC, omental metastases, and non-omental metastases from 10
465 HGSC patients. Blue and red bars on the right indicate which genes belong to the primary ovarian
466 HGSC stromal gene signature (blue) and the omental metastasis stromal gene signature (red).

467 Transcripts for GSTA2 (from the original primary ovarian HGSC stromal gene signature) and
468 LPREL2 (from the original omental metastasis stromal gene signature) were missing in the
469 GSE133296 data set. The signature score was defined as the average z-score of a z-score-transformed
470 GSE133296 data set. The average gene signature scores and average unweighted ratio of the signature
471 scores are shown at the bottom of the heatmap. Asterisks indicate patients for which primary ovarian,
472 omental metastasis, and non-omental metastasis samples clustered together. **(B-D)** Dot plots of the

473 ratio of z-scores from the omental metastasis stromal gene signature (positive unweighted value) and
474 primary ovarian HGSC stromal gene signature (negative unweighted value) in **(B)** primary ovarian
475 HGSC, omental metastases, and non-omenta metastases in the GSE133296 data set; **(C)** different sites
476 of sample collection in the GSE9891 data set (excluded from the analysis were tumors of low
477 malignant potential, non-serous tumors, one bone metastasis, and tumors lacking annotation of the
478 collection site); and **(D)** different sites of sample collection in the GSE2109 data set (included in the
479 analysis were ovarian tumors of all types and histologies that have been annotated by the site of
480 sample collection; some sites have been grouped in this graph; for original annotation, please see
481 **Table S5**). The GSTA2 transcript was missing in the GSE9891 and GSE2109 data sets. The bars
482 indicate average ratio of z-scores in each group.

483
484 **Fig. 5. TCGA primary ovarian Mes-HGSC are enriched for a stromal gene signature of omental**
485 **metastases.** **(A)** Euclidean clustering heatmap of expression values of 2 public stromal gene signatures
486 (derived from laser-capture microdissected stromal cells in matched primary ovarian HGSC and
487 omental metastases from 11 patients with HGSC) applied to the TCGA primary ovarian HGSC
488 samples classified as the Immunoreactive, Mesenchymal, Proliferative and Differentiated molecular
489 subtypes (excluded from the analysis were 4 samples that were not collected from the ovary and 81
490 samples that did not cluster among the 4 molecular subtypes). The primary ovarian HGSC stromal
491 signature was represented by 20 of the original 21 genes (GSTA2 transcript was missing in the
492 TCGA data set). The signature score was defined as the average z-score of a z-score-transformed
493 TCGA data set. Average gene signature scores and the average unweighted ratio of signature scores
494 are shown at the bottom of the heatmap. **(B)** Dot plot of the ratio of z-scores from the omental
495 metastasis stromal gene signature (positive unweighted value) and primary ovarian HGSC stromal
496 gene signature (negative unweighted value) in the Immunoreactive, Mesenchymal, Proliferative and
497 Differentiated molecular subtypes in the TCGA data set. **(C)** Dot plots of Spearman correlation of
498 stromal signature z-scores and percent of epithelial cancer cells present in histological sections of
499 tumor samples in the TCGA data set.

500

501

502 **SUPPLEMENTARY FIGURES**

503

504 **Fig. S1.** Kaplan-Meier plot of overall survival and disease-free survival using the 15-gene
505 mesenchymal signature (average expression) in the TCGA data set. Samples include grade 2+3 HGSC.

506

507 **Fig. S2.** Robustness of the Mes 15-gene signature in classifying Mes-HGSC. **(A)** Euclidean clustering
508 heatmaps of expression values of the 15-gene signature defined by NanoString analysis and the 100-
509 gene signature defined by Verhaak et al. (7) in the ovarian TCGA data set in which samples had been
510 previously classified into the Immunoreactive, Mesenchymal, Proliferative and Differentiated
511 molecular subtypes. The signature score was defined as the average z-score of a z-score-transformed
512 TCGA data set. Average gene signature scores are shown at the bottom of each heatmap. **(B)**
513 Spearman correlation of gene signature scores between Mes 15-gene set (NanoString) and Mes 100-
514 gene set (Verhaak). **(C)** Levels of signature scores in the Immunoreactive, Mesenchymal, Proliferative
515 and Differentiated molecular subtypes. The 15-gene Mes subtype gene set is equally effective in
516 identifying Mes-HGSC as the standard 100-gene Mes subtype gene set defined by Verhaak et al. (7).

517

518 **Fig. S3.** Derivation of the Mes 15-gene signature z-score in different gene expression data sets.
519 Expression values for the 15-gene gene sets are shown as heatmaps of Euclidean clustering analysis
520 **(A)** GSE135712, **(B)** GSE133296, and **(C)** GSE73168. Average gene signature scores are shown at the
521 bottom of each heatmap. **(D)** Relative enrichment of the Mes 15-gene signature in EpCam-positive
522 epithelial cells isolated from primary ovarian HGSC, matched metastases, and ascites samples from 5
523 patients (3 with duplicate samples). Excluded from the analysis were samples from 3 patients with
524 ovarian tumors of low malignant potential. The bars represent median relative enrichment levels in
525 each group of samples.

526

527

528 **SUPPLEMENTARY TABLES**

529

530 **Table S1.** Gene expression datasets and associated publications.

531

532 **Table S2.** 15-gene and 100-gene signatures of the Mes molecular subtype. Genes overlapping between
533 the 15-gene and 100-gene signatures are highlighted in yellow.

534

535 **Table S3.** 15-gene signature NanoString mRNA values and algorithm for classifying the Mes subtype
536 in 24 patient-matched primary, metastatic, and recurrent HGSC.

537

538 **Table S4.** Performance of the 15-gene gene classifier from Table S2 in identifying Mes and non-Mes
539 molecular subtypes in the TCGA data set.

540

541 **Table S5.** Metastasis site groups in the GSE2109 data set.

542

543 **References**

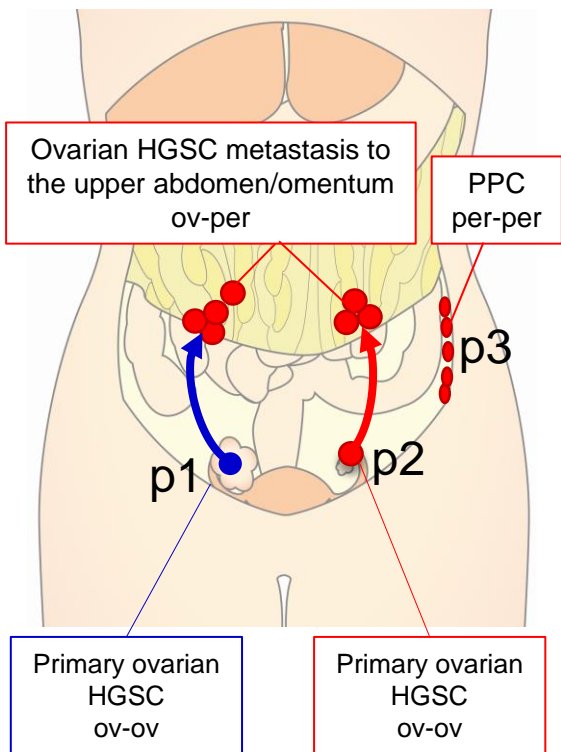
- 544
- 545 1. Matulonis UA, Sood AK, Fallowfield L, Howitt BE, Sehouli J, Karlan BY. Ovarian cancer.
- 546 Nat Rev Dis Primers 2016;2:16061
- 547 2. Eckert MA, Pan S, Hernandez KM, Loth RM, Andrade J, Volchenboum SL, *et al.* Genomics of
- 548 Ovarian Cancer Progression Reveals Diverse Metastatic Trajectories Including Intraepithelial
- 549 Metastasis to the Fallopian Tube. Cancer Discov 2016;6(12):1342-51
- 550 3. McPherson A, Roth A, Laks E, Masud T, Bashashati A, Zhang AW, *et al.* Divergent modes of
- 551 clonal spread and intraperitoneal mixing in high-grade serous ovarian cancer. Nat Genet
- 552 2016;48(7):758-67
- 553 4. Schwarz RF, Ng CK, Cooke SL, Newman S, Temple J, Piskorz AM, *et al.* Spatial and
- 554 temporal heterogeneity in high-grade serous ovarian cancer: a phylogenetic analysis. PLoS
- 555 Med 2015;12(2):e1001789
- 556 5. Brodsky AS, Fischer A, Miller DH, Vang S, MacLaughlan S, Wu HT, *et al.* Expression
- 557 profiling of primary and metastatic ovarian tumors reveals differences indicative of aggressive
- 558 disease. PLoS One 2014;9(4):e94476
- 559 6. Lee JY, Yoon JK, Kim B, Kim S, Kim MA, Lim H, *et al.* Tumor evolution and intratumor
- 560 heterogeneity of an epithelial ovarian cancer investigated using next-generation sequencing.
- 561 BMC Cancer 2015;15:85
- 562 7. Verhaak RG, Tamayo P, Yang JY, Hubbard D, Zhang H, Creighton CJ, *et al.* Prognostically
- 563 relevant gene signatures of high-grade serous ovarian carcinoma. J Clin Invest
- 564 2013;123(1):517-25
- 565 8. Cancer Genome Atlas Research N. Integrated genomic analyses of ovarian carcinoma. Nature
- 566 2011;474(7353):609-15
- 567 9. Jia D, Liu Z, Deng N, Tan TZ, Huang RY, Taylor-Harding B, *et al.* A COL11A1-correlated
- 568 pan-cancer gene signature of activated fibroblasts for the prioritization of therapeutic targets.
- 569 Cancer Lett 2016;382(2):203-14
- 570 10. Zhang S, Jing Y, Zhang M, Zhang Z, Ma P, Peng H, *et al.* Stroma-associated master regulators
- 571 of molecular subtypes predict patient prognosis in ovarian cancer. Sci Rep 2015;5:16066
- 572 11. Zhang Q, Wang C, Cliby WA. Cancer-associated stroma significantly contributes to the
- 573 mesenchymal subtype signature of serous ovarian cancer. Gynecol Oncol 2018
- 574 12. Vargas HA, Micco M, Hong SI, Goldman DA, Dao F, Weigelt B, *et al.* Association between
- 575 morphologic CT imaging traits and prognostically relevant gene signatures in women with
- 576 high-grade serous ovarian cancer: a hypothesis-generating study. Radiology 2015;274(3):742-
- 577 51
- 578 13. Torres D, Kumar A, Wallace SK, Bakkum-Gamez JN, Konecny GE, Weaver AL, *et al.*
- 579 Intraperitoneal disease dissemination patterns are associated with residual disease, extent of
- 580 surgery, and molecular subtypes in advanced ovarian cancer. Gynecol Oncol 2017;147(3):503-
- 581 8
- 582 14. Liu Z, Beach JA, Agadjanian H, Jia D, Aspuria PJ, Karlan BY, *et al.* Suboptimal cytoreduction
- 583 in ovarian carcinoma is associated with molecular pathways characteristic of increased stromal
- 584 activation. Gynecol Oncol 2015;139(3):394-400
- 585 15. Wang C, Armasu SM, Kalli KR, Maurer MJ, Heinzen EP, Keeney GL, *et al.* Pooled Clustering
- 586 of High-Grade Serous Ovarian Cancer Gene Expression Leads to Novel Consensus Subtypes
- 587 Associated with Survival and Surgical Outcomes. Clin Cancer Res 2017;23(15):4077-85

- 588 16. Torres D, Kumar A, Bakkum-Gamez JN, Weaver AL, McGree ME, Wang C, *et al.*
589 Mesenchymal molecular subtype is an independent predictor of severe postoperative
590 complications after primary debulking surgery for advanced ovarian cancer. *Gynecol Oncol*
591 2018
- 592 17. Shilpi A, Kandpal M, Ji Y, Seagle BL, Shahabi S, Davuluri RV. Platform-Independent
593 Classification System to Predict Molecular Subtypes of High-Grade Serous Ovarian
594 Carcinoma. *JCO Clin Cancer Inform* 2019;3:1-9
- 595 18. Torres D, Wang C, Kumar A, Bakkum-Gamez JN, Weaver AL, McGree ME, *et al.* Factors that
596 influence survival in high-grade serous ovarian cancer: A complex relationship between
597 molecular subtype, disease dissemination, and operability. *Gynecol Oncol* 2018;150(2):227-32
- 598 19. Tan TZ, Heong V, Ye J, Lim D, Low J, Choolani M, *et al.* Decoding transcriptomic intra-
599 tumour heterogeneity to guide personalised medicine in ovarian cancer. *J Pathol* 2018
- 600 20. Gao B, Lindemann K, Anderson L, Fereday S, Hung J, Alsop K, *et al.* Serous ovarian and
601 primary peritoneal cancers: A comparative analysis of clinico-pathological features, molecular
602 subtypes and treatment outcome. *Gynecol Oncol* 2016;142(3):458-64
- 603 21. Cheon DJ, Tong Y, Sim MS, Dering J, Berel D, Cui X, *et al.* A collagen-remodeling gene
604 signature regulated by TGF-beta signaling is associated with metastasis and poor survival in
605 serous ovarian cancer. *Clin Cancer Res* 2014;20(3):711-23
- 606 22. Eckert MA, Coscia F, Chryplewicz A, Chang JW, Hernandez KM, Pan S, *et al.* Proteomics
607 reveals NNMT as a master metabolic regulator of cancer-associated fibroblasts. *Nature*
608 2019;569(7758):723-8
- 609 23. Tothill RW, Tinker AV, George J, Brown R, Fox SB, Lade S, *et al.* Novel molecular subtypes
610 of serous and endometrioid ovarian cancer linked to clinical outcome. *Clin Cancer Res*
611 2008;14(16):5198-208
- 612 24. Gao Q, Yang Z, Xu S, Li X, Yang X, Jin P, *et al.* Heterotypic CAF-tumor spheroids promote
613 early peritoneal metastasis of ovarian cancer. *J Exp Med* 2019
- 614 25. Chen GM, Kannan L, Geistlinger L, Kofia V, Safikhani Z, Gendoo DMA, *et al.* Consensus on
615 Molecular Subtypes of High-Grade Serous Ovarian Carcinoma. *Clin Cancer Res* 2018
- 616 26. Aran D, Sirota M, Butte AJ. Systematic pan-cancer analysis of tumour purity. *Nat Commun*
617 2015;6:8971
- 618 27. Konecny GE, Wang C, Hamidi H, Winterhoff B, Kalli KR, Dering J, *et al.* Prognostic and
619 therapeutic relevance of molecular subtypes in high-grade serous ovarian cancer. *J Natl Cancer*
620 *Inst* 2014;106(10)
- 621 28. Zhang Z, Huang K, Gu C, Zhao L, Wang N, Wang X, *et al.* Molecular Subtyping of Serous
622 Ovarian Cancer Based on Multi-omics Data. *Sci Rep* 2016;6:26001
- 623 29. Tan TZ, Miow QH, Huang RY, Wong MK, Ye J, Lau JA, *et al.* Functional genomics identifies
624 five distinct molecular subtypes with clinical relevance and pathways for growth control in
625 epithelial ovarian cancer. *EMBO Mol Med* 2013;5(7):1051-66
- 626 30. Duda DG, Duyverman AM, Kohno M, Snuderl M, Steller EJ, Fukumura D, *et al.* Malignant
627 cells facilitate lung metastasis by bringing their own soil. *Proc Natl Acad Sci U S A*
628 2010;107(50):21677-82
- 629 31. Nieman KM, Kenny HA, Penicka CV, Ladanyi A, Buell-Gutbrod R, Zillhardt MR, *et al.*
630 Adipocytes promote ovarian cancer metastasis and provide energy for rapid tumor growth. *Nat*
631 *Med* 2011;17(11):1498-503
- 632 32. Nieman KM, Romero IL, Van Houten B, Lengyel E. Adipose tissue and adipocytes support
633 tumorigenesis and metastasis. *Biochim Biophys Acta* 2013;1831(10):1533-41

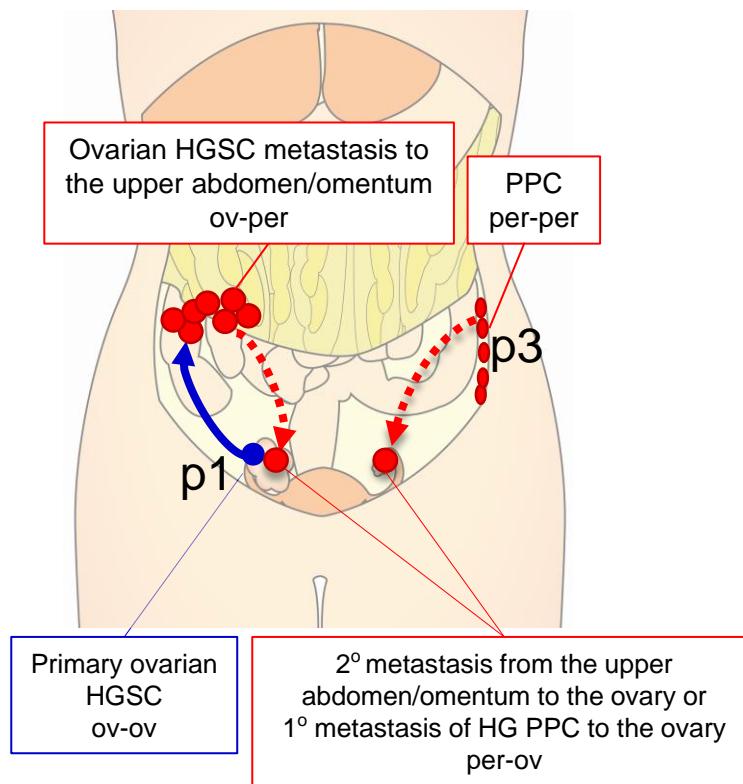
- 634 33. Riestter M, Wei W, Waldron L, Culhane AC, Trippa L, Oliva E, *et al.* Risk prediction for late-
635 stage ovarian cancer by meta-analysis of 1525 patient samples. *J Natl Cancer Inst* 2014;106(5)
636 34. Tucker SL, Gharpure K, Herbrich SM, Unruh AK, Nick AM, Crane EK, *et al.* Molecular
637 biomarkers of residual disease after surgical debulking of high-grade serous ovarian cancer.
638 *Clin Cancer Res* 2014;20(12):3280-8
639 35. Orsulic S, Karlan BY. Can molecular subtyping be used to triage women with advanced
640 ovarian cancer to Primary Debulking Surgery or Neoadjuvant Chemotherapy? *Gynecol Oncol*
641 2019;152(2):221-2
642 36. Nick AM, Coleman RL, Ramirez PT, Sood AK. A framework for a personalized surgical
643 approach to ovarian cancer. *Nat Rev Clin Oncol* 2015;12(4):239-45
644 37. Spencer JA, Weston MJ, Saidi SA, Wilkinson N, Hall GD. Clinical utility of image-guided
645 peritoneal and omental biopsy. *Nat Rev Clin Oncol* 2010;7(11):623-31
646 38. Rutten MJ, van Meurs HS, van de Vrie R, Gaarenstroom KN, Naaktgeboren CA, van Gorp T,
647 *et al.* Laparoscopy to Predict the Result of Primary Cytoreductive Surgery in Patients With
648 Advanced Ovarian Cancer: A Randomized Controlled Trial. *J Clin Oncol* 2017;35(6):613-21
649 39. Nagamine K, Kondo J, Kaneshiro R, Tauchi-Nishi P, Terada K. Ovarian needle aspiration in
650 the diagnosis and management of ovarian masses. *J Gynecol Oncol* 2017;28(4):e40

651

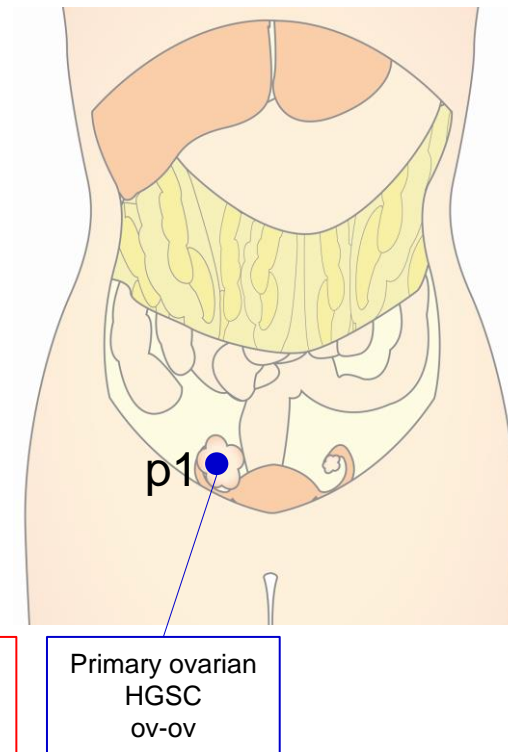
A Current model of intraperitoneal metastasis
Stage III HGSC



B Proposed model of intraperitoneal metastasis
Stage III HGSC



C Stage II HGSC

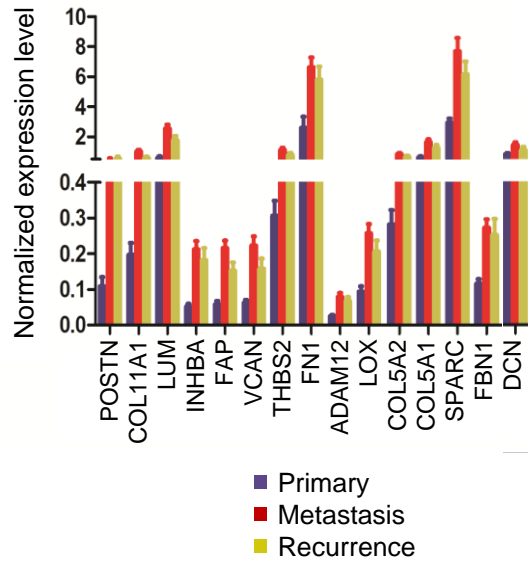


● Mes
● non-Mes

Legend	presumed tissue of origin	site of sample collection
ov-ov	ovary	ovary
ov-per	ovary	peritoneum
per-ov	peritoneum	ovary
per-per	peritoneum	peritoneum

Fig. 1

A Matched samples from 24 patients with stage III or IV HGSC

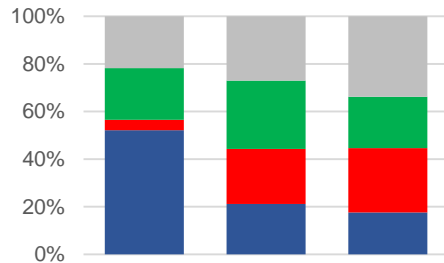


B

Patient	PRIMARY (ov-ov, III-IV)		METASTASIS (ov-per, III-IV)		RECURRENCE (ov-per, III-IV)	
	Mes	Site of sample collection	Mes	Site of sample collection	Mes	Site of sample collection
1	Mes	Left Ovary	Mes	Ileocecum	Mes	Rectosigmoid
2	Mes	Right Ovary	Mes	Omentum	non-Mes	Colon
3	Mes	Right Ovary	Mes	Colon	Mes	Omentum
4	Mes	Right Adnexa	Mes	Omentum	Mes	Omentum
5	Mes	Left Ovary	Mes	Omentum	Mes	Right Upper Quadrant
6	non-Mes	Ovary	Mes	Cul de Sac	non-Mes	Pelvis
7	non-Mes	Right Ovary	Mes	Omentum	Mes	Small Bowel
8	non-Mes	Right Ovary	Mes	Pelvis	Mes	Omentum
9	non-Mes	Ovary	Mes	Omentum	Mes	Lesser Omentum
10	non-Mes	Left Ovary	Mes	Omentum	Mes	Small Intestine
11	non-Mes	Right Adnexa	Mes	Omentum	Mes	Transverse Colon
12	non-Mes	Ovary	Mes	Omentum	non-Mes	Large Intestine
13	non-Mes	Right Ovary	Mes	Omentum	non-Mes	Periaortic Lymph Node
14	non-Mes	Ovary	non-Mes	Omentum	Mes	Pelvis
15	non-Mes	Left Ovary	non-Mes	Omentum	Mes	Rectum
16	non-Mes	Left Ovary	Mes	Abdominal Wall	non-Mes	Colon
17	non-Mes	Right Ovary	Mes	Anterior Wall	non-Mes	Right Inguinal Node
18	non-Mes	Right Ovary	Mes	Omentum	non-Mes	Pelvis
19	non-Mes	Left Adnexa	non-Mes	Periaortic Lymph Node	Mes	Rectosigmoid
20	non-Mes	Ovary	non-Mes	Peritoneal Lymph Node	Mes	Small Bowel
21	non-Mes	Right Ovary	Mes	Omentum	non-Mes	Liver
22	non-Mes	Right Ovary	Mes	Rectosigmoid	non-Mes	Intestine
23	non-Mes	Right Ovary	non-Mes	Right Upper Quadrant	non-Mes	Liver, Chordate Lobe
24	non-Mes	Right Ovary	Mes	Omentum	Mes	Rectosigmoid

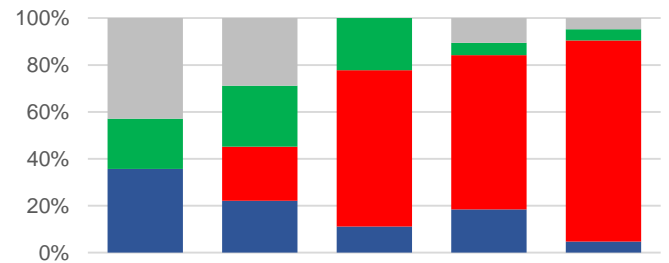
% Mes 20%
79%
58%

C



TCGA	ov-ov II	ov-ov III	ov-ov IV
Immunoreactive	12	76	13
Mesenchymal	1	83	20
Proliferative	5	103	16
Differentiated	5	97	25
Total	23	357	74
% Mes	4%	23%	27%

D

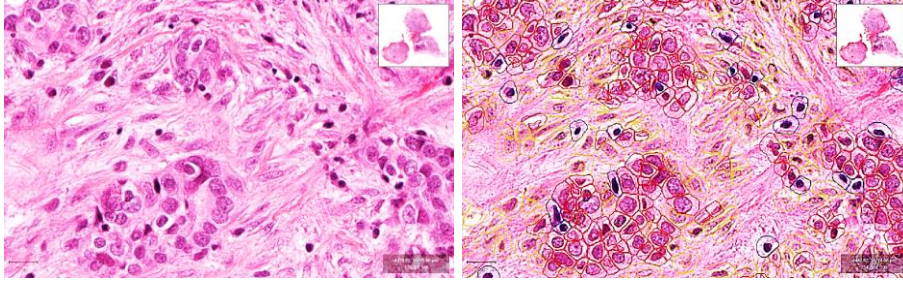
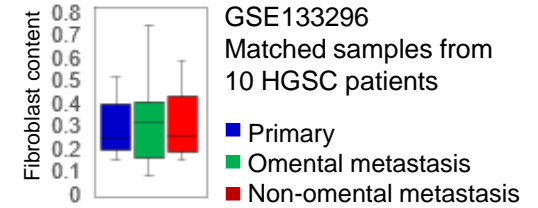


GSE9891	ov-ov I-II	ov-ov III-IV	per-ov II,III,IV	ov-per III-IV	per-per III-IV
Immunoreactive/C2	5	23	1	7	1
Mesenchymal/C1	0	24	6	25	18
Proliferative/C4	3	27	2	2	1
Differentiated/C5	6	30	0	4	1
Total	14	104	9	38	21
% Mes	0%	23%	67%	66%	86%

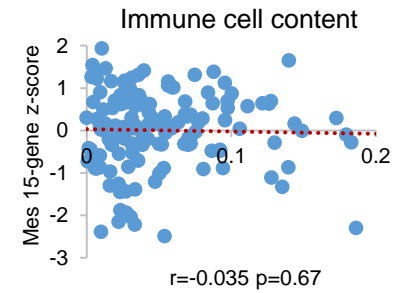
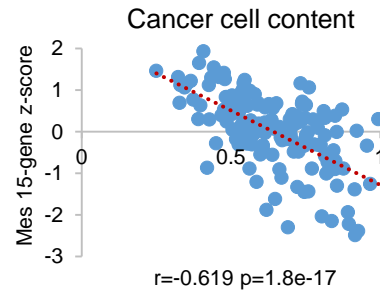
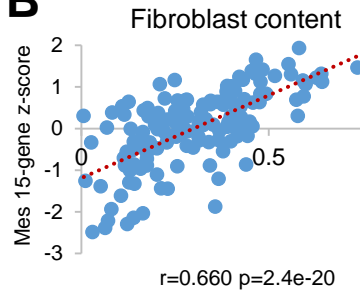
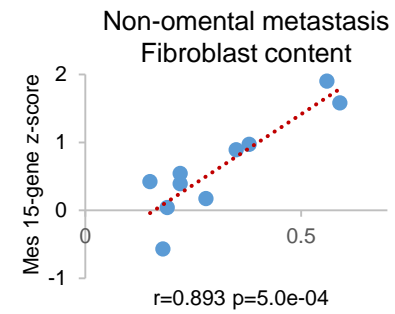
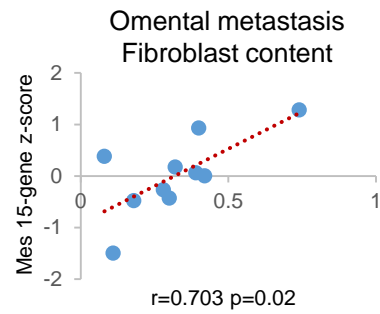
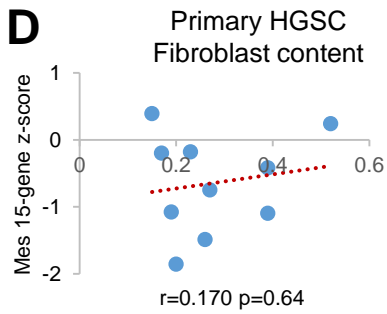
Fig. 2

AHGSC omental
metastases (n=152)

● Fibroblast
● Cancer cell
● Immune cell

**C**

ANOVA	Sum square	Mean square	p-value
Between	0.011	0.005	0.81
Within	0.669	0.025	-

B**D****Fig. 3**

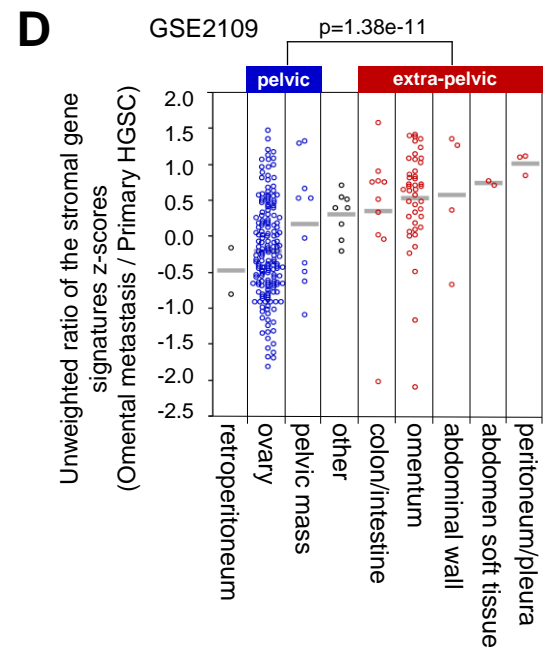
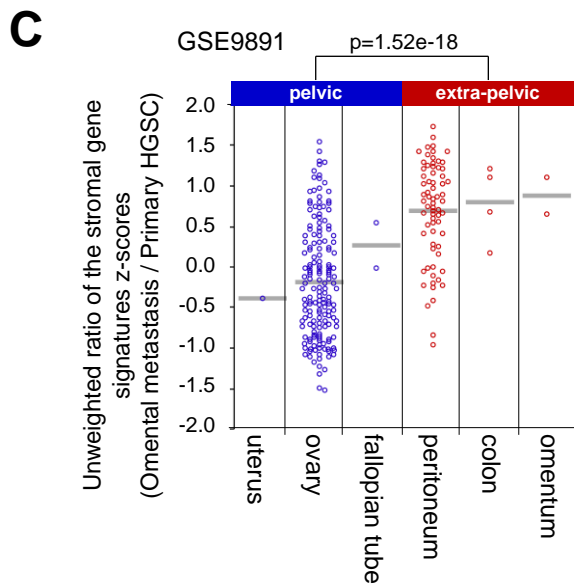
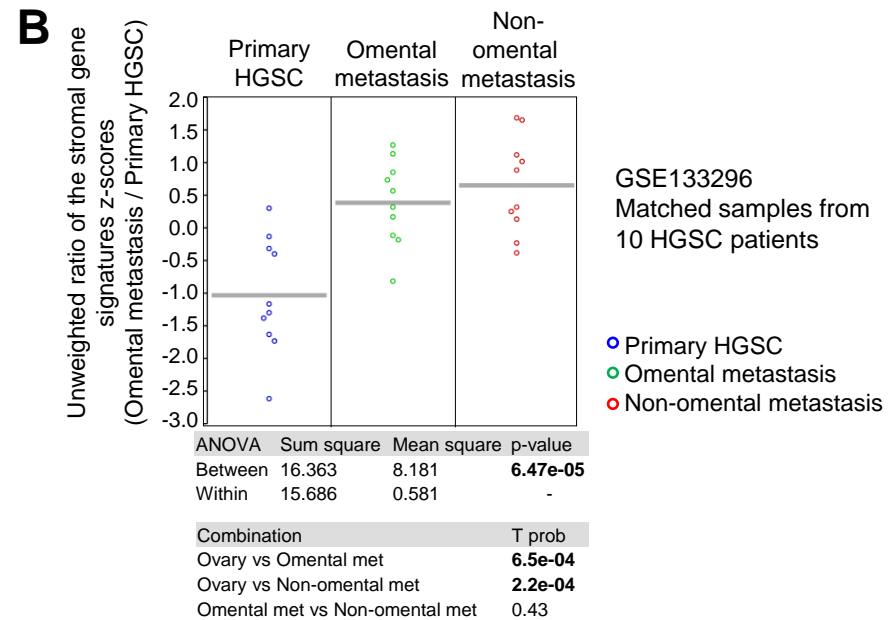
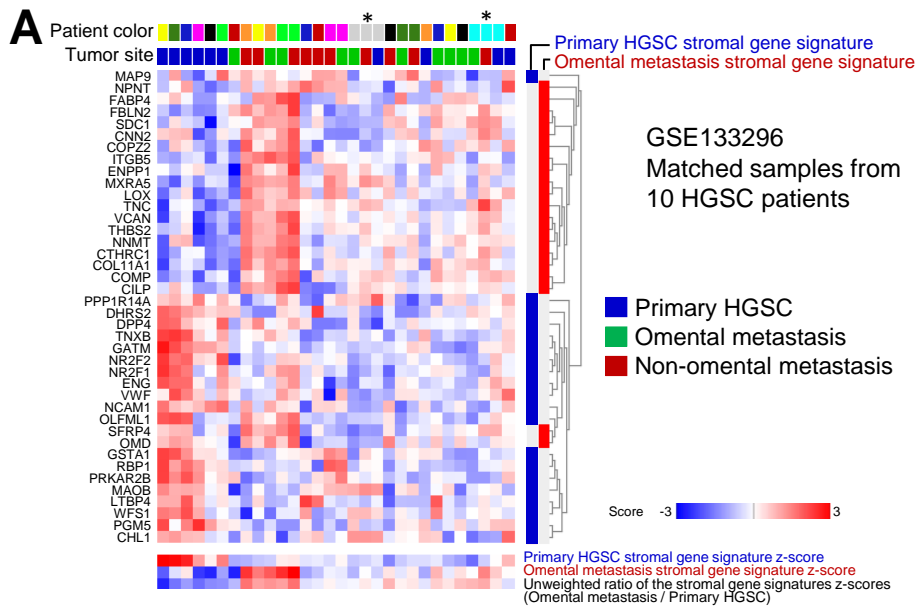


Fig. 4

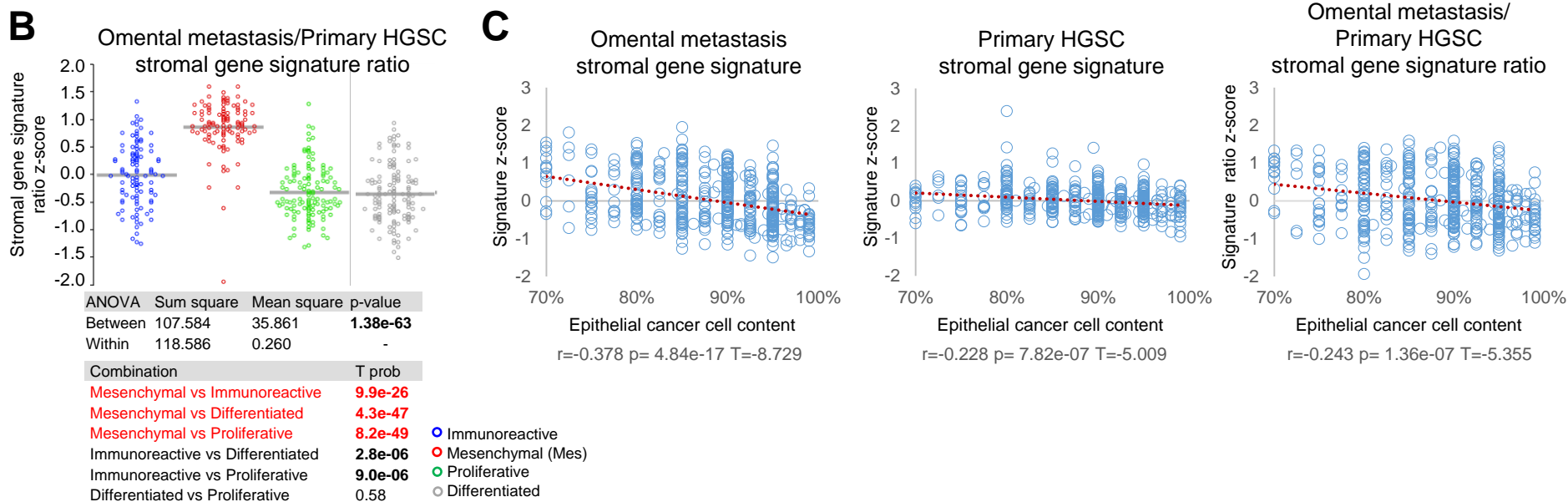
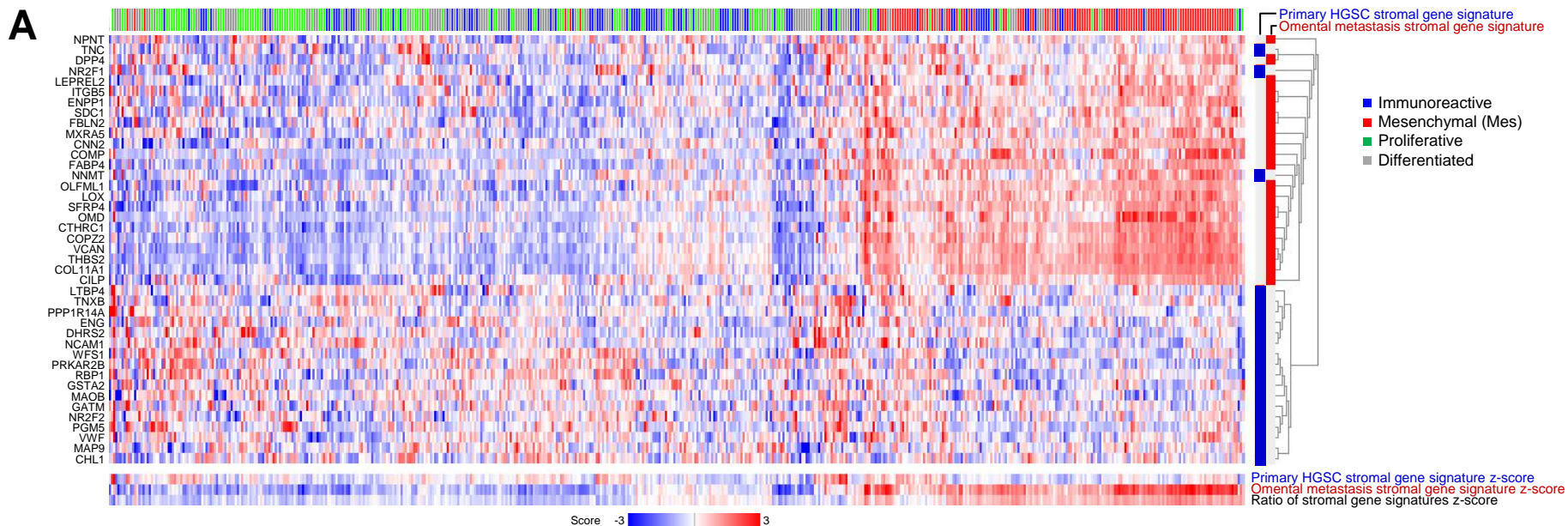


Fig. 5

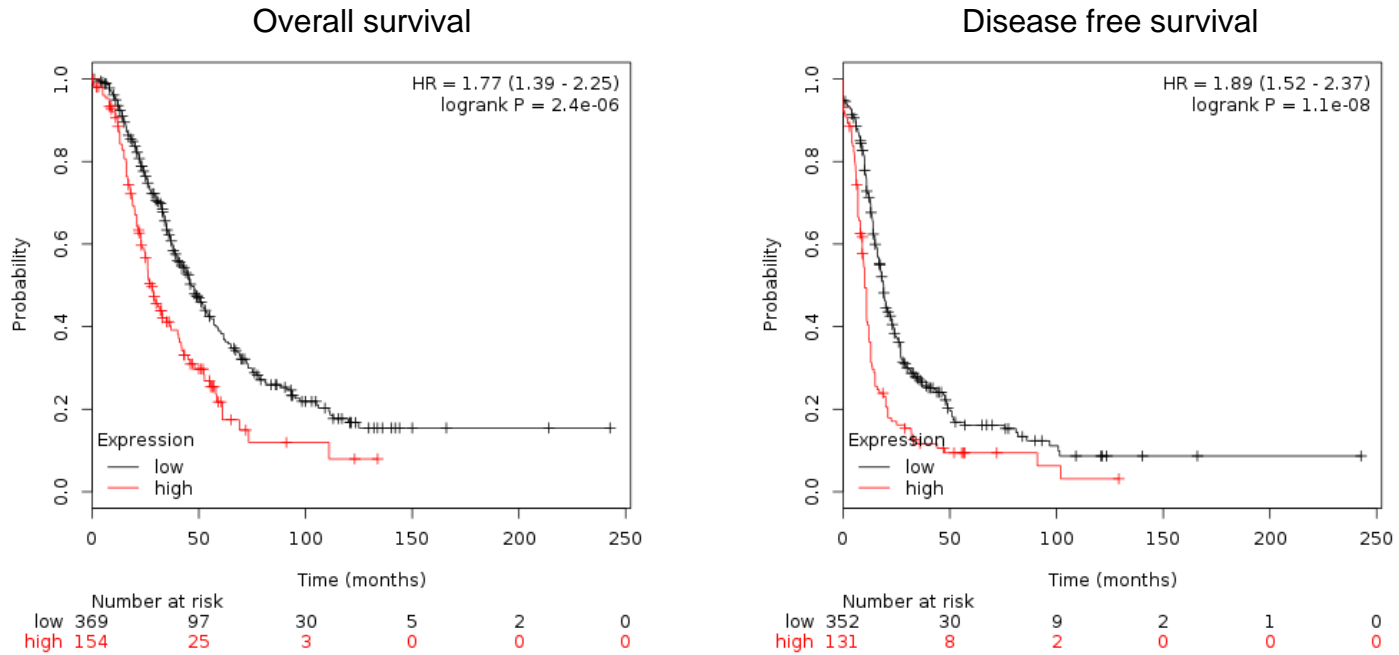
15-gene set

TCGA

Grade: 2+3

Histology: serous

Cutoff: compute best cutoff



Software used for analysis: Kaplan-Meier Plotter. Gyorffy B, Lanczky A, Szallasi Z. Implementing an online tool for genome-wide validation of survival-associated biomarkers in ovarian-cancer using microarray data of 1287 patients, *Endocrine-Related Cancer* 2012;19:197-208

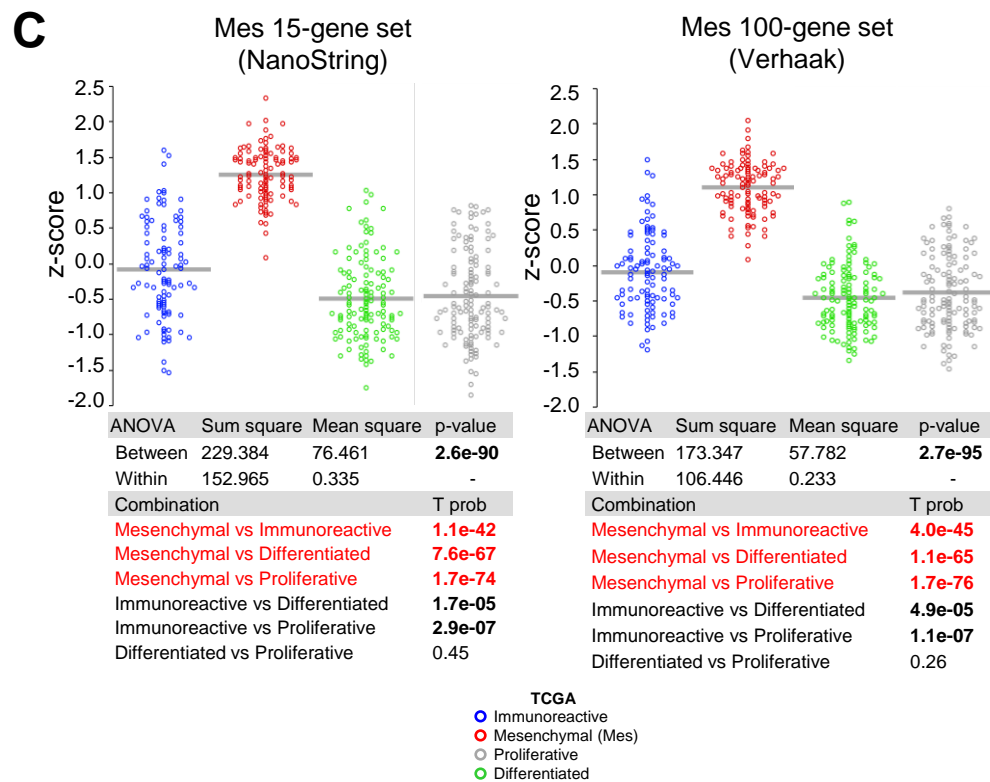
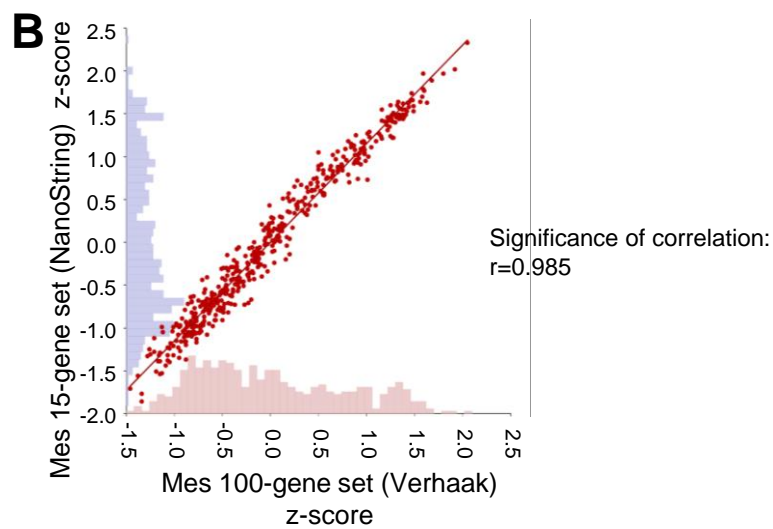
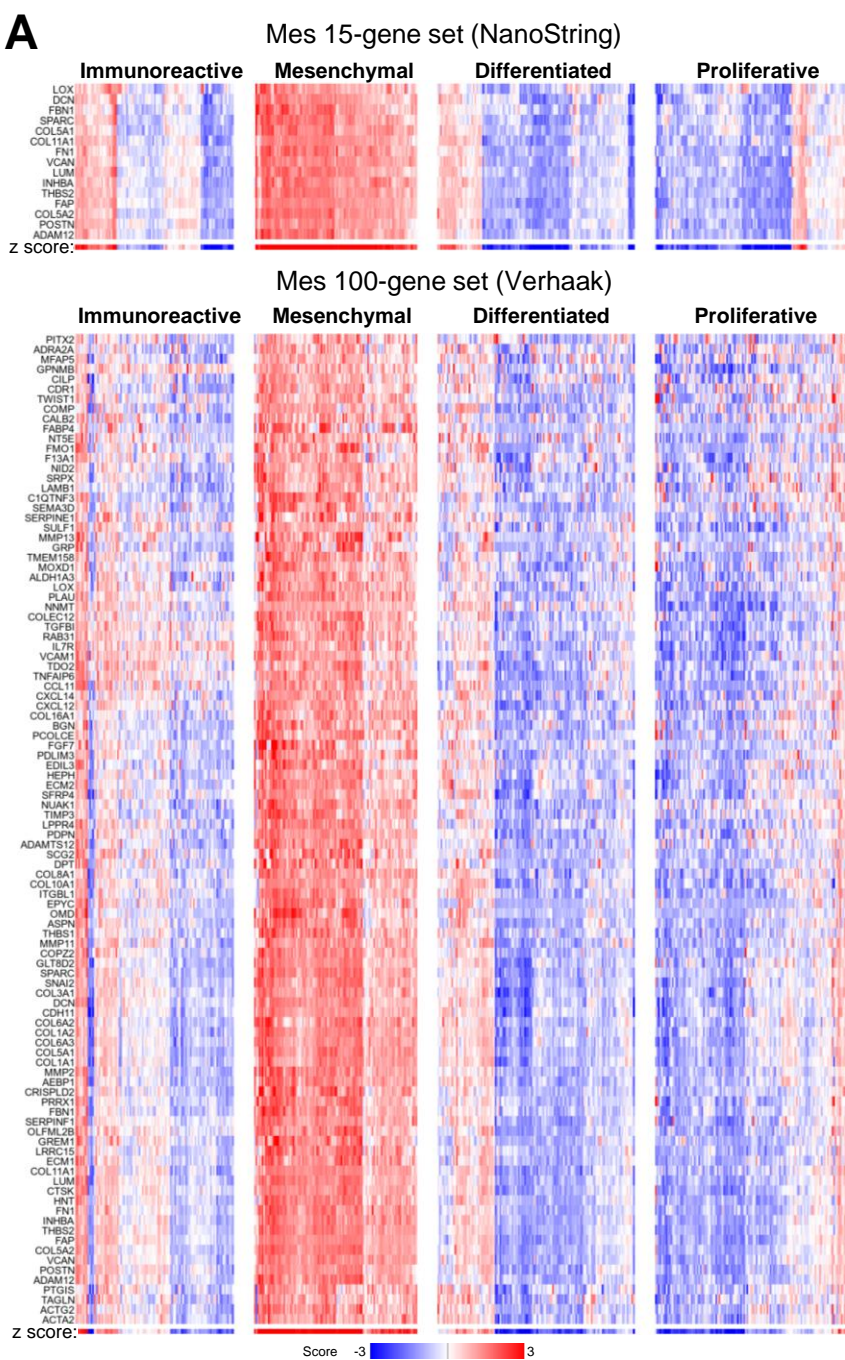


Fig. S2

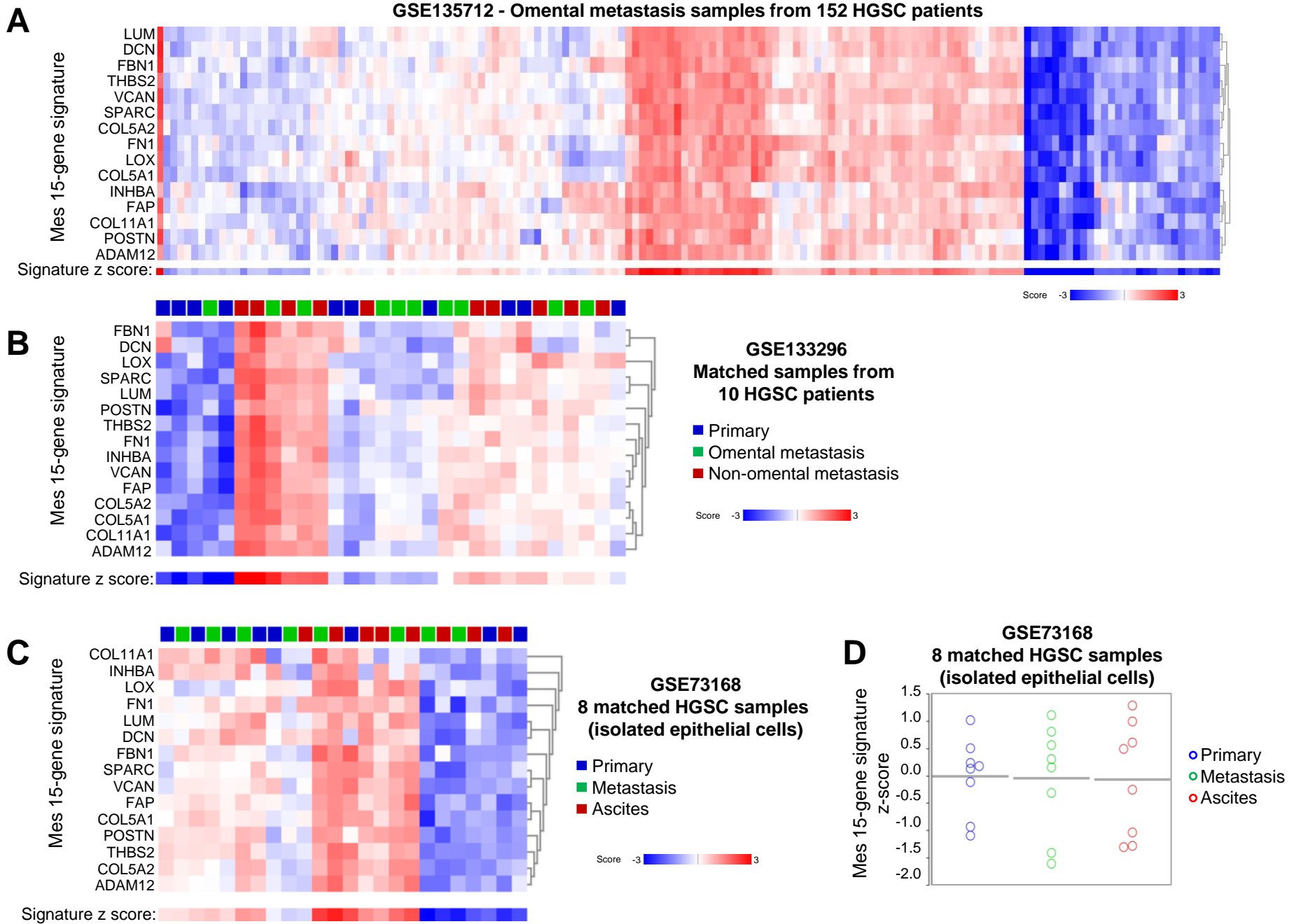


Fig. S3